IUSS
Scuola Universitaria Superiore Pavia

PhD degree in Biomolecular Sciences and Biotechnology

University School for Advanced Studies Pavia (IUSS)

The crosstalk between NuMA and multiple mitotic partners instructs division orientation in mammalian cells

Francesca Rizzelli

European Institute of Oncology (IEO), Milan

Supervisor: **Dr. Marina Mapelli**

European Institute of Oncology (IEO), Milan

Academic year 2019-2020; cycle XXXIII

TABLE OF CONTENTS

GLOSSARY

ABL1	Ableson Leukemia Kinase-1
ACD	Asymmetric Cell Division
AJ	Adherens Junction
APC	Adenomatous Polyposis Coli
BD	Binding Domain
BSA	Bovine Serum Albumine
Caco-2	Human Colorectal Adenocarcinoma Cells
CC	Coiled-Coil
CDK	Cyclin-Dependent Kinase
CM	Conditioned Medium/a
Coot	Crystallographic Object-Oriented Toolkit
CRC	Colorectal Cancer
Dkk1	Dickkopf-1 (Wnt signaling pathway inhibitor 1)
Dlg	Disc Large
DMSO	Dimethyl Sulfoxide
Dvl	Dishevelled
ECM	Extracellular Matrix
ESC	Embryonic Stem Cell
GFP	Green Fluorescent Protein
GoLoco	Galpha (i/o) - Loco
GSH	Glutathione Sepharose
GSK3β	Glycogen Synthase Kinase 3 Beta
GST	Glutatione S-Transferase
GTP/GDP	Guanosine Triphosphate/Diphosphate
$G\alpha_i$	The Alpha Subunit of Adenyl-Cyclase-Inhibitory Heterotrimeric G Protein
HEK293T	Human Embryonic Kidney 293 Cells
HeLa	Human Cervical Cancer Cells
Insc	Inscuteable
IP	Immunoprecipitation
ISC	Intestinal Stem Cell
JNK	c-Jun N-terminal Kinase
Lgl	Lethal Giant Larvae
LGN	Leu-Gly-Asn Repeat-Enriched Protein
LIC	Light Intermediate Chains
Lrp5/6	Low-Density Lipoprotein Receptor-Related Protein 5/6
MAPs	Microtubule-Associated Proteins

mCherry	Monomeric Red Fluorescent Proteins
MDCK	Madin-Darby Canine Kidney Cells
MTs	Microtubules
NLS	Nuclear Localization Signal
NuMA	Nuclear Mitotic Apparatus
OCD	Oriented Cell Division
Par	Partitioning-Defective
PD	Pull-Down
PDB	Protein Data Bank
Ric8A	Resistance to Inhibitors of Cholinesterase 8
SCD	Symmetric Cell Division
shRNA	Short-Hairpin RNA
SLS	Static Light Scattering
TCF/LEF	T-Cell Factor/Lymphoid Enhancer-binding Factor
TIPs	Microtubule ends tracking proteins
TPR	Tetratrico-Peptide Repeats

INDEX OF FIGURES

ABSTRACT

Mitotic progression sustains tissue morphogenesis and homeostasis supporting faithful segregation of the genetic material and correct positioning of the daughter cells within the tissue. The mitotic spindle is the main actor coordinating cell division, and what defines the position and orientation of the mitotic spindle have been object of intense investigation. Several pathways have been involved in establishing correct spindle orientation impinging on the evolutionarily conserved Gαi/LGN/NuMA complexes. During mitosis, the pool of cortical trimeric complexes orients the spindle by generating pulling forces on astral microtubules (MTs), via direct interaction of NuMA with the minus-end-directed MT motors dynein/dynactin. However, the exact mechanism by which MTs and dynein/dynactin are recruited and organized at the mitotic cell cortex still remains elusive. Dynactin is a multisubunit complex that increases dynein processivity by forming a stable complex in the presence of activating adaptors via the hook domain in Hook-family effectors, or a coiled-coil segment in CC1-box-containing adaptors.

The research activities of my PhD revealed that the N-terminal region of NuMA spanning residues 1-705 directly contacts both mitotic isoforms of dynein light intermediate chains (LIC1/2). This binding is mediated by the LIC C-terminal α1-helix analogously to what described for other known dynein/dynactin activating adaptors. Crystallographic studies showed that NuMA$^{1-153}$ folds as a hook domain that contacts LIC1/2. However, biochemical analyses showed that this region does not recapitulate entirely the NuMA/dynein interface. Interestingly, sequence alignments between NuMA orthologues and CC1-box-containing adaptors suggested the presence of a second binding site in the N-terminal portion of the NuMA coiled-coil, named the *CC1-box-like* motif and demonstrated important for the NuMA/LIC binding. Pull-down experiments showed that a double-mutant in the *CC1-box-like* motif impairs NuMA binding to LIC. Importantly, orientation rescue experiments conducted with NuMA truncation mutants lacking either of the LIC-binding interfaces showed that in HeLa cells both NuMA motifs are essential for proper spindle assembly and mitotic progression. These evidences support the notion that NuMA acts as a mitotic dynein/dynactin adaptor, forming a complex with two dynein motors and one dynactin. The organization of dynein motors at the cortex is orchestrated by NuMA interactions with LGN. With structural and biochemical studies, we showed that dimeric NuMA forms LGN/NuMA hetero-hexamers that generate subcortical protein networks promoting the assembly of dynein/dynactin clusters. MT co-sedimentation assays performed with the NuMA C-terminal region revealed that NuMA binds the MT lattice regardless of the tubulin tails, and

can interact also with α/β-tubulin dimers. These findings suggest that in mitosis cortically-anchored NuMA might organize spatially the dynein motors, and modulate the dynamics of astral MTs assisting the retrograde movements of dynein that are required for spindle positioning. Finally, a key question in the orientation field is how the division orientation is coordinated with tissue architecture. Recently, Wnt3 signaling appeared to be involved in spindle orientation. To dissect the molecular link between Wnt3 and orientation, we conducted immunoprecipitation assays in mitotic lysates from cells grown in Wnt3a-stimulated condition or Wnt3a signaling-inhibited pathway, which revealed that NuMA interacts with β-catenin, Dishevelled2 and Axin1 in both conditions. We will exploit this information to reconstitute mitotic complexes of NuMA with Wnt pathway components for structural studies.

1. INTRODUCTION

The research activities of my PhD focused on the biochemical and structural characterization of protein complexes orchestrating mitotic spindle assembly and positioning in mammalian cell divisions, with emphasis on the functional role of the dynein-interactor NuMA.

The following Introduction chapter will illustrate the principles, the functional roles and the molecular mechanisms instructing oriented cell divisions in vertebrates, with focus on the activities of microtubule motors.

1.1 The mitotic spindle

1.1.1 Spindle microtubule dynamics

Bipolar spindle formation is the pivotal event of mitosis, ensuring chromosomes separation within two daughter cells. Mitotic progression can be divided into five distinct phases: prophase, prometaphase, metaphase, anaphase, and telophase. In prophase, DNA replicated during S phase, condensates into chromosome ultrastructure with two visible sister chromatids. The two centrioles couples migrate at the opposite sites of the cell to form a bipolar spindle. Prometaphase starts when the nuclear envelope is complete disassembled (nuclear envelope breaks down, NEB) and ends when all the sister chromatids are bipolarly attached to the microtubules of the spindle. During metaphase the chromosomes align along the cell equator at the so-called metaphase plate before being separated in anaphase. The telophase completes the DNA segregation within two new nuclei, meanwhile the acto-myosin contractile ring divides cytoplasm; therefore, the cytokinesis completes the cell division (O Morgan 2007) (**Figure 1**).

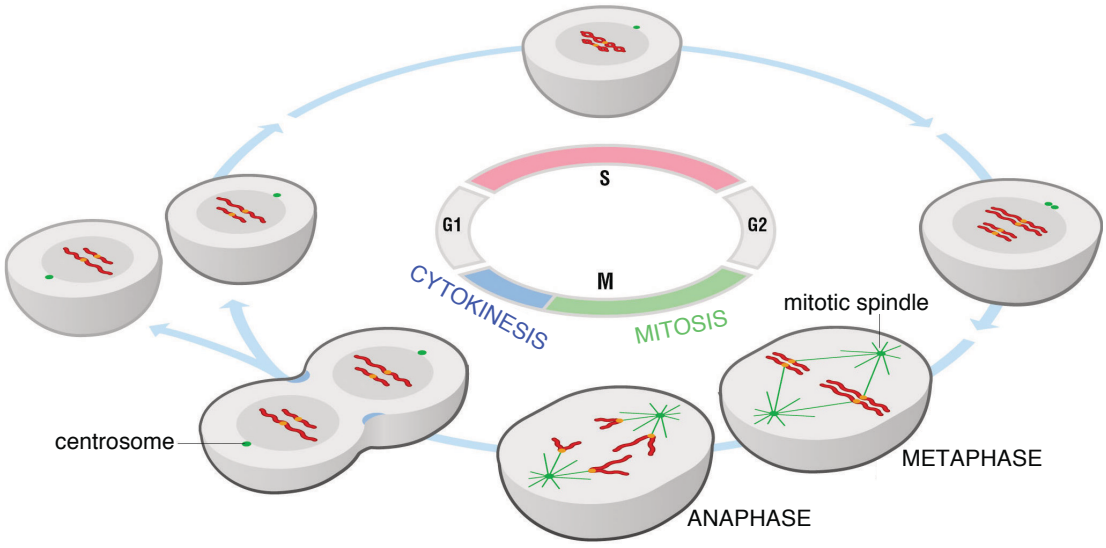

Figure 1. Eukaryotic cell cycle. During S phase the chromosomes and the centrosome are replicated. During mitosis, chromatids segregate, and the division of the genetic material and cytoplasm is completed during cytokinesis. G1 phase is the gap phase between M and S phases; G2 phase is the gap between S and M phases. *From O. Morgan D., The Cell Cycle: Principles of Control, 2007* (O Morgan 2007).

The main structural elements of the highly dynamic bipolar spindle are microtubule bundles. Microtubules (MTs) are long hollow cylinders composed by α,β-tubulin heterodimers subunit organized into 13 parallel protofilaments. In each protofilament, α-tubulin and β-tubulin proteins are longitudinally aligned head to tail, in the same orientation, conferring a discrete polarity at the MT ends. One end exposes β-tubulin, called the plus-end, whereas the other end is composed by α-tubulin and is known as the minus-end. The C-terminal tails of all tubulin monomers are found on the outer surface of the MTs (Nogales E., Wolf S.G., and Downing K.H. 1998). Both α and β-tubulin have GTPase activity, although the GTP-binding α-tubulin monomer is locked up at the dimer interface and is never hydrolyzed or exchanged (Garnham and Roll-Mecak 2012). As a result of this, the addition and removal subunits occur only at the MT ends. The two MT ends have a different rate of growth and shrinkage, with more pronounced rate at the plus-end. The dynamic polymerization and depolymerization rates coupled to GTP hydrolysis is called dynamic instability. This behavior is important for the assembly and function of the bipolar spindle in mitosis: the MT minus-ends are focused at two centrosomes, whereas the plus-ends emanate from spindle poles to cell cortical region and the center of the spindle (Desai and Mitchison 1997; Gierke, Praveen, and Torsten 2012).

MT assembly in cell exhibits distinct dynamic properties compared to pure tubulin *in vitro*, due to the action of numerous microtubule- or tubulin-associated factors that bind the lattice or the ends of MTs (Akhmanova and Steinmetz 2008). Kinesin-13 proteins bind the MT plus-ends and increase the rapidly shrinking rate (catastrophe phase) (Chatterjee et al. 2016) (**Figure 2B**), whereas the small protein Stathmin catches the heterodimers enhancing tubulin dissociation (Rubin and Atweh 2004). Opposite effect to MTs stabilizing is performed by ch-TOG (XMAP215 family member) (**Figure 2A**), EB1, and CLIP-170 in human cells that bind the plus-tips and increase the rapid growth phase (Akhmanova and Steinmetz 2008). These MAPs show uncommon tubulin binding domains: the MT binding domain (MTBD) of TOG family proteins consists of several HEAT-like repeats, a CH domain is found in EB1, and CLIP-170 associates with tyrosinated α-tubulin via a CAP-Gly domain (Brouhard and Rice 2018). MAPs can bind the MT lattice or interact with tubulin C-terminal tails. In

particular, ch-TOG preferentially binds to unpolymerized tubulin in a nucleotide independent manner, and stabilizes the weakly-attached tubulin dimer to the growing MT, so that a larger fraction of tubulin dimers is incorporated into the MT (Brouhard et al. 2008). The processivity of XMAP215 proteins at the MT plus-ends can be attributed to a combination of tubulin subunits binding by TOG domains and the dimers incorporation into the lattice via the interaction between the lattice-binding domain of protein and the acidic C-terminal tails of tubulin (Widlund et al. 2011) (**Figure 2A**). Otherwise, MAP-2 and tau proteins bind to the tubulin C-terminal acidic regions and stabilize the protofilaments (Al-Bassam et al. 2002).

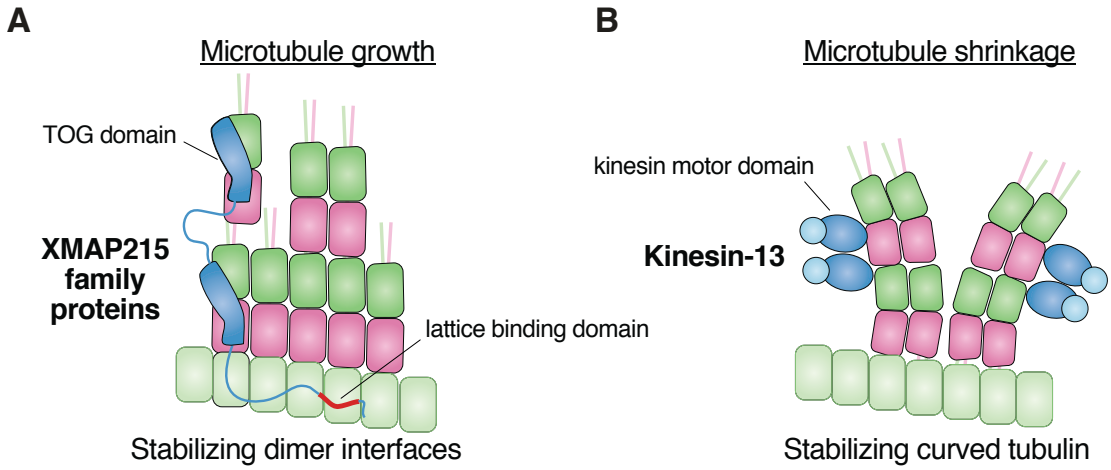

Figure 2. Effect of regulatory proteins on MT growth and shrinkage. Cartoon representation of two classes of microtubule-associated proteins (MAPs) at the MT ends regulating the MT grow or shrink. **A)** XMAP215 proteins (ch-TOG in human and Stu2 in budding yeast) promote rapid MT assembly at the plus-ends; thus, TOG domains-contained proteins positively regulate MT growth. **B)** Opposing its action are catastrophe factors such as Kinesin-13, a member of the kinesin motor protein superfamily. They destabilize the MT ends by binding and promoting highly curved tubulin conformation. *Adapted from Brouhard G. J. and Rice L. M., Nat Rev Mol Cell Biol, 2018* (Brouhard and Rice 2018).

Synthetic proteins helped to control MT dynamic instability in solution and proved to be useful tools to dissect the regulation of MT dynamics, both mechanistically and structurally. Pecqueur *et al.* characterized a Designed Ankyrin Repeat Protein 1 (DARPin1) that caps the MT plus-ends binding to the longitudinal interface of β-tubulin, and favoring the MT disassembly (Pecqueur et al. 2012). Notably, MT-targeting drugs suppressing the mitotic spindle dynamics are used in successful anti-cancer therapies. Specifically, colchicine,

vinblastine, nocodazole are natural toxins that disrupt the filaments polymerization reaction (Lu et al. 2012).

Another class of MT-associated proteins are the motor proteins with ATPase activity encompassing the kinesin (**Figure 2B**) and dynein families. They synergic act in mitotic spindle assembly, cortical force generators and spindle orientation (C. Zhu et al. 2005).

1.1.2 Mitotic spindle assembly

After NEB, the MTs self-organize into three main classes giving rise to a bipolar array of MT bundles focused and anchored at the spindle poles: kinetochore MTs, astral MTs and non-kinetochore MTs. Kinetochore MTs assemble in K-fiber bundles, which are attached to chromosomes at the kinetochores, and in anaphase physically pull sister chromatids apart to separate the two genomes. Astral MTs radiate from the spindle poles and anchor the mitotic spindle to the cell cortex sustaining spindle alignment in metaphase and elongation in anaphase (Kotak and Gönczy 2013). Whereas non-kinetochore MTs or interpolar MTs form an antiparallel array between the spindle poles and are implicated in positioning of the cleavage furrow (**Figure 3**). In late prophase, centrosome maturation begins the process of spindle self-organization (Dumont and Mitchison 2009; Prosser and Pelletier 2017). In animal somatic cells, at the onset of mitosis, the couple of centrosomes is organized in a pericentriolar matrix (PCM) in which two barrel-shaped centrioles and large numbers of tubulin ring complex (γ-TuRCs) are embedded (Kollman et al. 2011). The complex is mainly composed by γ-tubulin, which nucleate MTs at its minus-ends, allowing the plus-ends to grow outward. Several mitotic kinases such as the cyclin-dependent kinase 1 (CDK1), the Polo-like kinases (Plk1) and Aurora-A (Wang, Jiang, and Zhang 2014) are required in this process.

The concomitant centrosome separation and spindle self-organization around chromosomes is promoted by four main classes of motor proteins (**Figure 3**). Eg5 plus-end-directed kinesin cross-links antiparallel interpolar MTs and pushes the spindle poles apart. Eg5 is structured into homotetramers containing four motor domains engaging with two antiparallel MTs and slide them on one other (Kapitein et al. 2005). Selective removal of Eg5 or chemical inhibition of its motor activity (S-trityl-l-cysteine, STLC) prevents centrosome separation, resulting in the formation of monopolar spindles (Blangy et al. 1995; Giet et al. 1999).

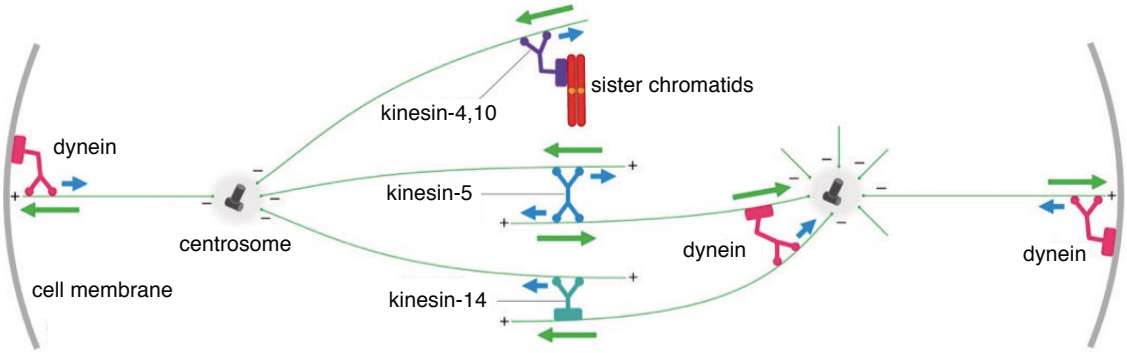

Figure 3. Spindle motors. Several types of motor proteins are particularly important in spindle function: Kinesin-5 (blue) cross-links antiparallel non-kinetochore MTs and pushes poles apart; Kinesin-14 (green) balances the actions of the Kinesin-5; cytoplasmic dynein (magenta) focuses MT minus-ends at the spindle poles, and anchors MT plus-ends at the cortex; Kinesins-4 and Kinesins-10 (purple) connect MTs to chromosome arms and pull them toward the poles in anaphase. Green arrows indicate the direction of MT movement; blue arrows indicate direction of motors movement along the MTs. The motor domains of kinesins and dynein are depicted as circles. *From O. Morgan D., The Cell Cycle: Principles of Control, 2007* (O Morgan 2007).

1.1.3 Mammalian dynein/dynactin complexes

Correct centrosomes separation requires the activity of the additional MT motor dynein (Kardon and Vale 2009). Human cytoplasmic dynein 1 (hereon dynein) is a 1.4 MDa complex composed of six different polypeptides, all of which are present in two copies: a single isoform of dynein heavy chain (DHC), two isoforms of the intermediate chains (DIC), two isoforms of the light intermediate chains (DLIC) and three dynein light chains (Roadblock, LC8, and TCtex) (Reck-Peterson et al. 2018). The two DHCs are linked together by an N-terminal dimerization domain (NDD) and contain a C-terminal AAA+ motor domain with a MTBD at the end of a long antiparallel coiled-coil stalk. Dynein moves along MTs by coupling ATP-induced conformational changes in the AAA+ ring with bending and straightening of the N-terminus (**Figure 4A**). Mammalian dynein assumes a Phi-particle conformation in an auto-inhibited state (Kiyomitsu 2019). Separation of the two motor domains increases dynein affinity for MTs, but still shows low processivity due to inverted conformation of MTBD (Toropova et al. 2019; Zhang et al. 2017). Recent structural analyses showed that dynein can form a ternary complex with dynactin and a cargo adaptor. This results in conformational changes of the motor domains that fully activate dynein motility (Urnavicius et al. 2018) (**Figure 4C**). Dynein and dynactin directly bind to each other through the interaction between the dynactin subunit p150^{Glued} and the DIC, whereas the adaptors generally interact with DLIC C-terminus and at the same time with the

dynactin's pointed-end complex (Olenick and Holzbaur 2019). The activating adaptors interact with dynein through a hook domain in hook-family adaptors or a coiled-coil segment in CC1-box-containing adaptors, and with dynactin through a conserved motif in a coiled-coil region referred to as spindly motif (**Figure 4B**). Furthermore, depending on the adaptor, one or two dynein can be part of the ternary complex. Complexes with two dyneins generate higher forces and walk faster on the MT tracks (Reck-Peterson et al. 2018) (**Figure 4C**). Hook3, BICD2 or BICDL1 are cargo adaptors identified in interphase. Spindly works as a mitotic cargo adaptor that activates dynein motility *in vitro* and at kinetochores (Gama et al. 2017). Moreover, recently Hook2 has been reported to act as a mitotic dynein adaptor at the spindle poles, required for mitotic progression and cytokinesis (Dwivedi et al. 2019). After nuclear envelope breakdown, the pool of dynein localized into the nucleus becomes involved in centrosomes separation (Gadde and Heald 2004). Besides its role in mitotic spindle formation, several lines of evidence demonstrated that in mitotic cells the Nuclear Mitotic Apparatus protein (NuMA) recruits dynein/dynactin at the cell cortex via its N-terminal portion, and places dynein on the spindle generating pulling forces on astral MTs (Kotak, Busso, and Gönczy 2012; Merdes et al. 1996, 2000; Okumura et al. 2018).

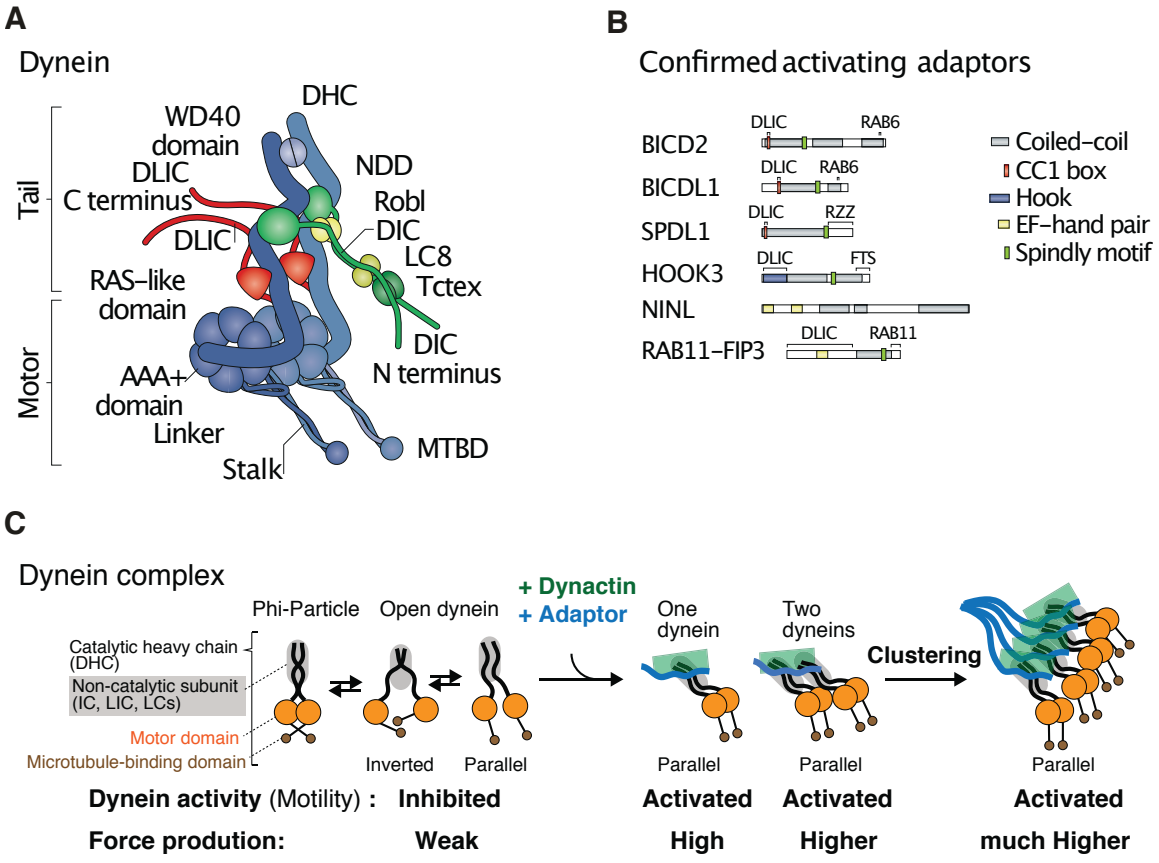

Figure 4. Structure and activation process of mammalian dynein. A) Cartoon of cytoplasmic dynein 1. The two dynein heavy chains (DHCs) are linked together by the N-terminal dimerization

domain (NDD) and have six C-terminal concatenated AAA+ motor domains with a MTDB at the end of a long antiparallel coiled-coil stalk. The dynein intermediate chains (DIC) have extended N-termini that bind dimers of the dynein light chains Roadblock (Robl), LC8 and Tctex. The dynein light intermediate chain (DLIC) has an extended C-terminus. **B)** Domain structures of known dynein-activating adaptors. Activating adaptors contain at least three different types of binding sites for DLIC C-terminus: the hook domain (blue box), the CC1-box (red box) and the EF-hand pair (yellow box). The spindly motif interacts with the pointed end of dynactin (green box). BICD2: Bicaudal D homologue 2; BICDL1: BICD family-like cargo adapter 1; SPDL1: Spindly; HOOK3: protein Hook homologue 3; NINL: ninein-like; RAB11-FIP3: RAB11 family-interacting protein. **C)** Dynactin and adaptors drive both the orientation of the dynein motors and the number of dynein molecules in the motor complex to generate higher forces. The possibility of dynein clustering might increase dynein forces on MTs. *Adapted from: Reck-Peterson S. L. et al., Rev Mol Cell Biol, 2018* (Reck-Peterson et al. 2018)*; Kiyomitsu T. et al., Curr Opin Cell Biol, 2019* (Kiyomitsu 2019).

1.2 Mitotic spindle orientation

1.2.1 Functional role of mitotic spindle orientation

In multicellular organisms, tissue morphogenesis and maintenance are established by spatio-temporal regulation of cell shape rearrangements and cell divisions. The mitotic spindle is the main actor coordinating mitotic progression. Its position, and hence the placement of the division plane, is particularly relevant in the so-called *oriented divisions* (Oriented Cell Divisions, OCDs), including epithelial symmetric divisions (Symmetric Cell Divisions, SCDs) and asymmetric stem cell divisions (Asymmetric Cell Divisions, ACDs) that contribute to the correct tissue development (Morin and Bellaïche 2011) (**Figure 5**). Spindle positioning within the plane of epithelia shapes tissue architecture with an equal partitioning of cellular components. Upon cytokinesis, SCD results in two identical daughters. Human cells undergoing symmetric cell division led to the Hertwig's rule, according to which cells divide depending to their longest axis (Oscar Hertwig 1884). Recent works have provided novel insights into when and how epithelial cells adhere to Hertwig's rule, as well as how tension and polarity contribute to division orientation (Finegan et al. 2019; Scarpa et al. 2018). Converging evidences revealed that oriented divisions require mechanisms in which the mitotic spindle aligns along a specific axis–determined by cellular polarity, that is generally inherited by the tissue in which the cell is integrated. In vertebrate tissues, epithelial polarity arises by opposing forces between the apical Par3/Par6/aPKC polarity complex and baso-lateral Scribble/Dlg/Lgl proteins (Bergstralh, Haack, and St Johnston 2013). Moderately anisotropic cells only partially obey Hertwig's rule, with imperfect alignment of the spindle axis both in unperturbed conditions and upon mechanical cell

stretching, while elongated cells favour division along the major axis. Moreover, by culturing single cells on adhesive micropatterns of defined shape, Théry *et al.* described that the distribution of actin retraction fibers connecting the mitotic cell with the substrate, rather than the cell shape, predicts spindle orientation (Théry et al. 2007). Based on these observations, retraction fibers were proposed to provide a memory of the interphase adhesion of the cell since interphase adhesion controls the distribution of retraction fibers (van Leen, di Pietro, and Bellaïche 2020).

In the developing skin, divisions along the apico-basal axis are associated to tissue stratification and asymmetric fate specification of the two daughter cells (**Figure 5A**). ACDs occur only in stem cells and sustain the stem cell self-renewal process, in which upon division one cell retains stemness while the other one undergoes differentiation (Bergstralh, Dawney, and St Johnston 2017; Santoro et al. 2016). Oftentimes, stemness is maintained by contacts with microenvironments known as *niches* (Fuchs and Chen 2013). The concept of *niche* is defined as a "specific anatomic location that regulates how stem cells participate in tissue regeneration, maintenance and repair" (Scadden 2014). Stem cells can also divide via proliferative symmetric divisions to amplify the stem cell pool. One of the best-characterized vertebrate system dividing asymmetrically is the stem cell compartment of the developing murine skin (described in details in following **paragraph 1.2.2**). It is becoming clear that in multicellular organisms, the balance between symmetric and asymmetric mitoses must be heavily controlled to prevent aberrant growth and tissue disorganization. Consistently, disruption of the mechanisms governing mitotic spindle orientation are often associated with loss of tissue architecture and tumor-like proliferation (Knoblich 2010). Although, several mechanisms might correct the misorientation of the mitotic spindle (Bergstralh, Lovegrove, and St. Johnston 2015), in the absence of corrective cell death or reintegration, spindle misorientation is alone sufficient to induce epithelial to mesenchymal transition (EMT) phenotype (Nakajima et al. 2013).

In both SCDs and ACDs, cells respond to specific stimuli instructing spindle orientation, which derive from extrinsic signals including growth factors, cell-matrix contacts, and cell-cell contacts (Tuncay and Ebnet 2016), as well as from cell geometry (as described above) and intrinsic factors, such as membrane associated proteins localizing in specific cortical domains.

1.2.2 Model systems for study spindle orientation in mammalian tissue and single cells

The core components driving spindle orientation and their regulation have been discovered in invertebrate *in vivo* models (Morin and Bellaïche 2011). Although the players involved in

spindle orientation are highly conserved throughout evolution, transferring the molecular knowledge acquired in invertebrates to vertebrate systems has proven difficult (Pietro, Echard, and Morin 2016; Santoro et al. 2016). Mouse skin progenitors and intestinal stem cells represent the mammalian model systems of oriented cell divisions (**Figure 5**). During development in mice, basal skin progenitors form a monolayer attached to a basement membrane via integrins and are connected to one another by E-cadherins (Fuchs 2016). This arrangement defines their apico-basal polarity, with Par proteins present at the apical regions. At the early stages of skin development, the progenitors divide symmetrically with mitotic spindle parallel to the basement membrane to amplify the stem-cell pool and enlarge the epithelium. At a later stage, the divisions switch to vertical, with the spindle perpendicular to the basement membrane to allow skin stratification. Thus, the ACD generates a progenitor remaining in the basal layer and a daughter cell that is located in the supra-basal layer (Williams et al. 2011). In skin progenitors, the switch from planar SCDs to vertical ACDs has been ascribed to the apical localization of key proteins implicated in spindle orientation including mInsc (the mammalian ortholog of Inscuteable), LGN (a cortical adaptor), NuMA, and dynein/dynactin MT motors (Lechler and Fuchs 2005) (**Figure 5A**). External stimuli might also contribute to instruct spindle orientation and determine daughter cell identity. In fact, by orienting the mitotic spindle perpendicular to the *niche* surface, only the daughter cell physically contacting the *niche* will retain stemness whereas the other will start a program of differentiation. Consistently, the extracellular matrix (ECM) that composed the basement membrane of skin and rich of growth factors can be considered as *niche.* A well-characterized adult stem cell *niche* in vertebrates is the base of intestinal crypts of the small intestine (**Figure 5B**), endowed with a high rate of regeneration. The small intestine is formed by a monolayer epithelium folding into villi and crypts (Barker 2014). Intestinal stem cells (ISCs) localize at the bottom of the crypts intercalate with Paneth cells that work as *niche.* Paneth cells generate a Wnt3 gradient, decreasing long the crypts, which is crucial to maintain stemness limited to the crypt base. Planar cell divisions of cells within the monolayer ensure crypts maintenance driving migration from the bottom of the crypt up to the villi, and sustain differentiation from ISCs to transit-amplifying (TA) progenitors (Sato et al. 2011). TA progenitors, in turn, differentiate into the variety of cells populating the villi to replace the epithelial cells. The crypts homeostasis disruption lead to intestinal tumors and colorectal cancers (CRCs), which are often promoted by the aberrant behavior of cancer stem cells residing at the bottom of the intestinal crypts (Zeuner et al. 2014). How deregulated intestinal cancer cells initiate and sustain intestinal tumors remains an outstanding open question.

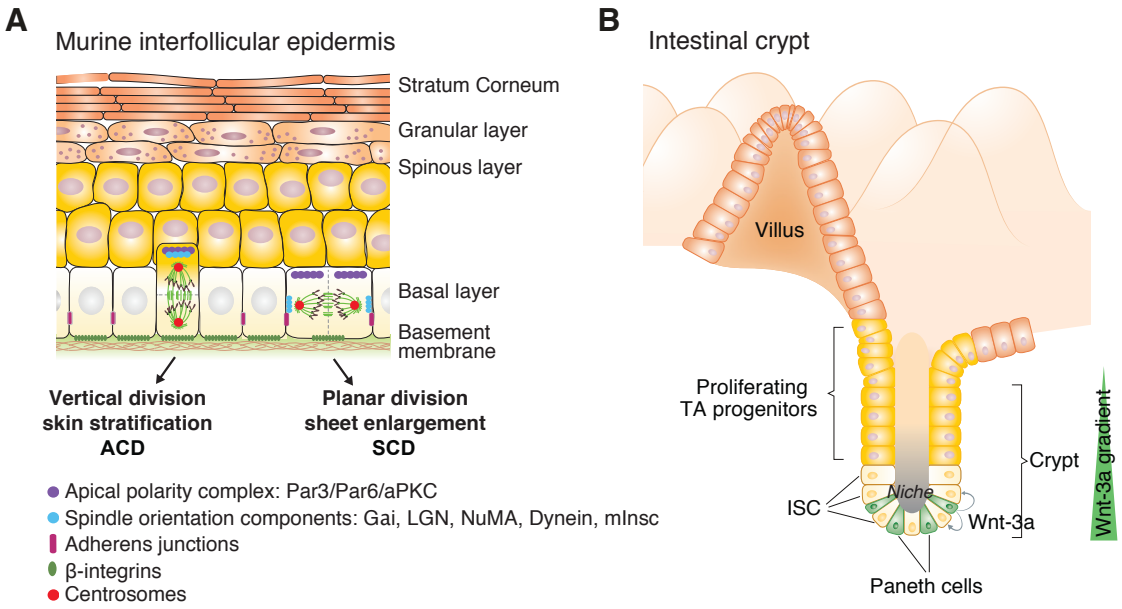

Figure 5. Oriented cell divisions sustain tissue morphogenesis and integrity. The players driving spindle orientation have been discovered *in vivo* system, which remain a useful tool for study the spindle orientation process dynamics. **A)** Murine epidermal progenitors switch from SCDs to ACDs ensuring the correct skin development. The contacts with the basement membrane (*niche*) through β1-integrins (green) and with the other cells of the monolayer through adherens junctions (magenta), and the apically restricted Par complex Par3/Par6/aPKC (purple) define the progenitor apico-basal polarity. **B)** The small intestine is formed by a monolayered epithelium folding into villi and crypts. At the crypt base, ISCs are interspersed among the Paneth cells (green) secreting Wnt ligands and thus acting as *niche*. ISCs proliferate along the crypt axis, through which Wnt production is reduced, and differentiates into transit-amplifying (TA) progenitors. TA progenitors, in turn, differentiate into the variety of cells to replace the epithelial cells. *Adapted from Santoro A. et al., EMBO Rep, 2016* (Santoro et al. 2016).

In addition, *in vitro* cultured cells are frequently used to molecularly investigate the spindle orientation mechanisms. Experiments with isolated embryonic stem cells (ES cells) demonstrated that Wnt3a-ligand-coated beads induce asymmetric ES cell divisions with the mitotic spindle oriented perpendicular to the bead, suggesting that localized Wnt3 signaling is sufficient to orient stem cell divisions (Habib et al. 2013) (**Figure 6D**). These experiments not only proved a Wnt3-driven stemness at single cell level but also provides an *in vitro* experimental setting to study the effect of localized Wnt-signals. Specifically, after cytokinesis the daughter cell in contact with Wnt3 beads inherits β-catenin (the intracellular downstream effector of Wnt3 signaling) and expresses pluripotency genes, while the more distal cell shows hallmarks of differentiation including Nanog, Rex1, and Stella (Habib et al. 2013).

Symmetric polarized cell divisions have been studied in three-dimensional cultures of MDCK (Madin-Darby Canine Kidney) and Caco-2 (from human epithelial colorectal adenocarcinoma) cells, which provided a simple model of monolayered epithelia. By culturing them in Matrigel, 3D cysts with a single central lumen and defined apico-basal polarity are generated. Cysts grow by oriented divisions in which the spindle aligns perpendicularly to the apico-basal polarity axis (Hao et al. 2010; Jaffe et al. 2008; Wei et al. 2012; Zheng et al. 2010) (**Figure 6A**). Defective spindle orientation commonly generates multi-lumen cysts. Basic spindle positioning pathways have also been analysed in non-polarized cells in culture, such as HeLa cells (from human cervical cancer), which undergo symmetrical divisions with the spindle axis aligned to the cell-substrate adhesion plane in a β1-integrin-dependent manner (Toyoshima and Nishida 2007) (**Figure 6B**). Notably, experiments in mice indicate that ablation of β1-integrin results in misoriented metaphases and anaphases in epithelial tissues including murine developing skin (Lechler and Fuchs 2005). Systems in which cells are cultured on surfaces of defined geometry, which dictate a specific shape and adhesion pattern to the cells, have been set up to study the role of the extracellular matrix (ECM) and external forces in inducing a specific spindle orientation (**Figure 6C**).

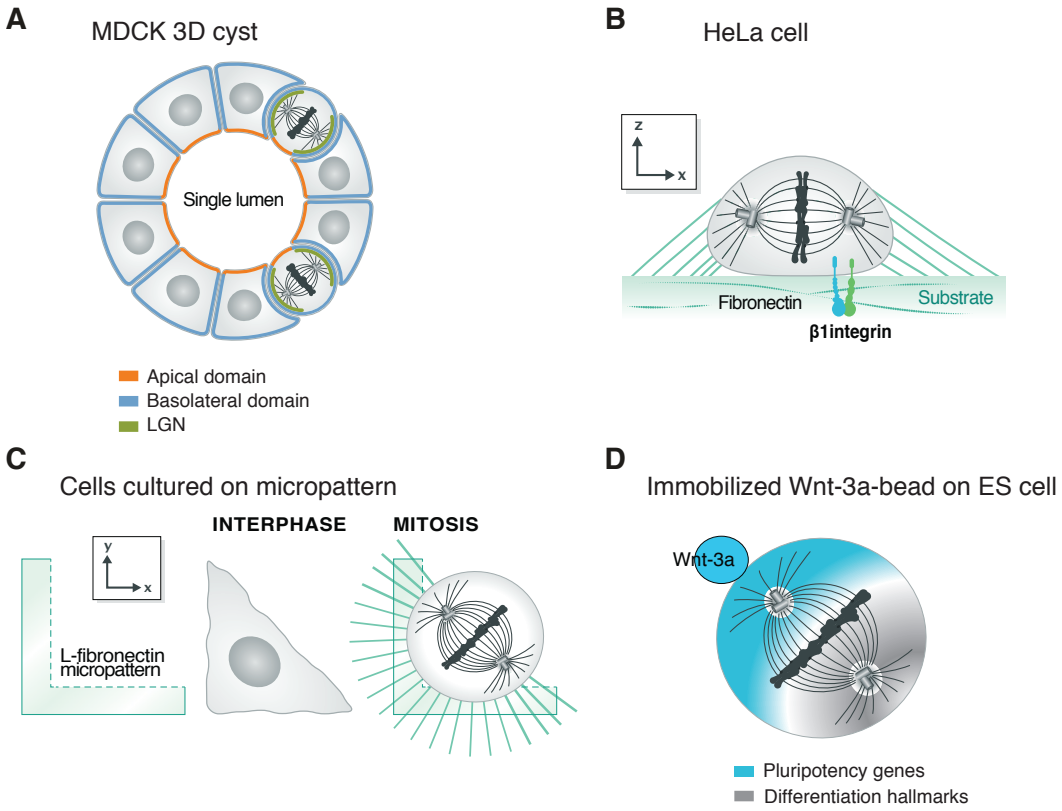

Figure 6. Models for study spindle orientation in single cells. In mammalian system, *in vitro* cultured cells are used to molecularly study the spindle orientation processes. **A)** Cartoon of MDCK/Caco-2 cyst with a central lumen and defined polarity domains, cultured in Matrigel. Spindle orientation occurs in the plane of epithelium and it is dictated by the lateral cell cortex localization of LGN. **B)** Model of the x, z view of a HeLa cell in metaphase plated on a fibronectin-coated support, where the mitotic spindle is oriented parallel to the substrate via β1-integrin. The actin-rich retraction fibers that form upon mitotic round-up are shown in light green. **C)** Model of the x, y view of a mammalian cell cultured on micro surfaces of defined geometry, which dictates a specific shape and adhesion pattern to the cell. The orientation is dependent on the distribution of actin retraction fibers, as well as on astral MTs. **D)** In the presence of a localized Wnt3a source (blue bead), the embryonic stem (ES) cell orients the spindle toward the bead. In this context, after cytokinesis the daughter cell proximal to the Wnt bead expressed pluripotency genes, while the more distal one showed hallmarks of differentiation. *Adapted from di Pietro F. et al., EMBO Rep, 2016* (Pietro, Echard, and Morin 2016).

As widely discussed in the next paragraphs, the synergic activities between the external and internal cues converge on the recruitment of dynein/dynactin MT motors to specialized cortical areas to define the mitotic spindle placement, and accordingly, division orientation. Cues from the cell cortex are transmitted to the mitotic spindle by cortical force generators assembled on Gαi/LGN/NuMA complexes, which in turn out to be in an evolutionary conserved mechanism.

1.3 External stimuli driving spindle orientation

1.3.1 Adhesion and cell-cell junctions in mitosis

At mitotic entry, the actin cytoskeleton undergoes dramatic rearrangement in a process known as mitotic cell rounding, in which cells organize a stiff acto-myosin cortex, and partially detach from the substrate to assume a more spherical shape. Mitotic round-up is essential to establish a cell geometry that provides space for mitotic spindle formation and stiffness to counterbalance forces exerted by cortical motor proteins on the astral MTs (Pietro, Echard, and Morin 2016; F. Rizzelli et al. 2020). In epithelial tissues, mitotic round up is accompanied by reorganization of cell junctions (Lancaster and Baum 2014). Interphase *focal adhesions*, formed by focal adhesion kinase (FAK), talin, paxillin, vinculin, connect the cell cytoplasm with extracellular cell matrix (ECM) via the cytoplasmic tail binding of the β1-integrin subunit of integrin transmembrane receptors. Although it is though that these cell-matrix connections disassemble in mitosis (Marchesi et al. 2014), recent studies in HeLa cells suggest that some FAK, paxillin, vinculin complexes remain

during cell round up in proximity of the actin retraction fibers to maintain substrate adhesion memory and the interphase geometry cues, referred to as *mitotic focal adhesions* (Taneja et al. 2016) (**Figure 7**).

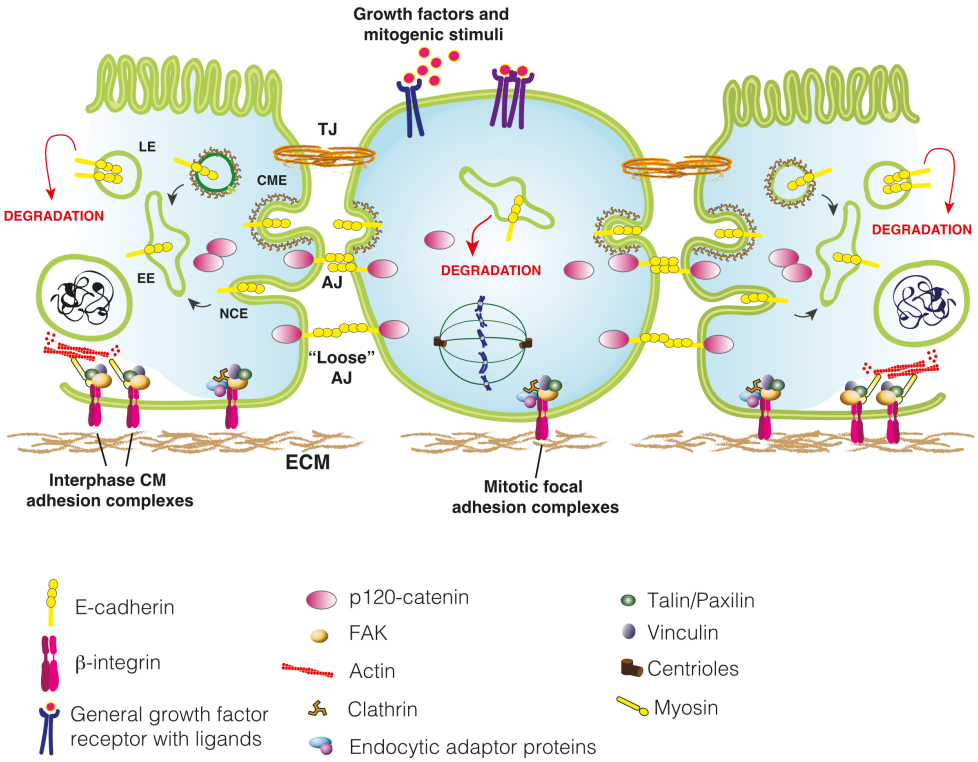

Figure 7. Role of cell-matrix and cell-cell junctions in mitosis. In epithelial polarized cells, two type of adhesive structures are present, which connect the cell to the extracellular matrix: the *cell matrix* (CM) *adhesions* and the *mitotic focal adhesions*. The CM adhesions represent the canonical focal adhesion complexes, which links the extracellular matrix to the actin cytoskeleton through the myosin. The mitotic focal adhesions are devoid of myosin and therefore miss the connection to the actin cytoskeleton. These latter are the ones retained during mitosis. Endocytosis regulates assembly and remodeling of *adherens junctions* (AJs). A small fraction of E-cadherin is constantly internalized and recycled back to the plasma membrane. The major described pathway of E-cadherin internalization is clathrin-mediated enocytosis (CME), but depending on the cell type, it can be endocytosed also through non-clathrin-mediated enocytosis (NCE). Growth factors and mitogenic stimuli accelerate E-cadherin turnover from the plasma membrane (PM), both in the mitotic cell as well as in the neighbouring cells, leading to E-cadherin targeting for lysosomal degradation. This causes a decrease in E-cadherin PM levels and a rearrangement of AJs that become 'loose', thus facilitating furrow ingression and cytokinesis. *Adapted from Rizzelli F. et al., Open Biol, 2020* (Francesca Rizzelli et al. 2020).

Moreover, several lines of evidence reported that intercellular junctions are maintained throughout divisions. In mitosis, *adherens junctions* (AJs) - together with *tight junctions* (TJs) – maintain cells within the epithelium, and also contribute to spindle orientation (F. Rizzelli et al. 2020). In MDCK cells in monolayer and in basal keratinocyte progenitors (**Figure 5A**), E-cadherin-based AJs are maintained laterally (Baker and Garrod 1993; Reinsch and Karsenti 1994). Molecularly, E-cadherin cytoplasmic tail recruits p120-catenin through its juxta-membrane domain (JMD), and β-catenin via its catenin binding domain (CBD). β-catenin associates with the actin-binding protein α-catenin, mediating the association of AJs with the actin cytoskeleton (Niessen and Gottardi 2008). Comparison of the JMD/p120-catenin and CBD/β-catenin complexes reveals that both catenins utilize a basic inner groove of the armadillo domain and an exposed N-terminal hydrophobic surface to recognize charged and hydrophobic stretches of the JMD and CBD, respectively (Huber and Weis 2001; Ishiyama et al. 2010) (**Figure 8**). During epithelial cell division, E-cadherin/p120-catenin association take place at the basolateral PM, where p120-catenin stabilizes E-cadherin by preventing its endocytosis (Ishiyama et al. 2010) (**Figure 7**). E-cadherin turnover from the PM, both in the dividing cell as well as in the neighbouring cells, has shown to be important to ensure a proper cleavage furrow formation during planar cell divisions. Upon depletion of E-cadherin or β-catenin or in the presence of β-catenin mutations, the cytokinesis is impaired (Guillot and Lecuit 2013). Moreover, in the basal layer of murine developing skin, the absence of α-catenin causes the loss of cortical Par3 and LGN, randomizes NuMA localization at the cortex and leads to spindle misorientation (Lechler and Fuchs 2005). In several mammalian cell lines, Gloerich *et al.* showed that LGN is recruited to cell–cell junctions by direct binding to the cytosolic tail of E-cadherin during interphase, and during mitotic entry NuMA is released from the nucleus and competes with E-cadherin for the binding to LGN (Gloerich et al. 2017). Mutational analyses showed that E-cadherin/LGN binding required a negatively charged region within the E-cadherin JMD (DEE758-760), which is reminiscent of how p120-catenin bind to E-cadherin and LGN binds to NuMA (Gloerich et al. 2017) (described in details in **paragraph 1.4.1**, **Figure 10C**).

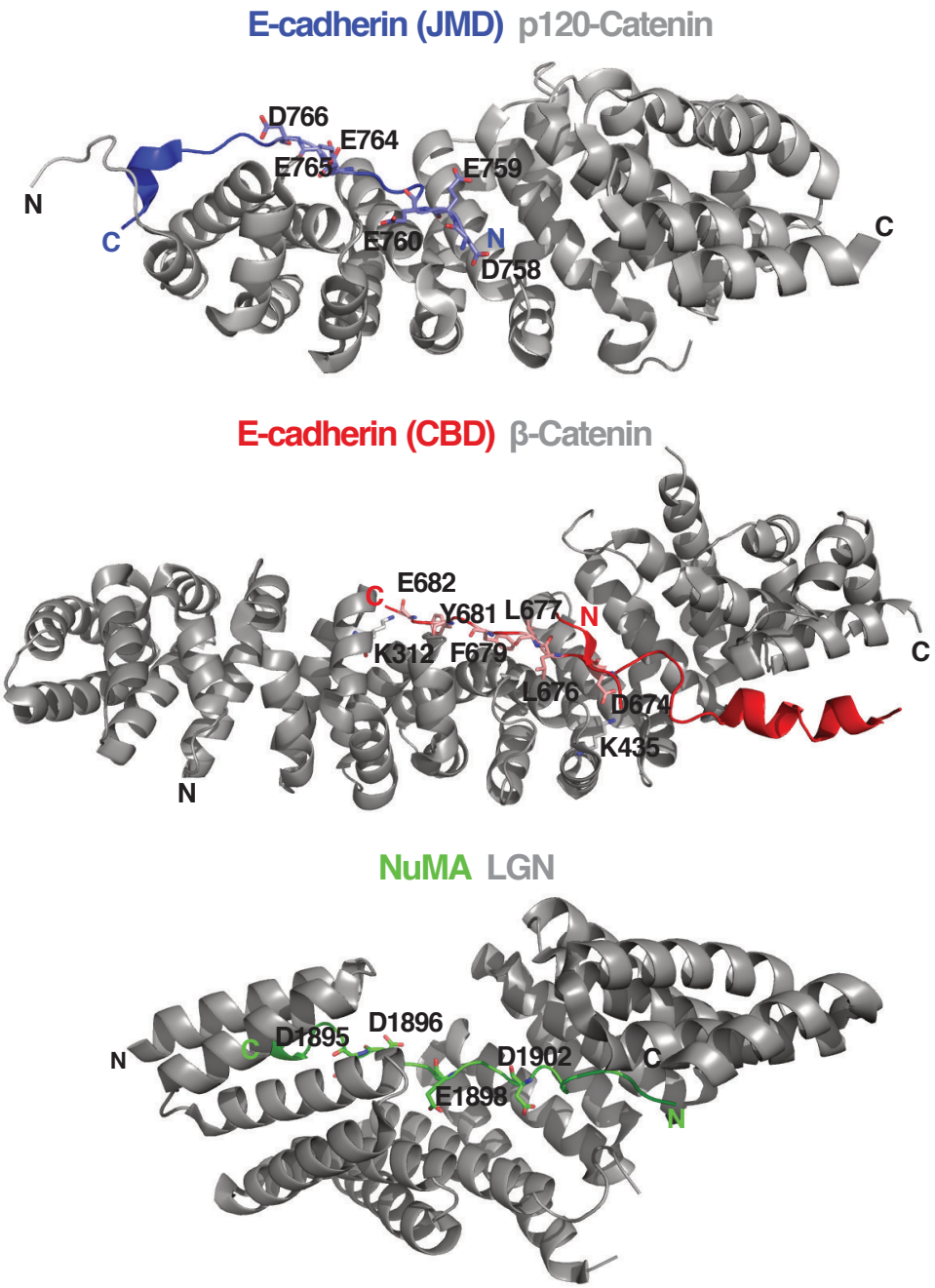

Figure 8. **Structural determinants of complexes involved both in AJs and spindle orientation.** Cartoon representation of JMD-E-cadherin/p120-catenin (PDB ID 3L6Y) (**top**), CBD-E-cadherin/β-catenin (PDB ID 1I7X) (**middle**) and NuMA/LGN (PDB ID 3RO2) (**bottom**) complexes. Three-dimensional structures of E-cadherin (blue) with p120-catenin and of NuMA (green) in complex with the TPR repeats of LGN, showing the negatively charged residues within E-cadherin and NuMA that establish binding to p120-catenin and LGN, respectively. The β-catenin binding domain of E-cadherin (red) contains hydrophobic amino acids, and the binding is sustained by lateral salt bridges. Three complexes reveal that both catenins and LGN show a basic helical groove (grey).

1.3.2 Wnt pathway components instructing mitotic spindle orientation

The Wnt proteins are lipid-modified growth factors that act as morphogens over short distances that, upon receptor binding, stimulate signaling in the responding cells to promote developmental and homeostatic processes (Routledge and Scholpp 2019). The Wnt pathway has been identified as regulator of mitotic spindle orientation in invertebrates and vertebrate systems. Immobilization of Wnt3a on beads was used to demonstrate that in mitosis mouse embryonic stem cells (mESCs) orient their spindle towards the bead, display polarization of Wnt-components in the cell proximal to the bead that retains stem cell fate (Habib et al. 2013) (**Figure 6D**). The molecular mechanisms underlying Wnt-dependent oriented asymmetric divisions is unknown. Wnt signaling is a very conserved pathway with multiple downstream branches (Sharma et al. 2018). In the canonical signaling, Wnt3 ligands bind to seven-pass transmembrane Frizzled (Fzd) receptors and co-receptors, the low-density lipoprotein receptor-related protein 5/6 (Lrp5/6). The formation of Wnt/Fzd/Lrp complexes leads to the recruitment of the so-called *destruction complex* to the plasma membrane: Dishevelled (Dvl) 2 proteins bind to Fzd and mediate the phosphorylation of the cytoplasmic tail of Lrp5/6, which then binds Axin (Gammons and Bienz 2018; Routledge and Scholpp 2019). Phosphorylated LRP6 (pLRP6), (Bilić et al. 2007) – an event mediated in mitosis by CDK14/cyclinY (Niehrs and Acebron 2012) - Dvl2, Axin1 and adenomatous polyposis coli (APC) are thought to form structures named signalosomes, that amplify the Wnt-signals. Lrp6 phosphorylation leads to inactivation of GSK3β, inhibits β-catenin phosphorylation and this way inducing its stabilization. Thus, the Wnt canonical pathway both enhances the half-life of cytosolic β-catenin and promotes its translocation to the nucleus through a JNK-dependent phosphorylation (M.-H. Lee et al. 2009), working with TCF/LEF to activate the transcription of Wnt-target genes (Gammons and Bienz 2018; Routledge and Scholpp 2019). Inhibition of JNK activity in keratinocytes promotes localization of β-catenin adhesion complexes to cell-cell contact sites (M.-H. Lee et al. 2009). Therefore, the cadherin-bound pool of β-catenin can be made available to Wnt pathway (Kam and Quaranta 2009), and during cell division Wnt stimulation could influence the cortical connections of β-Catenin at AJs, possibly facilitating the crosstalk between MTs, actin cytoskeleton and the plasma membrane. Wnt signaling components APC and Dvl affect MT dynamics and the attachment of the spindle to the kinetochores, β-catenin, Axin, GSK3β regulate chromosome segregation (Červenka and Čajánek 2018). In particular, β-catenin and Axin are present at mitotic centrosomes where they might be involved in MT nucleation and mitotic spindle assembly (Hadjihannas, Brückner, and Behrens 2010; Kaplan et al. 2004; Mbom, Nelson, and Barth 2013). Mutations in APC, often associated with colon cancer, have been correlated

with extensive chromosome and spindle aberration (Fodde et al. 2001). Inhibition of the Wnt pathway in HeLa cells through the ablation of LRP6, Fz2 and Dvl2 not only affects the spindle axis but also reduces astral MTs (Kikuchi et al. 2010). These findings rise the possibility that these Wnt-effectors are part of a novel spindle orientation mechanism. Consistently, in several invertebrate systems, a central role of the Dvl/NuMA/dynein axis in spindle orientation has been described (Johnston et al. 2013; Ségalen et al. 2010). In vertebrates, three isoforms of Dvl exist, two of which (Dvl2 and Dvl3) have been implicated in spindle orientation (Kikuchi et al. 2010; Y. Yang et al. 2014). In particular, the spindle orientation functions of Dvl3 seem to depend on its interaction with NuMA, that in mitotic HeLa cells is promoted by the activity of the deubiquitinase CYLD (Y. Yang et al. 2014). The orientation functions of Dvl2 seem to be related to its spindle pole localization, where it associates with and is phosphorylated by Plk1 (Kikuchi et al. 2010). Both NuMA and β-catenin bind to the actin cytoskeleton adaptor 4.1R (see **paragraph 1.4.2**) to ensure proper spindle orientation and preserve the integrity of adherent junctions, respectively (Mattagajasingh, Huang, and Benz 2009; S. Yang et al. 2009). Whether the three protein can be part of the same complex is unclear. Recently, Stolz *et al.* showed that Wnt/STOP pathway (Acebron et al. 2014) regulated by basal Wnt signaling during a normal cell cycle is required for proper spindle MT assembly and for faithful chromosome segregation during mitosis (Stolz et al. 2015).

1.4 Orientation and positioning of mitotic spindle

1.4.1 Structural organization of Gαi/LGN/NuMA/dynein conserved pathway

The best-characterised force generating complex at the cell cortex consists of an evolutionary conserved molecular pathway composed of the Gαi protein, LGN, NuMA, and dynein exerting spindle orientation and positioning functions. During mitosis, Gαi/LGN/NuMA trimeric complexes are localized to subcortical domains above the spindle poles, and direct the recruitment of the minus-end directed MT motor dynein (Morin and Bellaïche 2011; Pietro, Echard, and Morin 2016). The idea is that retrograde movement of cortically anchored dynein results in pulling force on the spindle poles ensuring the orientation and/or positioning of the spindle (**Figure 9**). The specific localization of Gαi/LGN/NuMA complex instructs the site of force concentration and the axis of spindle orientation. The assembly of Gαi/LGN/NuMA complexes at the cell cortex is orchestrated by four Gαi-GDP subunits anchored at the plasma membrane by N-terminal myristoyl group (**Figure 9**). Gαi subunits cover the whole cell inner surface with Gβγ, and what restricts

Gαi-GDP/NuMA/LGN localization is unclear (Peyre et al. 2011). Additional factors, and in particular polarity proteins, regulate the polarized cortical distribution of LGN and NuMA crescents (van Leen, di Pietro, and Bellaïche 2020; Morin and Bellaïche 2011) (**Figures 5A**). Moreover, a recent study proposes that the constitutive membrane protein of caveolae, Caveolin1, is implicated in instructing the distribution of Gαi/LGN/NuMA complexes based on interphase adhesion geometry. In HeLa cells cultured on the fibronectin pattern, Caveolin1 interacts and co-localizes with Gαi1 on the plasma membrane at the proximal end of retraction fibers and its depletion randomizes the orientation (Matsumura et al. 2016) (**Figure 9**).

The mammalian C-terminal LGN GoLoco domain contains four (three in *Drosophila* Pins and one in *C. elegans* GPR1-2) domains that, already in prometaphase, exclusively recognizes GDP-loaded Gαi (Willard, Kimple, and Siderovski 2004). In this non-canonical G-protein signaling pathway, intracellular guanine exchange factors (GEFs) such as Ric-8 catalyze the release of GDP from Gαi, limiting the concentration of Gαi-GDP molecules available for the interaction with LGN (Tall and Gilman 2005). Recent crystal and cryo-EM structures reveals that Ric-8A works as an unconventional GEF, exhibiting a chaperone activity towards Gα (McClelland et al. 2020). Ric8 is essential for execution of the asymmetric cell division in *C. elegans* and in *Drosophila* (Woodard et al. 2010), as well as the Ric8A isoform ensures mitotic spindle positioning in HeLa cells and cystogenesis in MDCK cells (Chishiki et al. 2017).

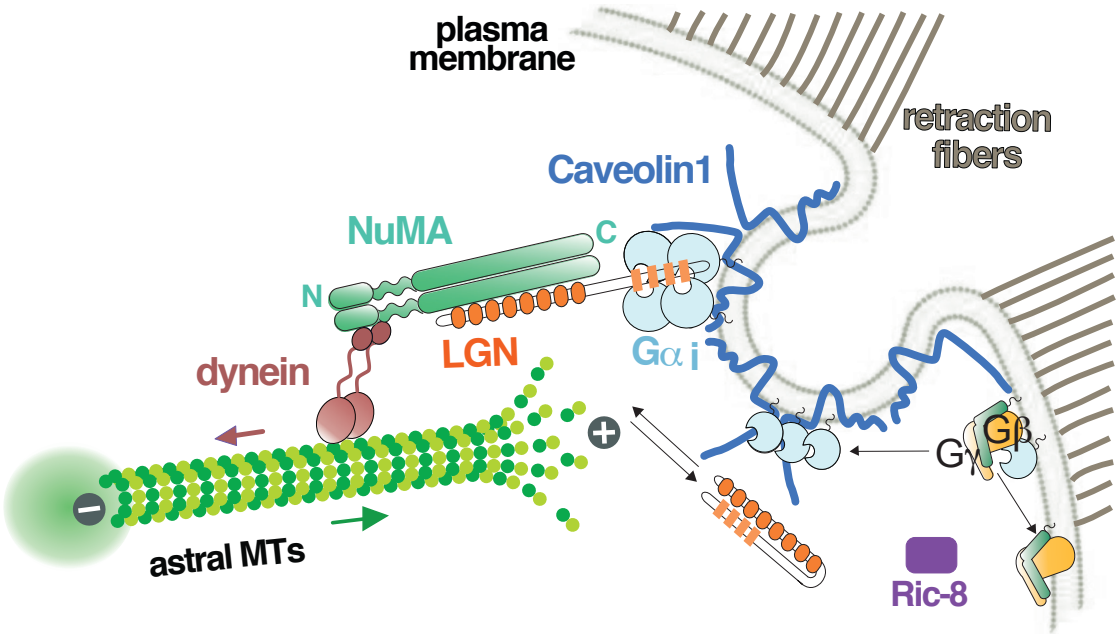

Figure 9. The mitotic spindle orientation pathway. In mitosis cortical Gαi/LGN/NuMA/dynein complexes are required to link the cell cortex to the spindle poles. The retrograde movement of dynein anchored at the plasma membrane by Gαi/LGN/NuMA complexes results in pulling forces on astral MTs (explained by the directions of the arrows). During mitotic cell rounding, Caveolin1, enriched at cortical regions near retraction fibers, recruits Gαi to drive mitotic spindle orientation. The GEF Ric-8 controls the timely activation of the Gαi/LGN/NuMA by catalysing the release of GDP from isolated Gαi subunits.

The scaffold protein LGN (Leu-Gly-Asn repeat-enriched protein) is composed by two main domains: eight N-terminal tetratricopeptide-repeats (TPRs) and four GoLoco motifs at the C-terminus, joined by a linker region of about 100 residues (**Figure 10A**). FRET studies demonstrated that LGN switches from a closed inhibited conformation in interphase to an opened one during mitosis (Du and Macara 2004). In the open conformation, the TPR domain mediates interactions with multiple binding partners, including Insc (Inscuteable), the polarity protein Afadin, and NuMA (Carminati et al. 2016; Culurgioni et al. 2011; J. Zhu et al. 2011) (**Figure 10C**). The structure of LGN-15-350 (LGN^{TPR} hereon) is composed of 16 α helices arranged into eight sequential helix-turn-helix TPR repeats, each one structured in two antiparallel α helices, referred to as A and B, which form the inner and outer surface of a superhelical conformation, respectively. Interestingly, LGN^{TPR} shows different structural features compared to canonical TPR motifs because it presents an insertion between the helices A and B of fourth repeat that determines a superhelix distortion resulting a more concave inner surface (**Figure 10B**). The LGN^{TPR} domain recognises its binding partners and its own GoLoco C-terminal region via a set of asparagines in the inner surface (Culurgioni et al. 2011; Pan et al. 2013; Yuzawa et al. 2011; J. Zhu et al. 2011) (**Figure 10C**). After nuclear envelope breakdown, NuMA is released from the nucleus and recruited at the cortex by binding to the TPR region of LGN. A small C-terminal peptide of NuMA spanning residues 1899-1926 has been shown to bind LGN^{TPR} with a 1:1 stoichiometry, similarly to cortical adaptor Insc (Culurgioni et al. 2011; J. Zhu et al. 2011). Thus, Insc and NuMA compete for the binding to LGN with Insc displaying a five-fold higher affinity compared to NuMA. The LGN-GoLoco3-4 contacts only the TPRs1-6 and TPRs5-8 of LGN (**Figure 10C**), while Insc and NuMA binding to LGN involve a further binding interface (the N-terminal α-helix on TPRs6-8) increasing the affinity. This could be the explanation about the role of Insc/NuMA to promote LGN open conformation. Moreover, other evidences show that the LGN opening requires the synergistic binding of NuMA and several

Gαi subunits (Smith and Prehoda 2011), suggesting that the linker of LGN contributes to stabilize intra-molecular interactions keeping LGN in the closed conformation.

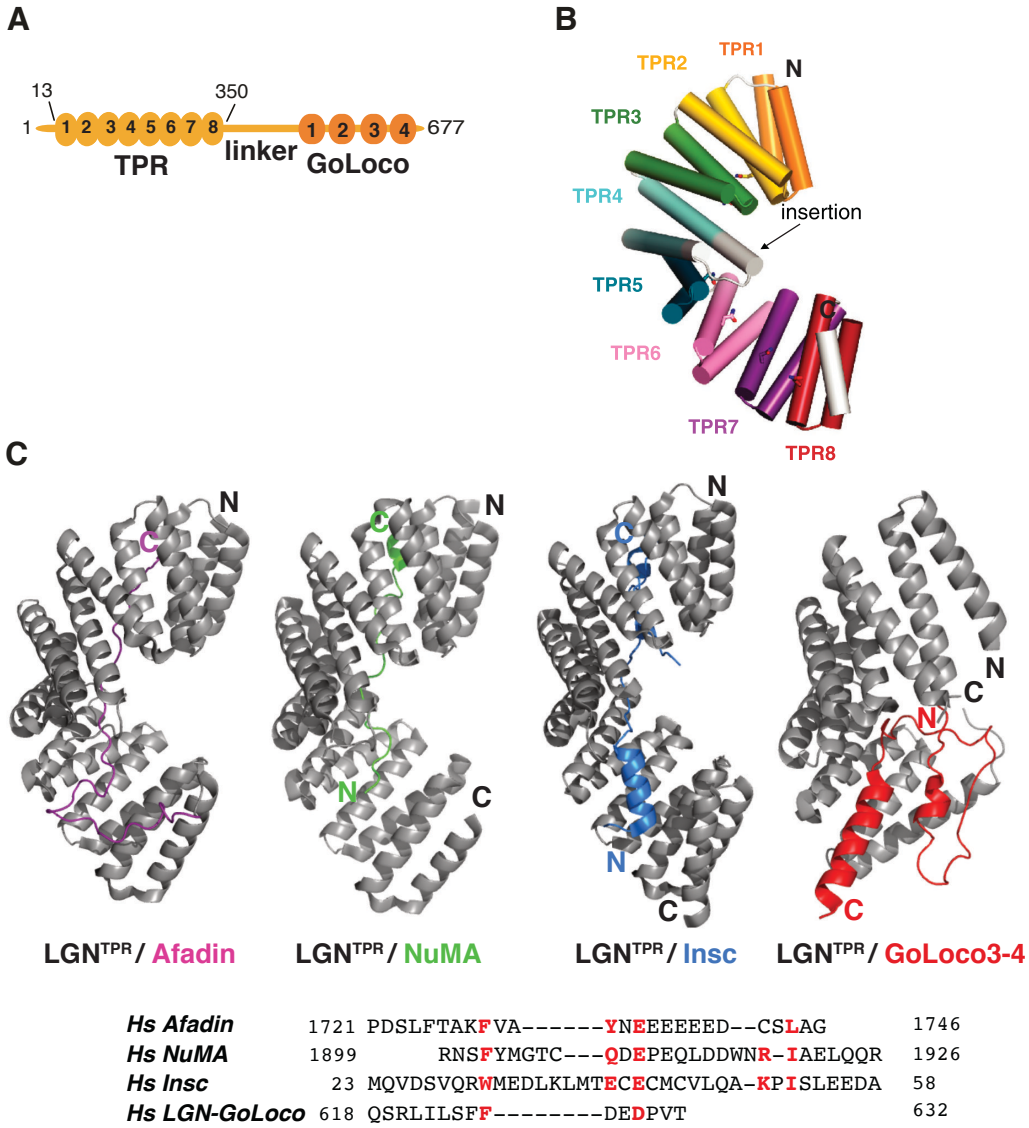

Figure 10. LGN architecture and overall structure with TPR binding partners. A) Domain structure of full-length LGN, with the eight N-terminal TPR repeats and the C-terminal GoLoco region joined by a linker region of 100 residues. **B)** Cartoon representation of LGN^{TPR} architecture. Each TPR repeat consists of two antiparallel helices represented as cylinders. *From Culurgioni S. et al., PNAS, 2011* (Culurgioni et al. 2011). **C) Top:** Cartoon representation of LGN^{TPR}/Afadin$^{1709-1746}$ (PDB ID 5A6C), with the Afadin peptide fused with the TPR domain of LGN shown in purple, whereas LGN is show in grey; LGN^{TPR}/NuMA$^{1899-1926}$ (PDB ID 3RO2), with the NuMA peptide shown in green; the LGN^{TPR}/Insc$^{23-69}$ complex (PDB ID 3SF4), with Insc in blue; topology of LGN^{TPR} in complex with GoLoco$^{593-651}$ (PDB ID 4JHR); the GoLoco fragment encompasses the 3rd and the 4th GoLoco motif, and is shown in red. **Bottom:** structure-based sequence alignment of the LGN^{TPR} interactors. The conserved residues involved in the binding to LGN are highlighted in red.

NuMA$^{1899\text{-}1926}$ binds to the LGN^{TPR} superhelix in an antiparallel manner. In this interface, the interaction between NuMA and LGN is mainly mediated by electrostatic interactions and hydrogen bonds (J. Zhu et al. 2011).

In line with the reconstituted interactions between Gαi, LGN and NuMA, in mitotic cells the pool of trimeric Gαi/LGN/NuMA complexes at the cortex associates with dynein/dynactin, promoting the onset of MT-pulling forces (Kotak, Busso, and Gönczy 2012).

1.4.2 Spatial-temporal regulation of spindle orientation players

In vertebrate cells, the mitotic spindle is assembled in prometaphase with a random orientation, and then orients during metaphase to adopt the final division axis observed in anaphase (Kiyomitsu 2015; Kotak, Busso, and Gönczy 2012). In prometaphase HeLa cells, LGN is uniformly recruited at the cell cortex, while in metaphase it localizes at two cortical regions restricted above the spindle poles, together with NuMA and dynein/dynactin (Kiyomitsu and Cheeseman 2012). In the same study, the authors observed that in metaphase dynein shows an asymmetric cortical placement that is negatively regulated by spindle pole proximity, this way determining oscillations that contribute to spindle centering (Kiyomitsu 2015; Kiyomitsu and Cheeseman 2012). The cortical asymmetric distribution of dynein is due to Plk1 kinase activity, which disrupts the association between dynein/dynactin and LGN/NuMA when poles are in close proximity to the cortex (Kiyomitsu and Cheeseman 2012). Recently, Doumont showed that NuMA is required for force generation at MT minus-ends, and that its depletion impairs dynactin localization at the poles (Hueschen et al. 2017). Thus, a pool of NuMA localizes at the spindle poles, and at the same time NuMA can be recruited at the cortical regions via direct interaction with LGN in metaphase and with the cell cortex in anaphase (Du et al. 2002; Kotak and Gönczy 2014; Seldin, Muroyama, and Lechler 2016). These findings converge in a recent work from Sana *et al.* demonstrating that Plk1 directly interacts and phosphorylates NuMA, negatively regulating its localization at the cell cortex (Sana et al. 2018). Besides Plk1 regulation, the enrichment of NuMA at the cortex is finely regulated by several kinases activity. Our lab recently demonstrated that in metaphase HeLa cells, Aurora-A kinase regulates the mobility of NuMA among the spindle poles and the cell cortex by phosphorylating Ser1969 (Gallini et al. 2016). In HeLa cells and mouse keratinocytes, the ABL1 kinase positively regulates the NuMA cortical localization through the phosphorylation of Tyr1774, via an unknow mechanism (Matsumura et al. 2012). In anaphase, NuMA enriches at the cortex, and results in an additional increasing of cortical dynein/dynactin localization that drive strong pulling forces for sister chromatids

segregation and spindle elongation. In metaphase, CDK1 phosphorylation impairs the direct association of NuMA (residues 1996-2074) with the lipids bilayer at the levels of PIP/PIP2 sites, possibly by electrostatic repulsion between negative charges of the phospho-groups (Kotak, Busso, and Gönczy 2013, 2014; Zheng et al. 2014). By contrast in anaphase, CDK1 activity is inhibited by cyclinB degradation and counterbalanced by the phosphatase PP2A activity (Kotak, Busso, and Gönczy 2013) promoting LGN-independent targeting of NuMA at the cell cortex. The increasing cortical localization of NuMA also involved the 4.1R cytoskeleton protein binding to the NuMA region encompassing residues 1788-1819 (Kiyomitsu and Cheeseman 2013; Mattagajasingh, Huang, and Benz 2009; Seldin et al. 2013). However, the Gonczy lab showed that loss of cortical NuMA upon depletion of 4.1G/R might be an indirect effect of cortical acto-myosin disruption (Kotak, Busso, and Gönczy 2014). Moreover, they proposed that the region containing the 4.1G/R binding site (1699-1876) is rather an additional phospholipid interacting region (**Figure 11**).

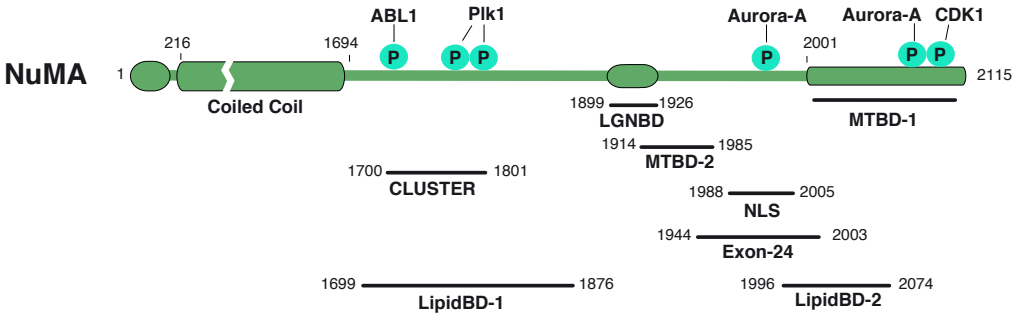

Figure 11. Domain structure and phosphosites of human NuMA.

ABL1 phosphosite on Tyr1774 (ABL1): Matsumura, *Nat Commun*, 2012

Aurora-A phosphosites on Ser1969 and Ser2047 (Aurora-A): Gallini, *Curr Biol*, 2016

Clusterization domain (CLUSTER): Okumura, *eLife*, 2018

Lipid binding domain (LipidBD–1): Kotak, *EMBO J.*, 2014

Lipid binding domain (LipidBD–2): Zheng, *MBoC*, 2013

Nuclear localization signal (NLS): Gueth–Hallonet, *Exp. Cell Res.*, 1996

LGN binding domain (LGNBD) or NuMA^{PEPT}: Zhu, *Mol. Cell*, 2011

Microtubules binding domain (MTBD–1): Gallini, *Curr Biol*, 2016

Microtubules binding domain (MTBD–2): Du & Macara, *Curr Biol*, 2002

Plk1 phosphosites on Ser1833 and Ser1834 (Plk1): Sana, *Life Sci Alliance*, 2018

Together these findings demonstrate that localization of NuMA/dynein is tightly regulated throughout mitosis to ensure mitotic spindle positioning in metaphase and elongation during anaphase.

1.5 NuMA interaction landscape

Human NuMA is a 2115 residues protein, composed by a N-terminal globular domain linked to the C-terminal unstructured tail region by a long coiled-coil. In the first stage of mitosis, NuMA is involved in spindle poles focusing and organization (Khodjakov et al. 2003; Merdes et al. 1996; Silk, Holland, and Cleveland 2009). In HeLa cells and fibroblasts NuMA depletion results in defects on chromosome congression, poles misorganization, and dissociation of centrosomes from MT minus-ends (Haren et al. 2009; Merdes et al. 1996, 2000). As depicted in the previous paragraph, in the later mitosis NuMA ensures spindle orientation and chromosome segregation exerting pulling forces on astral MTs, in association with dynein/dynactin motors. However, the architecture of these pulling-machinery is unknown.

1.5.1 The NuMA N-terminal region

In mitotic HeLa cells, the N-terminal region of NuMA spanning residues 1-705 suffices to immunoprecipitate both the dynein intermediate chain (DIC) and the $p150^{Glued}$ subunit of dynactin (Kotak, Busso, and Gönczy 2012). Recently, in HCT-116 cells light-induced cortical targeting of NuMA1-705 results in dynein/dynactin recruitment at the cortex, but is not sufficient to generate pulling forces, suggesting that other sites and/or a supramolecular organization of forces are required (Okumura et al. 2018). Beside dynein/dynactin association, the functions of the N-terminal region of NuMA are poorly understood. Moreover, the putative function of NuMA as a mitotic dynein/dynactin-activating adaptor is unclear.

1.5.2 The NuMA C-terminal region

The C-terminus of NuMA performs multiple roles and harbors lipid binding domains (Kotak, Busso, and Gönczy 2013, 2014), a 4.1-binding region (see **paragraph 1.4.2**) (Mattagajasingh, Huang, and Benz 2009), a nuclear localization signal (NLS) (Gueth-Hallonet, Weber, and Osborn 1996), two MT binding regions, and an LGN-binding region (residues 1899-1926; as detailed in **paragraph 1.4.1**) (Culurgioni et al. 2011; J. Zhu et al. 2011) (**Figure 11**). One of the most studied functions of NuMA is its MT binding ability. Experiments with *Xenopus* extract proved that a region of the NuMA C-terminus is involved in MT aster formation by MT-bundling (Merdes et al. 1996), and its overexpression in HeLa cells induces MT-bundling *in vivo*. Co-sedimentation experiments with taxol-stabilized MTs identified that human NuMA spanning residues 1914-1985 interacts physically with MTs, and this region was initially depicted as the minimal domain required for MT binding (Haren

and Merdes 2002). Notably, the MTBD of NuMA partially overlaps with the LGN binding region opening the question whether LGN and MTs could compete for the interaction with NuMA. In the same work of Du and colleagues, co-sedimentation experiments with NuMA-1580-2115 in the presence of LGN^{TPR} indicated that binding of LGN impairs the interaction between NuMA and MTs. Moreover, LGN^{TPR} inhibits *in vitro* MT-bundling with NuMA fragment encompassing residues 1892-2015. However, the same authors found that NuMA-1914-1985 can perform MT-bundling even with the concomitant presence of LGN^{TPR} (Du et al. 2002). The NuMA MTBD functional activity was investigated in mouse and human cells by depleting a region corresponding to the exon-22 which encodes for the putative MT binding domain (Gallini et al. 2016; Seldin, Muroyama, and Lechler 2016; Silk, Holland, and Cleveland 2009). In mouse carrying a heterozygous mutation in the exon-22 region, the MT binding region of NuMA identified by Merdes (MTBD-2 in **Figure 11**) is involved in spindle poles focusing, and MTs attachment to kinetochore, and its depletion results in impaired NuMA localization at the poles and spindle misorientation (Seldin, Muroyama, and Lechler 2016; Silk, Holland, and Cleveland 2009). Depletion of the corresponding region in HeLa cells (exon-24 in the human NuMA gene, encompassing residues 1944-2003) impairs NuMA localization at the spindle poles (Gallini et al. 2016). Recently, we reported that a second MT binding region of NuMA spanning residues 2002-2115 lies at the C-terminus, that is able to bind concomitantly LGN and MTs, and promotes MTs-bundling *in vitro* (Gallini et al. 2016) (**Figure 12**).

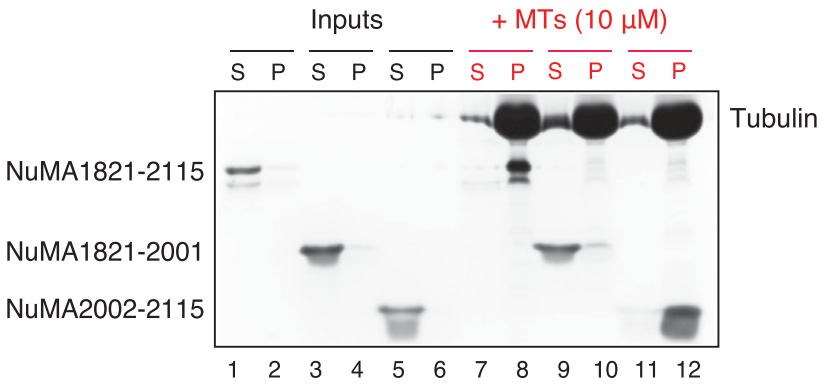

Figure 12. NuMA co-sediments simultaneously with MTs and LGN. Co-sedimentation of the NuMA C-terminal fragments (2 µM) with 9 µM MTs and 1 µM LGN^{TPR}. The supernatant (S) and pellet (P) fractions were analysed on SDS-PAGE followed by Coomassie staining. The solubility of the $NuMA^{Cter}$ fragments in the absence of MTs was tested (lanes 1-6). *From Gallini S. et al., Curr Biol, 2016* (Gallini et al. 2016).

Chang *et al.* reported that the interaction of NuMA with MTs is suppressed by steric blockage mediated by Importin-β. It binds to the N-terminal IBB (Importin-β binding) domain of the Importin-α in complex with NuMA region 1984-2010 - bearing the NLS (residues 1988-2005) – which interacts with Importin-α antiparallel helix scaffold (Chang et al. 2017) (**Figure 13**). Interestingly, the recent work by Kiyomitsu lab showed that only the cortical optogenetic targeting of NuMA fragment containing our discovered MT binding region (MTBD-1 in **Figure 11**) is able to generate pulling forces to displace the mitotic spindle (Okumura et al. 2018).

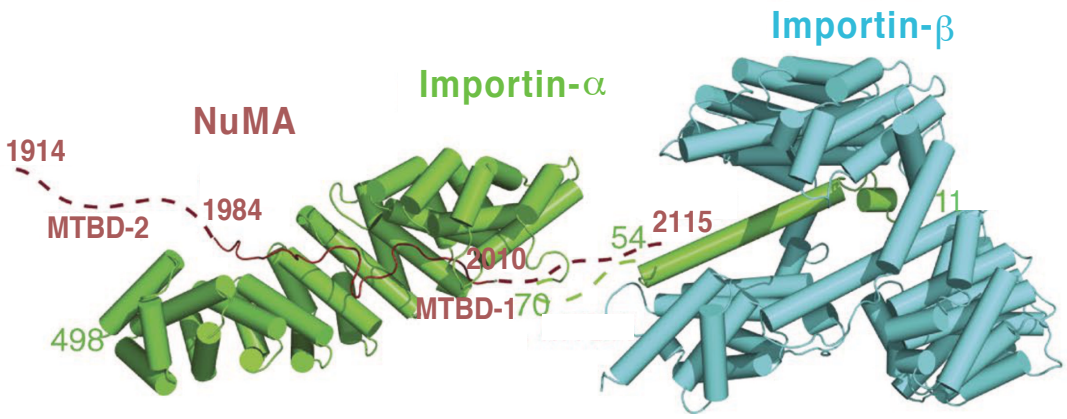

Figure 13. Importin-β regulates the C-terminal NuMA MT binding region. The MT binding region that lies C-terminal to the NLS in NuMA (aa 2010-2115; brown dotted line) is sterically blocked by Importin-β (light blue) that binds to the N-terminal IBB domain of Importin-α (green; PDB ID 1QGK). Two MT binding regions (MTBD-1/2) are indicated. *From Chang C.C., J Cell Biol., 2017* (Chang et al. 2017).

1.5.3 NuMA in interphase

During interphase NuMA localizes into the nucleus embedded into the nuclear matrix, except the nucleolar regions (Compton and Cleveland 1993). However, a recent study showed that NuMA can exist as a component of the nucleolus upon induced nucleolar stress (Jayaraman et al. 2017). In interphase, the nuclear localization of NuMA depends on importins' activity, which binds to the NLS of NuMA (encompassing residues 1988-2005) (Gueth-Hallonet, Weber, and Osborn 1996) (**Figure 13**). In the nucleus, NuMA is involved in chromatin organization and double-strand DNA breaks (DSB) repairing in response to DNA damage (Vidi et al. 2014). Recently, Moreno *et al.* demonstrated that NuMA is a negative regulator of 53BP1 (P53-binding protein 1) in DNA DSB repair. 53BP1 interaction and colocalization with NuMA decrease in response to DSB supporting mechanism whereby

NuMA sequesters 53BP1 to prevent activation of the DNA damage response in the absence of DNA damage (Moreno et al. 2019). Electron microscopy investigation revealed that NuMA forms multi-arm oligomeric structures in the nucleus, suggesting a nuclear structural role (Harborth et al. 1999). The functional role of NuMA in interphase is poorly characterized, albeit very interesting.

1.6 Aims of the project

The great progresses made over the past years revealed that the spindle orientation is a finely regulated process, and that disruption of the mechanisms governing mitotic spindle orientation, if not corrected, are associated with tissue disorganization and tumor-like proliferation (Knoblich 2010). Several cellular pathways and external stimuli have been implicated in spindle orientation. The synergic signaling between the external and internal cues converges on the evolutionary conserved pathway consisting of Gαi/LGN/NuMA/dynein complexes. We know that in metaphase, NuMA accumulates at the cortex by association with LGN, and recruits dynein/dynactin minus-end directed MT motors. LGN in turn is targeted to the plasma membrane by direct interaction with multiple copies of the Gαi subunit of heterotrimeric G proteins inserting a myristoyl group in the lipid bilayer. Biochemical and structural studies identified the minimal binding domains of the NuMA/LGN interaction, showing that the small stretch of NuMA encompassing residues 1899-1926 binds the TPR domain of LGN with nanomolar affinity. The general idea is that the cortical force-generating machinery pulls on dynamic plus-ends of astral MTs to control spindle position and orientation. However, the exact mechanisms by which astral MTs and dynein/dynactin motors are recruited and organized at the mitotic cell cortex still remains elusive.

The functional role of extracellular signals and Gαi/LGN-independent pathways in determining the division orientation in epithelial tissues have just started to emerge. Remarkably, NuMA has been implicated in most of these newly characterized pathways as it is involved in recruiting dynein at the cell cortex. The Wnt3 ligand is a morphogen that stimulates morphogenesis during developmental and homeostasis processes in adulthood, mostly by regulating stem cell proliferation and self-renewal. Interestingly, several Wnt signaling effectors such as β-catenin, adenomatous polyposis coli (APC), Axin, Dishevelled, GSK3β have been implicated as direct regulators of spindle orientation and mitotic progression, however the molecular events underlying these activities remain largely unknown.

Based on these considerations, my PhD project aimed at 1) exploring the organizational principles of the NuMA/dynein interaction and addressing the role of NuMA as a dynein/dynactin-activating adaptor; 2) characterizing the properties of the newly discovered MT binding region of NuMA (residues 2002-2115). In addition, in the last period of my PhD I focused on 3) understanding whether and how Wnt3 signaling effectors cross-talk with NuMA to drive spindle orientation in mammalian cells.

2. RESULTS: NuMA as a mitotic adaptor of dynein/dynactin

All results discussed in this chapter are presented in the article "*Organizational principles of the NuMA-dynein interaction interface and implications for mitotic spindle functions*" published in Structure on July 2020 (Renna, Rizzelli, Carminati et al. 2020).
Specifically, my contribution to this work was the following:

- GST pull-down assays with purified proteins and mitotic cell lysates with the corresponding densitometric analyses;
- cloning of pCDH-mCherry-NuMA-Δ1-705;
- protein purification of His-NuMA$^{1-705}$, GST-LIC1/2 constructs for pull-down assays, and His-GFP-Hook3 expression test;
- interpretation of the experimental results.

2.1 NuMA$^{1-705}$ directly interacts with dynein light intermediate chains

In mitotic cells, the N-terminal region of NuMA spanning residues 1-705 (**Figure 14A left**) suffices to immunoprecipitate dynein and dynactin (Kotak, Busso, and Gönczy 2012). Recent structural studies revealed that the dynein-activating adaptors can recruit different number of dyneins via direct contacts to dynein light intermediate chains (LICs hereon) (I. G. Lee et al. 2018; Olenick and Holzbaur 2019; Urnavicius et al. 2018). The mammalian LICs, encoded by two closely related gene products, LIC1 and LIC2 are involved in several different types of cargo interactions and dynein-based movements (Reck-Peterson et al. 2018). In mitosis, distinct sub-populations of LIC1 and LIC2-containing dynein/dynactin complexes are required for proper metaphase to anaphase transition acting on the Spindle Assembly Checkpoint (SAC) inactivation (Mahale, Sharma, and Mylavarapu 2016). LIC proteins consist of an N-terminal GTPase-like domain binding to dynein heavy chain (DHC) followed by a less conserved unstructured C-terminal region that associates via the α1-helix with hook domains of Hook proteins and with CC1-box of other effectors (Reck-Peterson et al. 2018) (**Figure 14A right**). Based on these evidences, to test whether human NuMA could interact directly with LIC1/2, I designed pull-down experiments with purified proteins. First, I prepared a homogeneous and purified NuMA$^{1-705}$ fragment with an N-terminal 6xHis-tag to be used as pray protein, and GST-fusion LIC1/2 fragments encompassing the full-length or the C-terminal region to be used as bait (GST-LIC1$^{1-523}$, GST-LIC1$^{390-523}$, GST-LIC2$^{1-492}$, GST-LIC2$^{379-492}$). Then, to screen the ability of the GST-LIC1/2 fragments to bind NuMA$^{1-705}$, I immobilized the GST fusion proteins on Glutathione-Sepharose (GSH) beads at 0.8

µM concentration, and incubated them with 7 µM NuMA$^{1-705}$ in solution. After washes, the species retained on beads were separated on an SDS-PAGE, and detected with immunoblotting by an anti-His antibody. Detection of binding by immunoblotting has been the key to discriminate bait proteins from NuMA$^{1-705}$ that tends to degrade. This analysis revealed that all tested LIC1 and LIC2 constructs interacted with NuMA$^{1-705}$, with full-length LIC proteins displaying higher affinity than the C-terminal portions. Moreover, the C-terminal fragment of LIC1 showed slightly higher affinity for NuMA compared with the C-terminus of LIC2 (**Figure 14B**).

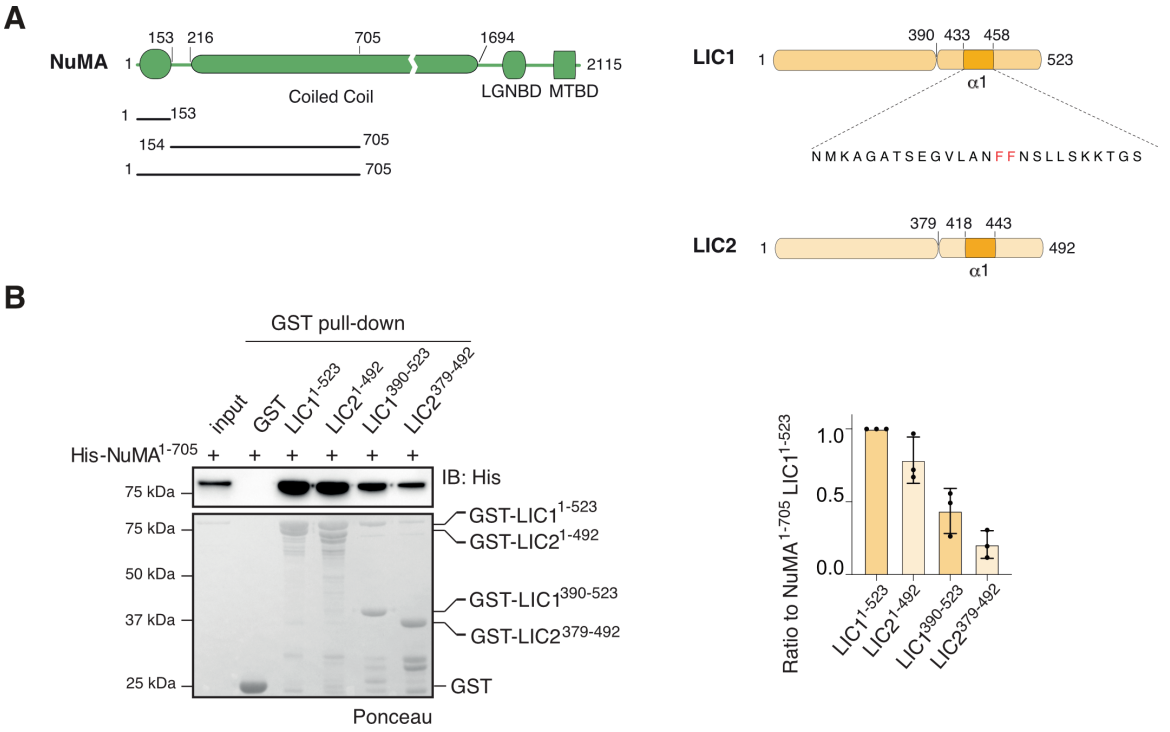

Figure 14. NuMA interacts with dynein LIC1 and LIC2. A) Schematic representation of the domain structures of human NuMA and dynein LIC1 and LIC2 isoforms. Bold lines with numbers indicate protein subdomain used in this work. The LIC1 α1 primary sequence is shown with F447 and F448 shown in red. **B) Left:** Glutathione-S-transferase (GST) pull-down experiments with GST-tagged full-length or C-terminal portion of LIC1 and LIC2 bound to glutathione resin, and His-tagged NuMA$^{1-705}$ in solution. 0.8 µM of GST-LIC constructs (GST-LIC1$^{1-523}$, GST-LIC1$^{390-523}$, GST-LIC$^{21-492}$, GST-LIC2$^{379-492}$), immobilized on glutathione beads, was incubated for 1h on ice with 7 µM of purified His-NuMA$^{1-705}$. Pull-down assays were conducted in 100 µl of pull-down buffer composed of 50 mM Tris-HCl pH 7.4, 0.1 M NaCl, 3 mM DTT, 0.1% Tween, 0.1% Triton X-100, and 0.07% Na deoxycholate. After washes, proteins bound to beads were separated by SDS-PAGE and then transferred onto a nitrocellulose membrane for 1.5 hours at 100 V for immunoblotting. Membranes were blocked with 5% milk solution in TBS and 0.1% Tween for 1 hour and incubated with an anti-His antibody at room temperature for 2 hours; 150 ng of His-NuMA$^{1-705}$ were used as input. GST

proteins used in the experiment were visualized by Ponceau staining. **Right:** ratio of bound NuMA$^{1-705}$ band intensity to NuMA$^{1-705}$/LIC1$^{1-523}$ signal. Densitometric analysis of His-NuMA$^{1-705}$ bands in the immunoblot was carried out using ImageLab (Bio-Rad Laboratories). For each band, equally-sized boxes were drawn, signal intensity was integrated, and background subtracted. The ratio of the intensity of each band to wild-type His-NuMA$^{1-705}$ from three independent experiments is presented in the right panel with SDs calculated in Prism. Mean and SD are shown for three independent experiments.

2.2 NuMA N-terminus head folds into a hook domain

2.2.1 NuMA has a monomeric head

Sequence inspection revealed that NuMA$^{1-705}$ contains a globular region comprising residues 1-153, followed by a coiled coil (**Figure 14A left**). In order to explore the interface between NuMA$^{1-705}$ and dynein, we cloned NuMA$^{1-153}$ and NuMA$^{154-705}$ into a pETM-14 vector for bacterial expression and His-tag for affinity purification. We further checked the oligomeric state of the samples. Static Light Scattering (SLS) analyses revealed that the globular domain of NuMA$^{1-153}$ is monomeric in solution (**Figure 15A**), while from residue 154 to 705 a dimeric portion starts (**Figure 15B**). Furthermore, SLS experiment showed the monodispersity of the NuMA$^{1-153}$ purified sample, which revealed the presence of a homogenous population of molecules with a molecular weight consistent with the theoretical one (**Figure 15C**). Therefore, we decided to use this N-terminal pure and monodispersed fragment of NuMA$^{1-153}$ for crystallographic studies.

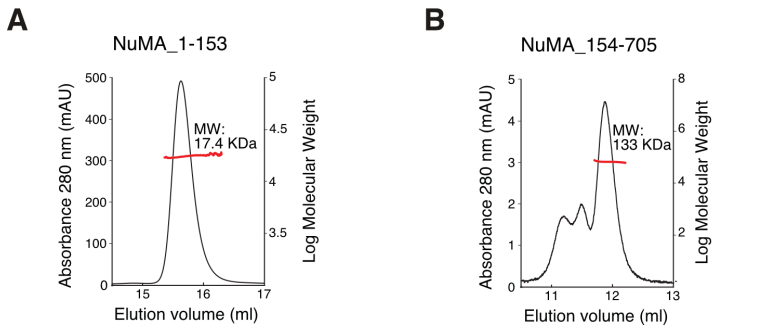

C

	Molecular Weight (KDa)		
	Theoretical monomer	Theoretical dimer	Measured (SLS)
NuMA_1-153	17.4	/	17.4
NuMA_154-705	64	128	133

Figure 15. NuMA$^{1-153}$ has a monomeric head and a dimeric coiled-coil. A) Static Light Scattering (SLS) analysis on NuMA$^{1-153}$ indicating that the sample is monodisperse and monomeric in solution. **B)** SLS analysis on NuMA$^{154-705}$ indicating that in solution the sample is polydisperse with a main dimeric population. **C)** Table comparing the theoretical molecular weight of monomeric and dimeric form of NuMA$^{1-153}$ and NuMA$^{154-705}$, and the molecular weights measured by SLS. Static-Light-Scattering (SLS) analyses of His-NuMA$^{1-153}$ and His-NuMA$^{154-705}$ were performed on a Viscotek GPCmax/TDA instrument equipped with two TSKgel G3000PWxl columns (Tosoh bioscience) in

series. The system was equilibrated in a buffer containing 10 mM Tris-HCl pH 6.8, 0.1 M NaCl, 5% glycerol for NuMA$^{1-153}$, and in a buffer containing 10 mM Hepes pH 7.5, 0.1 M NaCl, 5% glycerol for His-NuMA$^{154-705}$, and calibrated with BSA. Typically, 75 ml of purified samples concentrated at about 1.5 - 2 mg/ml were loaded on the columns.

2.2.2 NuMA$^{1-153}$ folds as a hook domain like hook-dynein/dynactin adaptors

X-ray diffraction quality crystals of NuMA$^{1-153}$ were obtained by Cristina Renna, a PhD student in the lab, and the determination of the crystal structure of NuMA$^{1-153}$ was carried out by Manuel Carminati, a postdoctoral fellow in our group, and Sebastiano Pasqualato, head of the Biochemistry Unit at IEO (see Material and Methods for crystallization and structure determination details, **paragraph 6.4**). The structure was solved by single-wavelength anomalous diffraction (SAD) method on Se-Met containing crystals, and refined to 1.5 Å resolution with a final R_{free} of 21.5% and good stereochemistry. The final model covers all the 153 residues of the construct.

The crystal structure revealed that NuMA$^{1-153}$ folds into a hook domain, a variant of the Calponin-homology (CH) domain, displaying the canonical 7 helices found in several hook family dynein/dynactin-activating adaptors, plus 2 short helices at the C-terminus (**Figures 16A** and **17C**). NuMA$^{1-153}$ differs from the hook domains of the other dynein-activating adaptors such as Hook2 and Hook3 (Dwivedi et al. 2019; I. G. Lee et al. 2018) for 2 topological features. The first one is the presence of an extra helix α9 that packs against helix α8 and inserts residues Leu147, Phe150, and Leu151 of α9 into a hydrophobic pocket formed by helices α7 and α1. This helix α9 contributes to further stabilize the core of the fold. In addition, NuMA$^{1-153}$ does not contain the two α8 helical fragments named α8a and α8b in Hook3 (**Figures 16B** and **17C**), but shows an extended flexible conformation (that we named α7-α8 loop) encompassing residues 111-117 (**Figure 17C**).

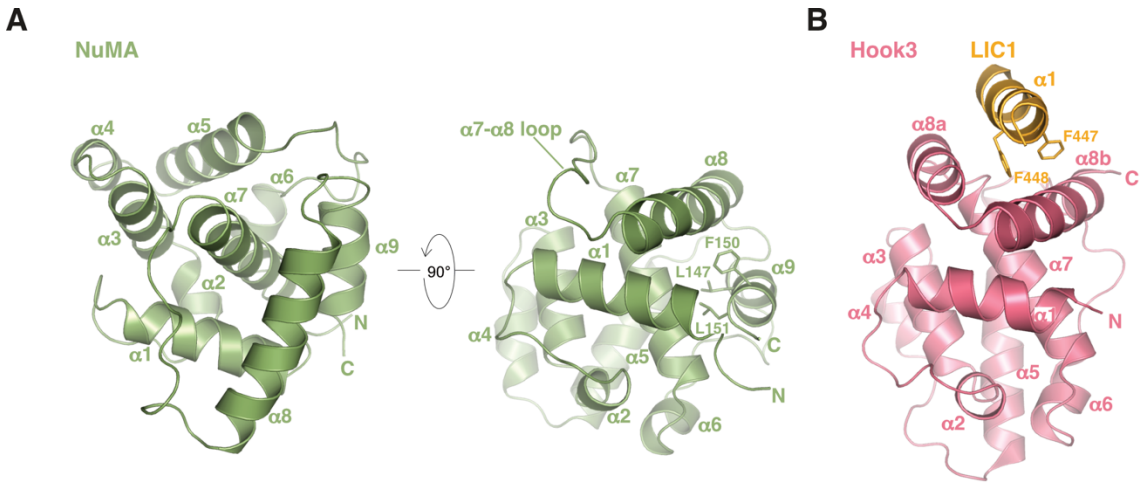

Figure 16. NuMA$^{1-153}$ folds into a hook domain. A) Cartoon representation of the crystal structure of NuMA$^{1-153}$ viewed at the indicated orientations. Hydrophobic residues stabilizing the helix α9 are shown in ball-and-sticks. **B)** Cartoon representation of the crystal structure of Hook3 in complex with LIC1 α1 (PDB: 6B9H) (I. G. Lee et al. 2018) shown as pink and gold cartoons. Hook3 is shown in the same orientation as NuMA in A on the right panel. The side chains of Phe447 and Phe448 of LIC1 α1 are shown as balls-and-sticks.

2.3 NuMA$^{1-153}$ shares with the hook adaptors the binding region for LIC

To assess whether the hook domain of NuMA is able to recognize the C-terminal region of LIC1 and LIC2, we conducted size exclusion chromatography (SEC) experiments with purified proteins. At millimolar concentration only a small fraction of NuMA$^{1-153}$ enters a complex with the LIC1 and LIC2 tails, meaning that the downstream NuMA$^{1-153}$ fragment coiled-coil region is required for full binding of LIC (data not shown (Renna et al. 2020)). Therefore, I tried to characterize biochemically the binding interface between the hook domain of NuMA and LIC1/2 chains. Structural studies on the Hook proteins showed that the helix α1 of LIC1 fits into a hydrophobic cavity of the hook domain organized by the Hook3 helices α8a and α8b, in which the conserved residues Met140^{Hook3}, Gln147^{Hook3} and Ile154^{Hook3} contact Phe447^{LIC1} and Phe448^{LIC1} (**Figure 17A**). Based on sequence alignment of the hook domain of human NuMA with Hook1, Hook2, Hook3 (**Figure 17C**) and structural evidences (**Figure 17B**) we generated NuMA$^{1-705}$ point mutants in the region encompassing the α7-α8 loop and helix α8 and tested their ability to bind LIC1 in a pull-down experiment (**Figure 17B**). I conducted this experiment with 7 μM of His-NuMA$^{1-705}$ mutants in which Arg114, Trp116, Tyr121, Gln124, Leu131, Leu135 were substituted with alanine, and GST-LIC1, GST-LIC2 full-length immobilized on GSH beads. The assay revealed that alanine substitutions on Gln124^{NuMA} and Leu131^{NuMA} abrogate binding to LIC1, as well as alanine replacement on Arg114^{NuMA} and Leu135^{NuMA}, whereas the Trp116Ala^{NuMA} and Tyr121Ala^{NuMA} mutations do not affect NuMA$^{1-705}$ binding to LIC1 (**Figure 17D**). Importantly, Gln124^{NuMA} and Leu131^{NuMA} corresponds to Gln147^{Hook3} and Ile154^{Hook3} that have been implicated in LIC1 binding in the Hook proteins. Analogous results were obtained in a pull-down experiment with GST-LIC2 adsorbed on beads (**Figure 17E**), indicating that the topology of the binding interface between NuMA and the two LIC isoforms is conserved.

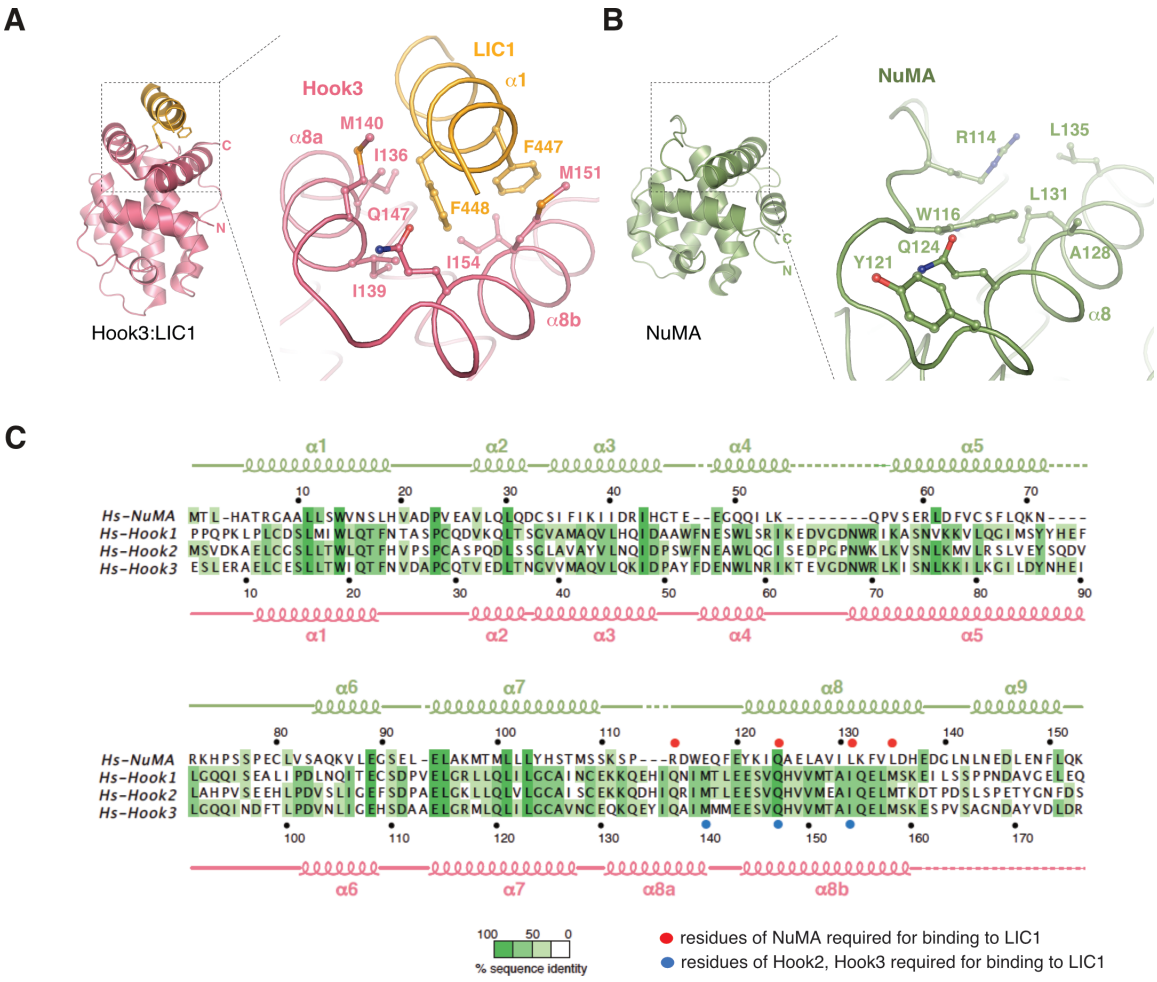
A
Hook3:LIC1
LIC1
α1
Hook3
α8a
M140
I136
Q147
I139
I154
F447
F448
M151
α8b
B
NuMA
NuMA
R114
L135
L131
W116
Q124
Y121
A128
α8
C
α1 α2 α3 α4 α5
Hs-NuMA MTL-HATRGAALLSWVNSLHVADPVEAVLQLQDCSIFIKIIDRIHGTE--EGQQILK--------QPVSERLDFVCSFLQKN----
Hs-Hook1 PPQPKLPLCDSLMIWLQTFNTASPCQDVKQLTSGVAMAQVLHQIDAAWFNESWLSRIKEDVGDNWRIKASNVKKVLQGIMSYYHEF
Hs-Hook2 MSVDKAELCGSLLTWLQTFHVPSPCASPQDLSSGLAVAYVLNQIDPSWFNEAWLQGISEDPGPNWKLKVSNLKMVLRSLVEYSQDV
Hs-Hook3 ESLERAELCESLLTWIQTFNVDAPCQTVEDLTNGVVMAQVLQKIDPAYFDENWLNRIKTEVGDNWRLKISNLKKILKGILDYNHEI
α6 α7 α8 α9
Hs-NuMA RKHPSSPECLVSAQKVLEGSEL-ELAKMTMLLLYHSTMSSKSP---RDWEQFEYKIQAELAVILKFVLDHEDGLNLNEDLENFLQK
Hs-Hook1 LGQQISEALIPDLNQTTECSDPVELGRLLQLILGCAINCEKKQEHIQNIMTLEESVQHVVMTAIQELMSKEILSSPPNDAVGELEQ
Hs-Hook2 LAHPVSEEHLPDVSLIGEFSDPAELGKLLQLVLGCAISCEKKQDHIQRIMTLEESVQHVVMEAIQELMTKDTPDSLSPETYGNFDS
Hs-Hook3 LGQQINDFTLPDVNLIGEHSDAAELGRMLQLILGCAVNCEQKQEYIQAIMMMEESVQHVVMTAIQELMSKESPVSAGNDAYVDLDR
α6 α7 α8a α8b
100 50 0
% sequence identity
residues of NuMA required for binding to LIC1
residues of Hook2, Hook3 required for binding to LIC1
D
GST pull-down
WT WT R114A W116A Y121A Q124A L131A L135A
His-NuMA1-705
IB: His
75 kDa
GST-LIC11-523
GST
Ponceau
inputs
His-NuMA1-705
IB: His
WT R114A W116A Y121A Q124A L131A L135A
Ratio to WT NuMA
1.0
0.5
0.0
WT R114A W116A Y121A Q124A L131A L135A
E
GST pull-down
WT WT R114A W116A Y121A Q124A L131A L135A
NuMA1-705
IB: His
75 kDa
GST-LIC21-492
GST
Ponceau

Figure 17. The hook domain of NuMA interacts with LIC1 and LIC2 dynein isoforms. A) Close-up view of the Hook3/LIC1-α1 complex, with balls-and-sticks representation of the residues at the binding interface. **B)** Close-up view of the α7-α8 loop and helix α8 of NuMA in the same orientation of Hook3 in panel A, with balls-and-sticks representation of the residues mutated in the pull-down experiments of followed panels D and E. **C)** Structure-based sequence alignment of the hook domain of NuMA and Hook proteins. Residues are coloured by percentage of sequence identity according to the alignment of different orthologues of NuMA, Hook1, Hook2 and Hook3. Red and blue circles indicate residues of NuMA, Hook2 and Hook3 required for LIC1 binding. **D) Left:** Pull-down assay with 0.8 μM of GST-LIC1$^{1-523}$ on glutathione resin, and 7 μM of His-NuMA$^{1-705}$ wild-type or carrying the mutations R114A, W116A, Y121A, Q124A, L131A, L135A in solution. Pull-down assays were performed in 100 μl of pull-down buffer consisting of 50 mM Tris-HCl pH 7.4, 0.1 M NaCl, 3 mM DTT, 0.1% Tween, 0.1% Triton X-100, and 0.07% Na deoxycholate. Proteins retained on beads were visualized by immunoblotting using anti-His antibody. Input proteins were analyzed by immunoblotting, and GST proteins on beads by Ponceau staining. **Right:** ratio of NuMA$^{1-705}$ mutants band intensity to wild-type NuMA$^{1-705}$ (WT) signal. Densitometric analyses of wild-type and mutants His-NuMA$^{1-705}$ bands in the immunoblots were carried out using ImageLab (Bio-Rad Laboratories). For each band, equally-sized boxes were drawn, signal intensity was integrated, and background subtracted. The ratio of the intensity of each band to wild-type His-NuMA$^{1-705}$ from three independent experiments is presented with SDs calculated in Prism. Mean and SD are shown for three independent experiments. **E)** The same GST pull-down assay shown in panel D was performed on LIC2 isoform.

2.4 The coiled-coil of NuMA contributes to the NuMA/LIC interaction

2.4.1 A motif into the coiled-coil of NuMA is homologous to the CC1-box

The evidences provided so far made us consider that the hook domain of NuMA does not fully recapitulate the NuMA interaction with LIC1 and LIC2, and that NuMA$^{1-705}$ could harbour additional LIC-interaction motifs. As previously mentioned (described in **paragraph 1.1.3**), dynein-activating adaptors show at least three different types of binding sites for LIC chains: the hook domain, the CC1-boxes, and pairs of EF hands (Olenick and Holzbaur 2019; Reck-Peterson et al. 2018). Sequence alignments analyses excluded the presence of EF-hand domains within NuMA$^{1-705}$ fragment, but showed the existence of a conserved motif spanning residues 360-385 in the coiled-coil region (**Figure 18A**). Interestingly, CC1-box-containing effectors share the consensus sequence (D/E)-x-x-x-A-A-x-x-G-x-x-(L/V)-(L/V), that aligns with the conserved region found within the NuMA coiled-coil encompassing residues 360-385, that we refer to as *CC1-box-like* motif hereon (**Figure 18B**). The *CC1-box-like* motif does not entirely conform to the A-A-x-x-G

consensus sequence as the alanine couple A368-A369^{NuMA} is out of frame of one residue and the Gly is entirely missing.

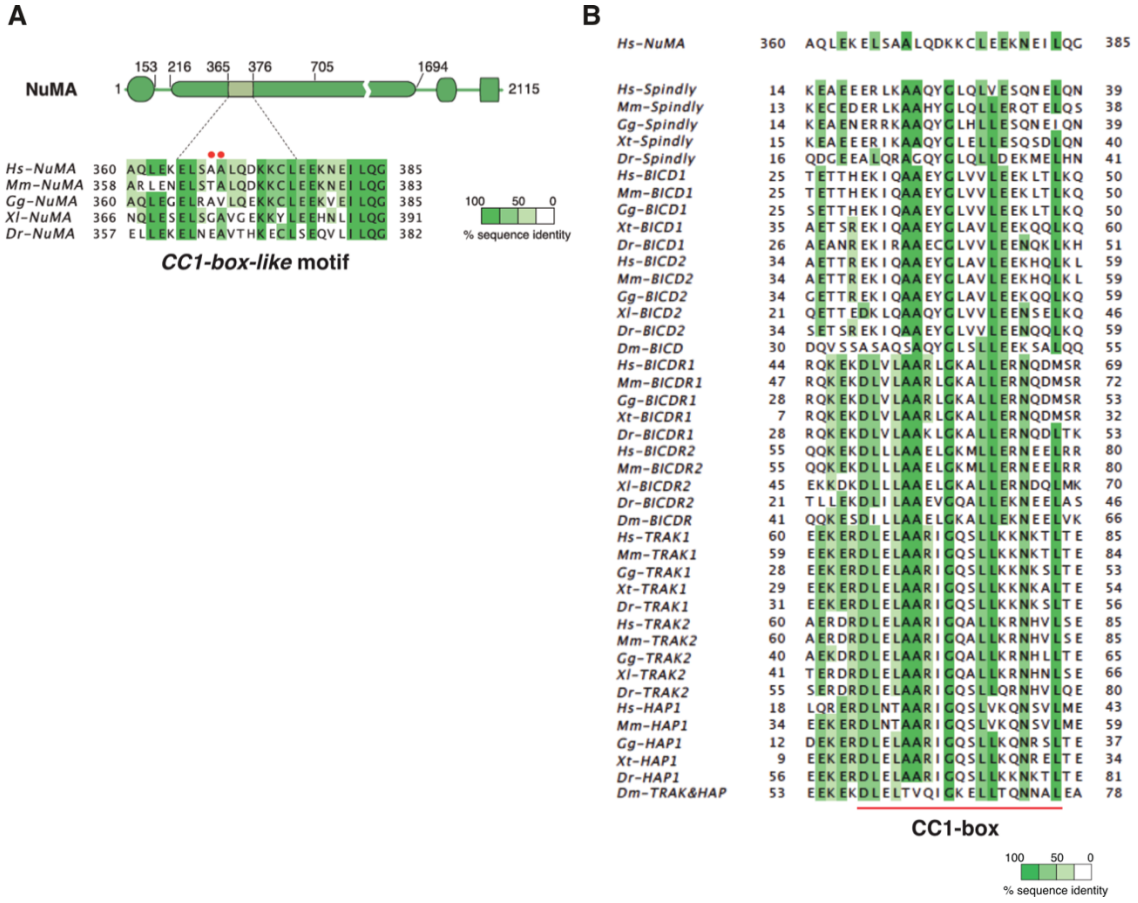

Figure 18. NuMA contains a CC1-box-like motif. A) Sequence alignment of NuMA orthologues, showing the CC1-box-like motif at residues 360-385 of the coiled-coil region of NuMA. Residues are coloured by percentage of sequence identity with Ala-368 and Ala-369 of human NuMA marked with red circles. **B)** Sequence alignment between the N-terminal region of human NuMA from 360 to 385 residues and different orthologues of known CC1-box containing dynein adaptors; *Hs: Homo sapiens, Mm: Mus musculus, Gg: Gallus gallus, Xt: Xenopus Tropicalis, Xl: Xenopus laevis, Dr: Danio rerio, Dm: Drosophila melanogaster.*

2.4.2 The *CC1-box-like* motif in the NuMA coiled-coil interacts with LIC

To check whether the analyzed motif in the NuMA coiled-coil is implicated in LIC recognition, I tested by pull-down assay the binding ability of the NuMA$^{1-705}$-A368V/A369V double mutant (**Figure 19**). The NuMA double mutation was designed in line with what done for the other CC1-box-containing dynein-activating adaptors, that have been shown to loose binding to LIC chains upon replacement of the alanine couple of the motif with valines (Gama et al. 2017; Schlager et al. 2014) (**Figure 18B**). In GST pull-down assay NuMA$^{1-705}$-

A368V/A369V shows only residual binding to LIC1 (**Figure 19A**) and LIC2 (**Figure 19B**). Nonetheless, observing the sequence alignment of NuMA orthologs (**Figure 18A**), we realized that only the alanine 369 of the human NuMA *CC1-box-like* motif is conserved within species. To test if the *CC1-box-like* motif identified works as conserved interface between NUMA and LIC1/2, I performed GST-LIC1 pull-down experiments with mitotic lysates from murine MC38 cells, in which a single alanine $A369^{NuMA}$ is present (**Figure 18A**), and compared the results with lysates of human HEK293T cells. Both murine and human endogenous NuMA associate with purified human LIC1 (**Figure 19C**). The experiment highlighted that $A369^{NuMA}$ is essential for the NuMA/LIC binding, which it is conserved throughout species.

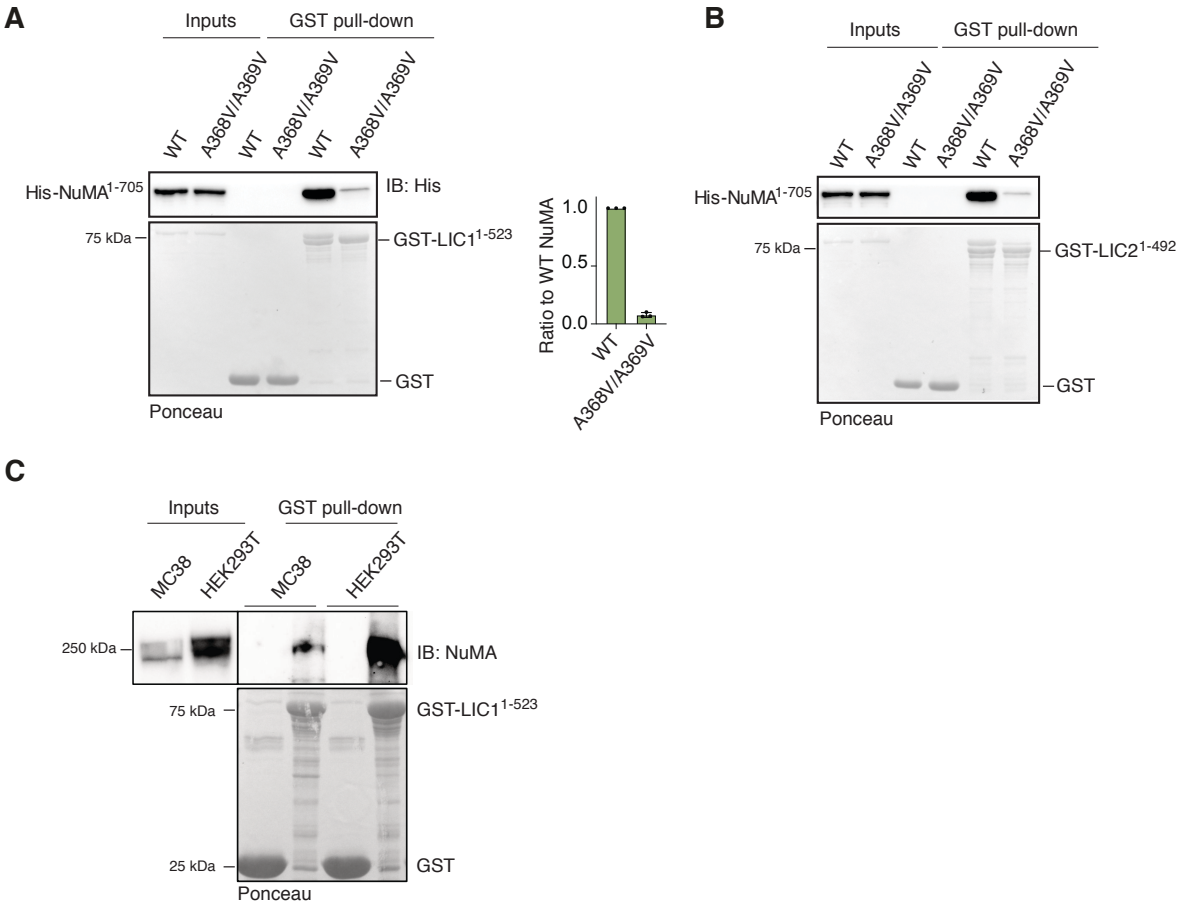

Figure 19. Characterization of the binding of the *CC1-box-like* motif of NuMA to LIC1/2. A) Left: Pull-down assay with GST-$LIC1^{1-523}$ on glutathione resin, and purified His-$NuMA^{1-705}$ wild-type or carrying the Ala368Val/Ala369Val mutation in solution. Proteins retained on beads and input proteins were analyzed by immunoblotting using anti-His antibody. GST proteins used in the experiment were visualized by Ponceau staining. **Right:** Ratio of band intensity to the wild-type $NuMA^{1-705}$ signal. Mean and SD are shown for three independent experiments. GST pull-down assays with purified proteins and densitometric analyses were performed as in **Figure 14** and **Figure**

17. **B)** The same GST pull-down assay shown in panel A performed with the GST-LIC2 isoform. **C)** GST-LIC1 full-length adsorbed on GSH resin was incubated with MC38 or HEK293T mitotic lysates. The pull-down assay was performed with extracts of murine MC38 and human HEK293T cells treated with 0.33 mM nocodazole (Sigma Aldrich) for 16 h to enrich the population of prometaphase cells. After harvesting, cells were lysed by sonication in 50 mM Hepes pH 7.5, 50 mM NaCl, 1.5 mM EDTA, 1.5 mM $MgCl_2$, 1mM DTT, 10% glycerol, 0.01% Tween20, protease (Calbiochem) and phosphatase inhibitors (Sigma), and cleared by centrifugation. 1 mg of extracts (at about 10 mg/ml for MC38 cells, and 5 mg/ml for HEK293T cells) was incubated with 2 μM GST-LIC1 immobilized on glutathione beads for 2 hours at 4 °C, with gentle agitation on wheel. Beads were washed 3 times with 0.5 ml lysis buffer, and species retained on beads were analyzed by SDS-PAGE and blotted with mouse anti-NuMA antibody (Mapelli lab). The blot on the left shows the NuMA expression levels in the two cell lines: 20 μg of MC38 and HEK293T mitotic lysates were loaded as input.

2.5 Both the hook domain and the *CC1-box-like* motif of NuMA contact the α1 helix of LIC1

LIC1 has been shown to contact dynein-activating adaptors via a C-terminal α1-helix coding for two conserved phenylalanines, Phe447 and Phe448 (Reck-Peterson et al. 2018). Thus, to assess whether NuMA interacts with LIC chains similarly to other dynein-activating adaptors, I performed pull-down experiments between $NuMA^{1-705}$ and the double mutant LIC1-F447A/F448A on GSH beads. In these experiments I also tested the $NuMA^{1-705}$-L131A hook domain mutant and $NuMA^{1-705}$-A386V/A387V double mutant that are impaired in LIC binding (**Figure 20**). Pull-down experiments showed that GST-LIC1-F447A/F448A is totally impaired in NuMA binding, indicating that both the hook domain and the *CC1-box-like* motif are implicated in contacting LIC1 α1. In summary, these findings suggest that NuMA interacts with dynein LIC1/2 via double binding interface comprising the hook domain and the coiled-coil region.

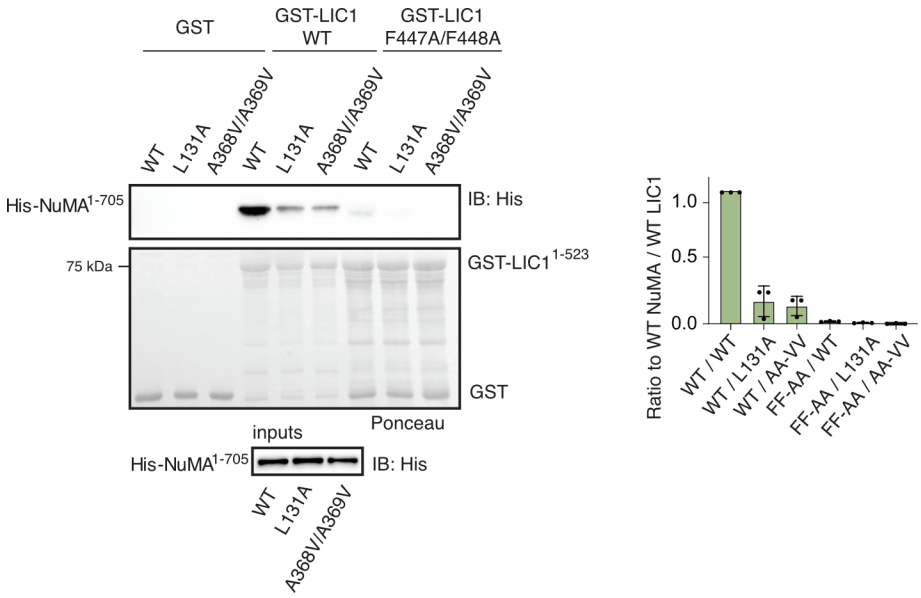

Figure 20. NuMA contains two binding interfaces for LIC1 α1. Left: Pull-down assay with 0.8 μM of GST-LIC1$^{1-523}$ wild-type or carrying the F447A/F448A mutation on beads, and 7 μM of purified His-NuMA$^{1-705}$ wild-type, or L131A, or A368V/A369V in solution. Proteins bound to beads were visualized by immunoblotting using anti-His antibody. GST proteins on beads were monitored by Ponceau staining, equal amounts of prey proteins were analyzed by immunoblotting. **Right:** Ratio of band intensity to the signal of binding between wild-type NuMA$^{1-705}$ and wild-type LIC1$^{1-523}$ (WT/WT). Mean and SD are shown for three independent experiments. GST pull-down assays with purified proteins and relative densitometric analysis were performed as in **Figure 14** and **Figure 17**.

We could not reconstitute the NuMA/LIC complex in solution at millimolar concentrations (data not shown (Renna et al. 2020)), due to the aggregation-prone behaviour of NuMA$^{1-705}$ that tends to aggregate above at 0.3 mM concentration. The evidence that the NuMA/LIC interaction cannot be reconstitute in SEC at millimolar concentrations suggests that the affinity of NuMA for LICs is substantially lower than the one measured between LIC1 and Hook3, whose K_D is about 12 μM (I. G. Lee et al. 2018). To verify this hypothesis, I conducted parallel pull-down experiments with GST-LIC1 adsorbed on GSH beads and increasing concentration of NuMA$^{1-705}$ or Hook3$^{1-552}$, a Hook3 fragment containing the hook domain followed by a segment of coiled-coil (**Figure 21A**). Importantly, we realized that His-NuMA and His-Hook3 are not recognized in the same manner by the anti-His antibody (**Figure 21B**). Thus, I decided to monitor the binding by Coomassie staining of 8% SDS-PAGE. This analysis revealed that Hook3 binds to LIC already at 1 μM concentration of the pray protein in solution, whereas 7 μM concentration of NuMA$^{1-705}$ are required to detect binding to LIC1 on the beads (**Figure 21C**).

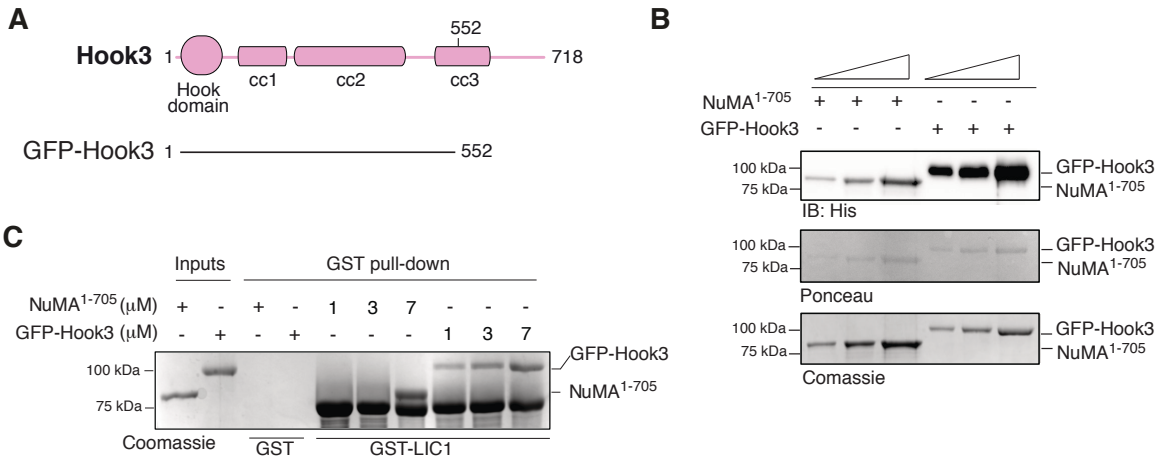

Figure 21. NuMA and Hook3 have a different binding affinity for LIC1. A) Schematic representation of Hook3 domain structures. The line with numbers indicates the protein subdomain used in the PD experiments of followed panels. **B)** Anti-His immunoblotting of increasing amount of GFP- Hook3$^{1-552}$ and NuMA$^{1-705}$. Ponceau staining and Coomassie staining detect the presence of the same amount of both proteins. **C)** Comparative analysis of NuMA$^{1-705}$ and Hook3 binding to LIC1. The pull-down experiment was performed with 0.8 μM of GST-LIC1 full-length, immobilized on glutathione beads, that were incubated with 1 μM, 3 μM or 7 μM of purified His-NuMA$^{1-705}$ or GFP-Hook3$^{1-552}$, similarly to what described for NuMA/LIC *in vitro* assay (**Figure 14** and **Figure 17**). After washes, proteins retained on beads were separated by SDS-PAGE and visualized by Coomassie staining.

2.6 Both NuMA/LIC binding interfaces are required for mitotic spindle orientation

Recently, Kiyomitsu *et al.* demonstrate that optogenetic targeting of NuMA to the mitotic cell cortex recruits and activates dynein to generate cortical pulling forces positioning the spindle (Okumura et al. 2018). We then set out to test whether both NuMA/LIC binding interfaces are relevant to recruit dynein/dynactin to the cell cortex to position the spindle. To address this issue, Chiara Gaddoni and Laura Pirovano in the lab cloned mCherry-NuMA truncation mutants devoid of the entire N-terminal portion (NuMA-Δ1-705) or of the individual LIC-binding domains (NuMA-Δ1-153 and NuMA-Δ154-705), and expressed these constructs in a HeLa cell line stably interfered for endogenous NuMA by short-hairpin RNA (shNuMA) (**Figure 22A**). Our aim was to test whether N-terminal NuMA mutants could rescue spindle orientation defects observed in HeLa cells lacking endogenous NuMA. It is know that NuMA depletion causes abnormal spindle morphology, multipolar mitoses, and chromosome congression errors (Hueschen et al. 2017). Thus, to assess only the spindle orientation functions of the NuMA truncation mutants, we analysed a subpopulation of

shNuMA HeLa cells that could assemble a bipolar spindle and properly congress chromosomes. For spindle orientation analyses, these HeLa cells were grown on fibronectin-coated coverslides, synchronized in metaphase by single thymidine block, and imaged in the x-z plane by confocal microscopy. Under these conditions, wild-type HeLa cells divide with the spindle aligned to the substratum (α-angle), whereas cells with compromised orientation mechanisms undergo oblique divisions. Quantifications of the metaphase spindle angle revealed that cells lacking NuMA undergo misoriented divisions that are rescued by full-length NuMA but not by NuMA/LIC binding interfaces truncation mutants (**Figures 22B** and **22C**). Notably, the point mutant NuMA-A368V/A369V restored spindle alignment to the substrate almost to the same extent of wild-type NuMA, suggesting that, in this kind of assay, the disruption of the CC1-box like is tolerated within the NuMA/dynein/dynactin complex. These results indicate that in HeLa cells the interaction of NuMA with dynein LIC mediates proper spindle positioning and orientation.

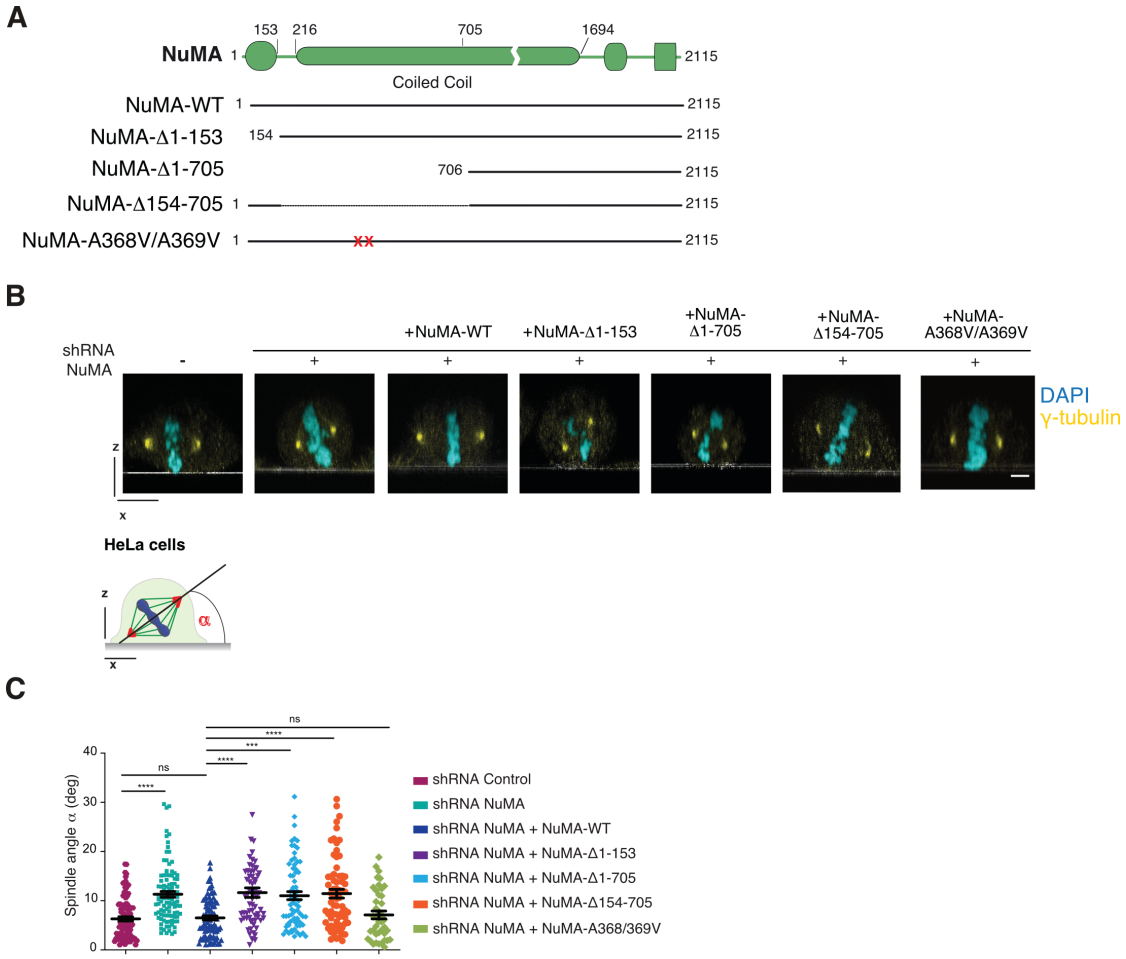

Figure 22. Analysis of spindle orientation in HeLa cells expressing NuMA/LIC binding interfaces mutants. A) Schematic representation of NuMA truncation mutants devoid of the entire N-terminus or the individual LIC-binding interface. **B)** Confocal sections of metaphase HeLa cells

transiently expressing a control shRNA, or stably depleted of endogenous NuMA and expressing mCherry-tagged NuMA-WT, NuMA-Δ1-153, NuMA-Δ1-705, NuMA-Δ154-705, or NuMA-A368V/A369V. Cells were stained with γ-tubulin (yellow) to visualize the poles, and with DAPI (blue) to show DNA. The white line represents the plane of the coverslip. Specifically, HeLa cells were plated on 13 mm coverslips coated with 5 μg/ml fibronectin and pre-synchronized with a single thymidine block/release. Cells were treated with thymidine (2.5 mM, Sigma T1895) for 24 hours, and then fixed 8 hours after the release. To visualize γ-tubulin, cells were fixed with 4% paraformaldehyde (PFA) for 10 minutes at room temperature, followed by permeabilization with 0.3% Triton X-100 in PBS for 5 minutes. Blocking was performed with 3% BSA in PBS for 1 hour at room temperature. Cells were stained with anti-γ-tubulin mouse (1:100, Abcam, ab11316) antibody in 3% BSA + 0.05% Tween-20, followed by incubation with anti-mouse AlexaFluor 647 (1:300, Jackson ImmunoResearch). DNA was stained with DAPI. Confocal images were acquired on a Leica SP8 confocal microscope controlled by Leica confocal software. For HeLa cells analysis, a 63X oil-immersion objective lens (HC PL APO 63X/1.40 OIL CS2) was used. All images were processed using the software Fiji. Notably, quantification of the orientation was performed by measuring the angle formed by a line passing through the spindle poles and the coverslip, as depicted in the scheme at the bottom left. Cells were imaged in x-z optical sections passing through the spindle poles, and the spindle angle was measured exploiting the angle tool of the software Fiji. **C)** Dot-plot showing the spindle axis angles distribution of HeLa cells imaged in panel B. Means ± SEM are shown for three independent experiments, with $n > 40$. Statistical analysis of the data was performed in Prism, the Kruskal-Wallis test was applied. **** indicates $p < 0.0001$; *** indicates $p < 0.001$; ns, not significant.

3. RESULTS: Cell cortex molecular contribution of NuMA to mitotic spindle orientation

Part of my PhD project was dedicated to the characterization of the NuMA/LGN oligomers, and the MT binding activity of NuMA, as described in the following paragraphs. Much of these experimental results are presented in the manuscript "*Hexameric NuMA:LGN structures promote multivalent interactions required for planar epithelial divisions*" published in Nature Communications on June 2019 (Pirovano et al. 2019).
Specifically, my contribution to the results discussed within this chapter was the following:

- immunoprecipitation experiments with mitotic HEK293T lysates;
- analytical SEC experiments of NuMA$^{2002-2115}$ or NuMA$^{1970-2089}$ and tubulin;
- MT co-sedimentation assays with several C-terminal fragments of NuMA;
- MT and tubulin Subtilisin-treatment for analytical SEC and MT co-sedimentation assays;
- protein crystallization experiments with NuMA/tubulin/DARPin1 complexes;
- plasmid generation (pETM14-His-NuMA$^{1970-2089}$, pETM14-His-DARPin1, pEGFP-GFP-LGN-WT/ΔOLIGO);
- protein purification (His-NuMA$^{1821-2115}$, His-NuMA$^{2002-2115}$, His-NuMA$^{1970-2089}$, His-DARPin1, Ndc80^{Bonsai});
- interpretation of the experimental results.

3.1 NuMA and LGN form oligomers in cells

3.1.1 NuMA/LGN oligomerization is required for orientation in HeLa cells

Biochemical studies conducted in our lab revealed that the portion of NuMA encompassing residues 1861-1928 (NuMA-LGN-Binding-Domain, NuMA^{LGNBD} hereon) and a longer TPR region of LGN spanning residue 1-409 (LGN^{TPR} hereon) are the minimal binding fragments required for high-order oligomers formation (**Figures 23A** and **23B**).
Simone Culurgioni from our lab with the help of Sebastiano Pasqualato determined the crystal structural of NuMA^{LGNBD} with LGN^{TPR}, revealing a hetero-hexameric arrangement with NuMA/LGN 3:3 complexes (**Figure 23C**). These complexes arrange in a donut-shaped architecture, whose backbone is formed by three TPR domains of LGN interacting in a head-to-tail manner, forming a central triangular cavity. In the donut, the interface between the C-terminal stretch of the NuMA^{LGNBD}, spanning residues 1900-1928, and LGN^{TPR} is identical to the one observed in the crystal structure of the 1:1 complex between the NuMA$^{1899-1926}$

and LGN^{TPR} (J. Zhu et al. 2011) (for more details see **paragraph 1.4.1)**, with the NuMA chain filling the groove formed by the TPR repeats of LGN. The additional flexible N-terminal stretch spanning residues 1861-1899 present in $NuMA^{LGNBD}$ interacts with the two adjacent LGN molecules.

Several approaches we used to assess whether LGN/NuMA hetero-hexamers exist in cells and their relevance for mitotic spindle orientation mechanisms. Laura Pirovano set spindle orientation assays in HeLa cells depleted of endogenous LGN and expressing a construct oligomerization deficient. Based on biochemical experiments, LGN^{1-350} and LGN^{13-409} fragments are unable to form oligomers in complex with NuMA (Pirovano et al. 2019). Therefore, from biochemical and structural evidences, Laura generated an LGN mutant depleted of the N-terminal region, encompassing residues 1-12, and the region downstream the TPR repeat (corresponding to the C-terminal helix of the TPR domain), encompassing residues 350-366, and then she expressed these constructs in a HeLa cell lines stably interfered for endogenous LGN (**Figure 23D**). This mutant, hereon referred as LGN-ΔOLIGO, retains the ability to bind NuMA with 1:1 stoichiometry because it contains a proficient TPR domain, but cannot oligomerize. This analysis confirmed that HeLa cells expressing the control shRNA divide by with the spindle parallel to the substratum, with a mean spindle angle of 5˚. In line with known literature, knockdown of LGN misorients the spindle to about 13˚. Expression of LGN-WT fully rescued the correct orientation, while expression of LGN-ΔOLIGO did not, with cells dividing with a mean angle of 13˚. These results highlighted that NuMA/LGN oligomerization is required to orient the mitotic spindle in HeLa cells.

Details about NuMA/LGN oligomerization biochemical and structural investigation, and the cell culture experiments were reported in published paper "*Hexameric NuMA:LGN structures promote multivalent interactions required for planar epithelial divisions*" (Pirovano et al., *Nat Commun*, 2019).

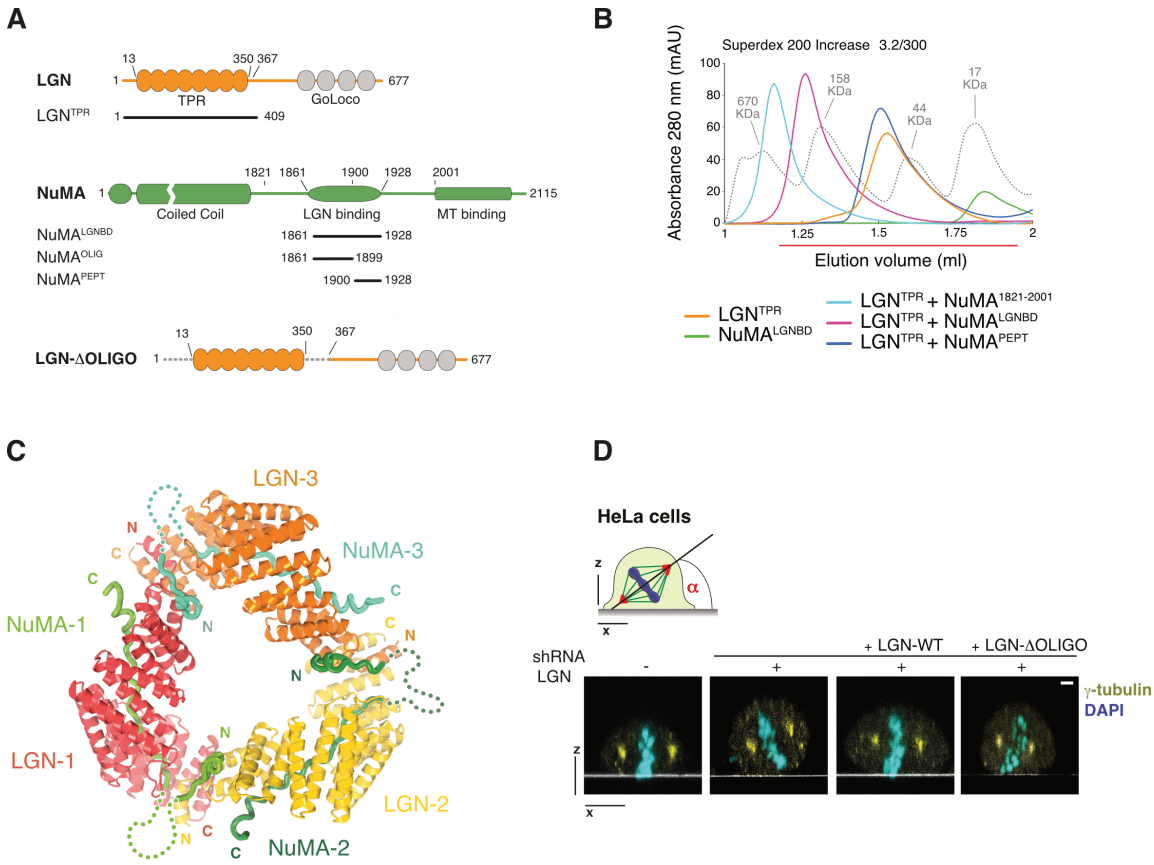

Figure 23. The hetero-hexameric LGN/NuMA complexes are required for spindle orientation in HeLa cells. A) Schematic representation of LGN and NuMA domain structures. Bold lines below the cartoons indicate proteins fragment used for the *in vitro* assay of figure B. LGN-ΔOLIGO is the construct used for the spindle orientation analysis shown in D. **B)** SEC elution profile of LGN^{TPR} (20 μM) in complex with $NuMA^{1821-2001}$ (20 μM, cyan), $NuMA^{LGNBD}$ (20 μM, purple) or $NuMA^{PEPT}$ (40 μM, blue). The elution profile of globular markers is reported in a dashed gray line. Notably, the early elution volume of $LGN^{TPR}/NuMA^{LGNBD}$ indicates that they form higher molecular weight species compared with the 1:1 stoichiometry of $LGN^{TPR}/NuMA^{PEPT}$. **C)** Cartoon model of the oligomer assembly. The first helix of one LGN^{TPR} molecule hooks on the last TPR repeat of an adjacent LGN^{TPR} domain, while the NuMA chains lines in the inner surface to the TPR domains and between them in an overall donut-like architecture. **D) Upper:** Cartoon depicting a metaphase HeLa cell. The spindle angle "α" is the angle formed by a line passing through the spindle poles (red) and the substratum. **Bottom:** Confocal x-z sections of HeLa cells depleted of endogenous LGN and expressing LGN-WT-mCherry or LGN-ΔOLIGO-mCherry. Cells were stained with γ-tubulin to visualize the spindle poles (yellow), and with DAPI to visualize the metaphase plate (cyan). The substratum is visible as a white line. *From Pirovano L. et al., Nat Commun, 2019* (Pirovano et al. 2019).

3.1.2 NuMA and LGN engage into high-order oligomers in cells

Another strategy to understand the existence of NuMA/LGN oligomers in cells has seen my direct contribution to this project. In particular, I set up a co-immuprecipitation experiment in HEK293T cells in which I used GFP-tagged LGN as the bait that binds α-GFP antibody conjugated to agarose beads (MBL) and FLAG-tagged LGN to check the co-immunoprecipitated interactors. The idea was to check whether two differently-tagged LGN molecules could be part of the same complex in mitotic cells. Because based on the structural and biochemical data the LGN/LGN interaction requires NuMA, we expected to find among the GFP-LGN interactors NuMA and FLAG-LGN, meaning that LGN/NuMA complexes with multiple copies of LGN assemble in cells. As negative control for this co-IP experiment we planned to co-transfect LGN-ΔOLIGO with GFP and with FLAG tags. In this case, we expected to IP GFP-LGN-ΔOLIGO and find only NuMA among the co-immunoprecipitated molecules, because of the binary interaction between NuMA and LGN is preserved even in absence of NuMA/LGN oligomerization. At the same time, we reasoned that the presence of endogenous NuMA, containing a long coiled-coil region which induces the self-dimerization (as shown by SLS analysis of $NuMA^{154-705}$, **Figure 15**), could promote interaction between LGN molecules regardless of the hexamer formation. As a consequence, even in the absence of NuMA/LGN oligomerization, we could see a second molecule of LGN in the co-immunoprecipitations. To overcome this problem, we generated a 293T cell line depleted of endogenous NuMA by expression of a shRNA against NuMA, and stably expressing the monomeric C-terminal portion of NuMA downstream of the coiled-coil, encompassing residues 1821-2115 and the LGNBD. Western blot analysis confirmed that the C-terminal NuMA construct was expressed in 293T cell depleted of the endogenous protein (**Figure 24A**). The GFP-IP experiments conducted in mitotic HEK293T lysates overexpressing GFP-LGN and FLAG-LGN revealed that only wild-type GFP-LGN co-immunoprecipitates wild-type FLAG-LGN with $NuMA^{1821-2115}$. Conversely, GFP-LGN-ΔOLIGO co-IPs only $NuMA^{1821-2115}$, and in lower amount compared to the wild-type protein (**Figure 24B**). These results fully support the notion that NuMA and LGN can assemble high-order oligomers in cells, and that mutations affecting the NuMA/LGN oligomer formation in vitro also impairs the oligomerization in cells. Moreover, this evidence suggests that NuMA/LGN oligomerization occurs independently of NuMA self-assembly, and that the hetero-hexamers we characterized *in vitro* are the key event in multivalent NuMA/LGN interactions in mitosis.

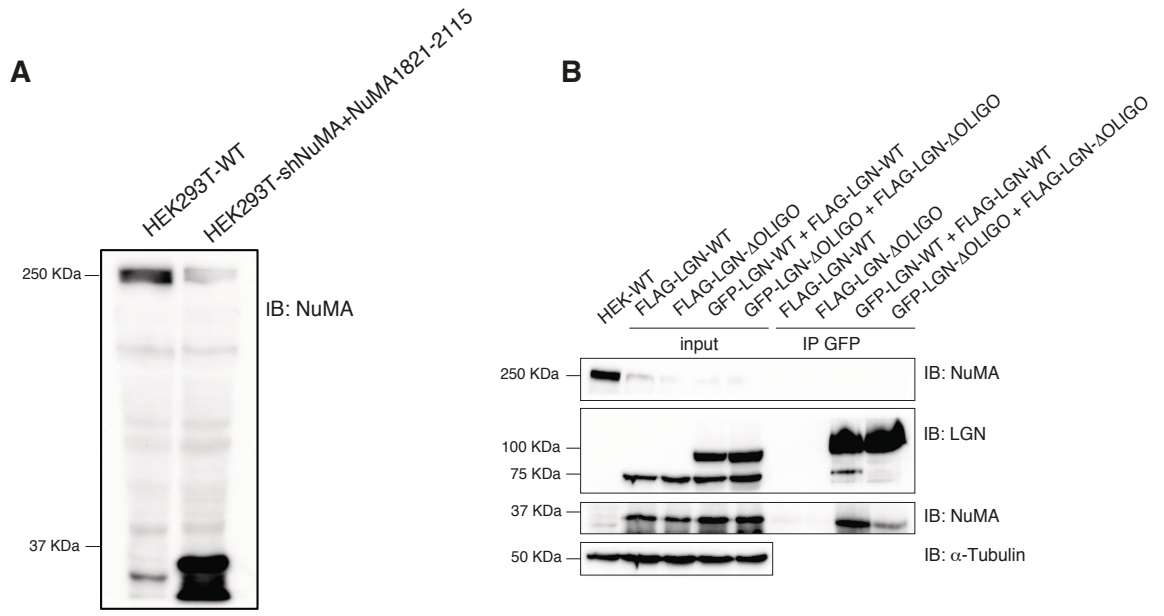

Figure 24. NuMA/LGN form high-order oligomers in mitotic cells. A) Western blot of mitotic lysates of HEK293T cell line stably depleted of endogenous NuMA and expressing NuMA$^{1821-2115}$. Primary antibody incubation was performed at room temperature for 2 hours with the following dilutions: mouse anti-NuMA (1:200, Mapelli lab), mouse anti-α-tubulin (1:600, Abcam, ab4074). **B)** GFP-immunoprecipitation of mitotic lysates of HEK293T cell line stably depleted of endogenous NuMA and co-transfected with 0.25 μg pEGFP-LGN-WT and 10 μg pCDH-LGN-WT-3xFLAG or 0.25 μg pEGFP-LGN-ΔOLIGO and 10 μg pCDH-LGN-ΔOLIGO-3xFLAG. Cells transfected with 5 μg pCDH-LGN-WT-3xFLAG or 5 μg pCDH-LGN-ΔOLIGO-3xFLAG were used as specificity control for the GFP-IPs, and wild-type cells were loaded to monitor NuMA depletion and NuMA$^{1821-2115}$ expression (IB anti-NuMA at 250 KDa for the endogenous protein and 37 KDa for NuMA C-terminal construct). α-tubulin was used as loading control for the inputs. Transfections of HEK293T cells were performed using Calcium Phosphate. In particular, two expression vectors have been mixed with 61 μl $CaCl_2$ and water, and then added to a bubbling solution of HBS (Hank's Buffered Saline, 50 mM HEPES, 280 mM NaCl, 1.5 mM Na_2HPO_4). The transfection mix was added to fresh medium after ten minutes incubation. 24 hours post-transfection cells were synchronized with 0.33 mM nocodazole (Sigma Aldrich) treatment for 16 hours before harvesting. Mitotic cells were lysed on ice in lysis buffer containing 75 mM Hepes pH 7.5, 1.5 mM, EGTA, 1.5 mM $MgCl_2$, 150 mM KCl, 0.1% NP40 and 15% glycerol and protease inhibitors, with 30 minutes 11,000 g. 300 μg of cleared lysates were incubated with 10 μl α-GFP antibody conjugated to agarose beads (MBL) for 2 hours at 4 °C, with gentle agitation on the wheel. After supernatant removal, beads were washed 4 times with 1ml lysis buffer, and Laemmli sample buffer was added to the beads. Input and IP samples were resolved by SDS-electrophoresis and transferred onto a nitrocellulose membrane for 18 hours at 30 V, 4 °C for immunoblotting. Membranes were blocked with 5% milk solution in TBS and 0.1% Tween for 1 hour and incubated at room temperature for 2 hours with mouse anti-LGN, mouse anti-NuMA, mouse anti-α-tubulin, mouse anti-FLAG.

3.2 The microtubules binding activity of NuMA

3.2.1 NuMA$^{2002-2115}$ binds soluble tubulin dimers

Previous work from our lab led to the identification of a MT binding region of NuMA spanning residues 2002-2115, which lies downstream of the LGN binding domain (Gallini et al. 2016), rather than overlapping with it as previously reported (Du et al. 2002; Haren and Merdes 2002) (for more details see **paragraph 1.5.2**). In *vitro* MT co-sedimentation assay demonstrated that NuMA$^{2002-2115}$ co-sediments with taxol-stabilized MTs, leaving LGN^{TPR} in the supernatant, while NuMA$^{1821-2001}$ encompassing the LGNBD does not (**Figure 12**), in agreement with the hypothesis that NuMA could simultaneously form hetero-hexamers with LGN and interact with the MTs. To better dissect the molecular basis for the MT binding activities of NuMA, first I tested the capability of NuMA$^{2002-2115}$ to bind the α,β-tubulin dimers as well as the polymerized MTs. To this aim I carried out SEC experiments by loading 1:1.3 molar ratio of purified α,β-tubulin and NuMA$^{2002-2115}$ on a Superdex-200 Increase 3.2/300 column, from which they eluted as a stoichiometric 1:1 complex, indicating that they interact physically (**Figure 25**).

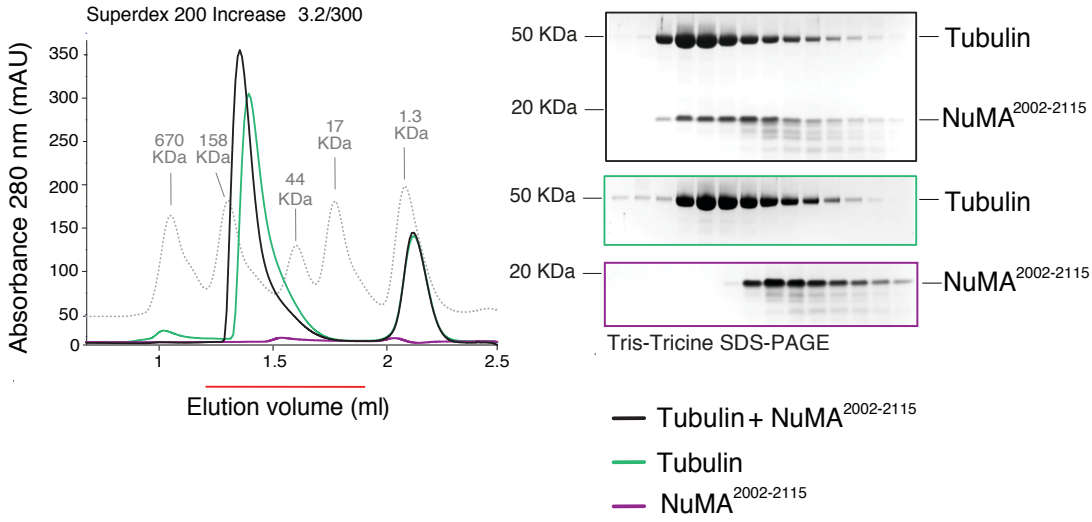

Figure 25. NuMA$^{2002-2115}$ binds α,β-tubulin dimers. SEC elution profile of α,β-tubulin (20 μM) and NuMA$^{2002-2115}$ (26 μM) showing that NuMA$^{2002-2115}$ binds α,β-tubulin dimers in solution (black line). SEC analysis was conducted loading the samples on a Superdex-200 Increase 3.2/300 column equilibrated in General Tubulin (GT) buffer (80 mM Pipes pH 6.8, 1 mM $MgCl_2$, 1 mM EGTA) supplemented with 60 mM NaCl and 1mM DTT. Eluted species were monitored by absorbance at 280 nm, subsequently checked by Tris-Tricine SDS-PAGE and visualized by Coomassie staining. The Coomassie-stained SDS-PAGE of the peak fractions corresponding to the horizontal red bar is shown on the right. Tris-Tricine increases the resolution of lower molecular weight NuMA$^{2002-2115}$

protein. The elution profile of globular markers is reported in a dashed grey line. Individual runs of α,β-tubulin (green line) and NuMA$^{2002-2115}$ (purple line) are shown for comparison.

3.2.2 NuMA recognizes the microtubule lattice

MTs associated proteins (MAPs) can bind hollow cylindrical MTs in several manners, as detailed in **paragraph 1.1.1**. To further characterize the capability of NuMA to associate with MTs *in vitro*, we asked whether the MTBD of NuMA can bind the MT lattice or the C-terminal tails. Therefore, I performed MTs co-sedimentation experiments with MTs lacking the tubulin tails. To this aim, paclitaxel-stabilized MTs were treated with Subtilisin A (Carlsberg) in a 1:50 weight ratio to remove the acidic tails by proteolytic digestion. Specifically, the cleavage occurs after Asp438 of α-tubulin and Gln433 of β-tubulin (Knipling, Hwang, and Wolff 1999). To check the proteolytic cleavage of MT tails, I used two methods. On one side, I run the proteolyzed sample on a 10% Tris-Glycine SDS-PAGE supplemented with the reagent Phos-TAG (**Figure 26A**). Phos-TAG SDS-PAGE delays the run of phosphorylated bands that associate with the Phos-TAG reagent, resulting in a consistent shift to higher molecular weights. The tubulin tails are hotspots for phosphorylation (Garnham and Roll-Mecak 2012). An alternative method that I used to confirm the MT tails cleavage was immunoblotting of the cleaved sample with rat anti-α-tubulin YL1/2 (monoclonal raised against the last 8 residues – GEEEGEEY – at the C-terminus of human α-tubulin) and mouse anti-β-tubulin JDR.3B8 (monoclonal, monoclonal raised against the C-terminus of human β-tubulin) antibodies that recognize specifically two epitopes of the α-tubulin and β-tubulin tails respectively (**Figure 26B**). Both methods confirmed that under the conditions used tubulin tails are efficiently removed. I then set out to test the ability of NuMA to associate with MTs lacking tubulin tails. In this experiments, I used a sample of Ndc80^{Bonsai} as negative control, that is known to recognize Subtilisin-treated MTs with a dramatically reduced affinity (Ciferri et al. 2008). 9 μM MTs with and without tails were incubated with 5 μM NuMA$^{2002-2115}$ or 1 μM Ndc80^{Bonsai}. After incubation, the reactions were subjected to high-speed centrifugation to separate the pellet (P) from the supernatant (S) fraction retained onto a cushion buffer on which the reaction mix was transferred to analysis (**Figure 26C**). These co-sedimentation assays showed that NuMA$^{2002-2115}$ pellets with MTs regardless of the presence of tubulin tails, indicating that NuMA directly recognizes MT lattice.

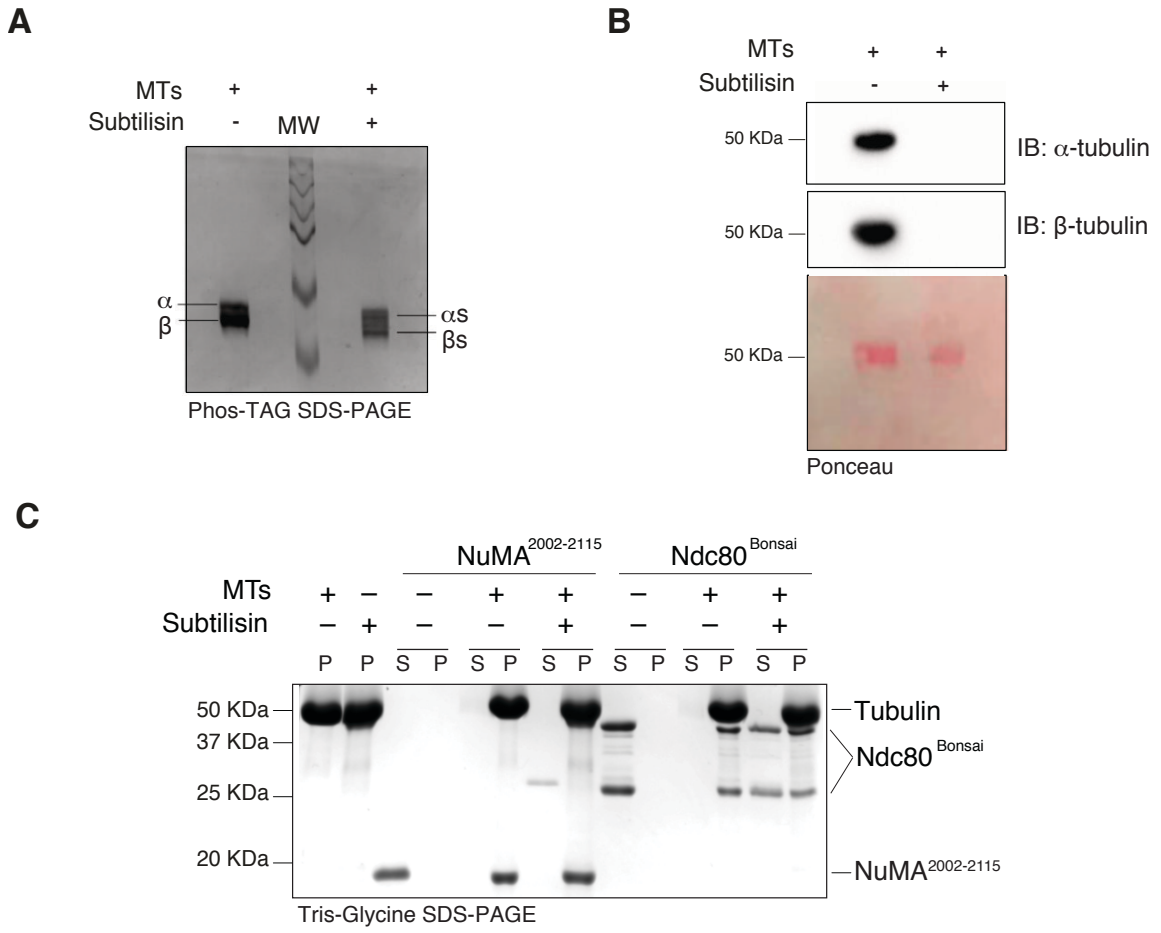

Figure 26. NuMA$^{2002-2115}$ binds tubulin with and without tails. A) Coomassie blue-stained Phos-TAG SDS-PAGE of the same amount of untreated MTs (sample lane before markers molecular weight) or Subtilisin-treated MTs (sample lane after markers molecular weight) showing the cleavage efficacy. α/β-tubulin (Cytoskeleton Inc.) was polymerized into stable microtubules (MTs) according to the producer's instructions, and MT co-sedimentation assays were carried out as in Ciferri *et al.* (Ciferri et al. 2008). In order to remove the C-terminal tubulin tails, MTs were incubated with Subtilisin A (Carlsberg; Sigma-Aldrich) in a 1:50 weight ratio for 30 min at 30 °C. Proteolysis was stopped with the addition of 10 mM PMSF. The Phos-TAG SDS-PAGE (Wako Rure Chemical Industries, Ltd, AAL-107) is a phosphate-affinity gel electrophoresis technique developed to detect different phosphorylation states of proteins by using a separating gel containing Phos-TAG acrylamide. To prevent excessive heating of the gel, Phos-TAG SDS-PAGE was run at 80 V for 2 hours at room temperature. **B)** Western blot of paclitaxel-stabilized MTs loaded as control and Subtilisin-treated MTs incubated with specifically-recognized antibody for α and β-tubulin tails. **C)** Co-sedimentation assay performed with 9 μM paclitaxel-stabilized MTs with or without tubulin tails and 5 μM NuMA$^{2002-2115}$. For MT binding reactions, MTs were diluted to a final concentration of 9 μM in general tubulin (GT) buffer (80 mM PIPES pH 6.8, 1 mM $MgCl_2$, 1 mM EGTA) supplemented with 1 mM GTP, 50 μM Paclitaxel, and 60 mM NaCl. MTs with and without tails were incubated for 10 min at room temperature with NuMA$^{2002-2115}$ or 1 μM Ndc80^{Bonsai}, in a final volume of 50 μl. All reactions were incubated at room temperature for 15 minutes, transferred onto 100 μl of cushion

buffer (80 mM PIPES pH 6.8, 1 mM $MgCl_2$, 1 mM EGTA, 50 µM Paclitaxel, 50 % glycerol), and ultracentrifuged for 15 minutes at 400,000 g at 25 °C in a Beckman TLA100 rotor. Supernatant (S) and pellet (P) fractions were separated by SDS-PAGE and Coomassie stained. $Ndc80^{Bonsai}$ was used as a control of tail-dependent MT-binding. The solubility of $NuMA^{2002-2115}$ and $Ndc80^{Bonsai}$ in the absence of MTs was also tested.

3.2.3 $NuMA^{1970-2089}$ is the minimal C-terminal fragment that binds to MTs

During the purification protocol of the NuMA C-terminal region spanning residues 1945 to 2115 containing the MT binding region of NuMA-2002-2115, we noticed a stable degradation, that was assigned by mass spectrometry to three fragments encompassing residues 1970-2089, 1945-2059, and 1951-2067. To better understand the biochemical properties of these fragments, they were expressed and purified in large amount, as soluble proteins from *E.coli* production. I then tested the capability of new identified NuMA fragments to binds MTs *in vitro*, incubating 10 µM MTs with 7 µM C-terminal NuMA fragments, using $NuMA^{1821-2115}$ as positive control (**Figure 27**). $NuMA^{1970-2089}$ was found in the pellet fraction with MTs, whereas both $NuMA^{1945-2059}$ and $NuMA^{1951-2067}$ co-sedimented only partly with MTs. The assay indicated that $NuMA^{1970-2089}$ shows higher affinity to MTs compared to $NuMA^{1945-2059}$ and $NuMA^{1951-2067}$.

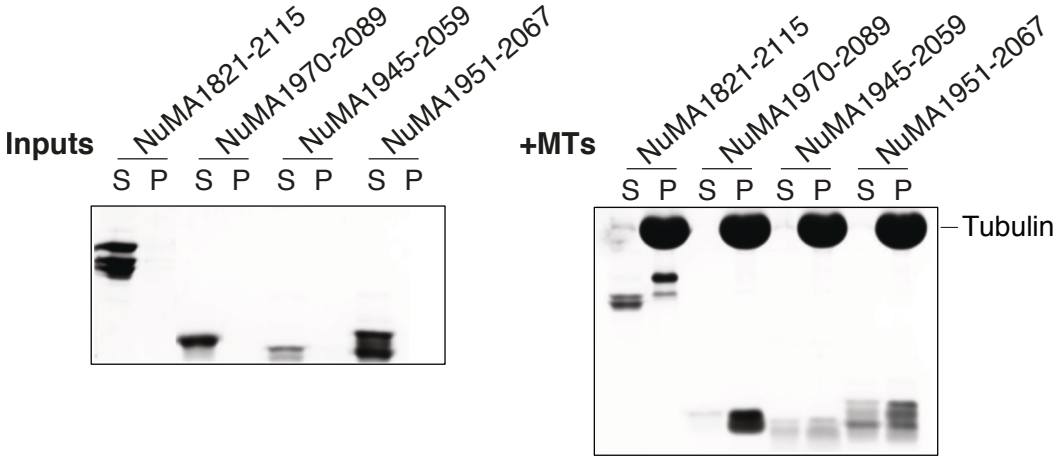

Figure 27. $NuMA^{1970-2089}$ is the shorter region that binds MTs with high affinity. Co-sedimentation assay performed with 10 µM paclitaxel-stabilized MTs and 5 µM $NuMA^{1970-2089}$, $NuMA^{1945-2059}$, $NuMA^{1951-2067}$ or $NuMA^{1821-2115}$ as positive control, as reported in **Figure 26**. Supernatant (S) and pellet (P) fractions were separated by SDS-PAGE and Coomassie stained.

3.2.4 NuMA$^{1970-2089}$/MTs binding interface involves both the lattice than tails

From large scale purification of NuMA$^{1970-2089}$ I obtained the highly pure sample, more stable than NuMA$^{2002-2115}$, which was prone to degradation (**Figure 25**). Thus, I decided to use this construct to determine the organizational principles of the NuMA/MTs interaction by X-ray crystallography. I first carried out Subtilisin-treated MT co-sedimentation experiments to ensure that this C-terminal NuMA fragment was endowed with the same MT binding ability of 2002-2115 construct (**Figures 25** and **26**). This experiment revealed that at the concentration used NuMA$^{1970-2089}$ does not completely sediment with MTs devoid of tubulin tails (**Figures 28A** and **28B**), indicating that in absence of the MT tails, NuMA$^{1970-2089}$ decreased the affinity with MTs, and that both the MT lattice and the tubulin tails are recognized by NuMA.

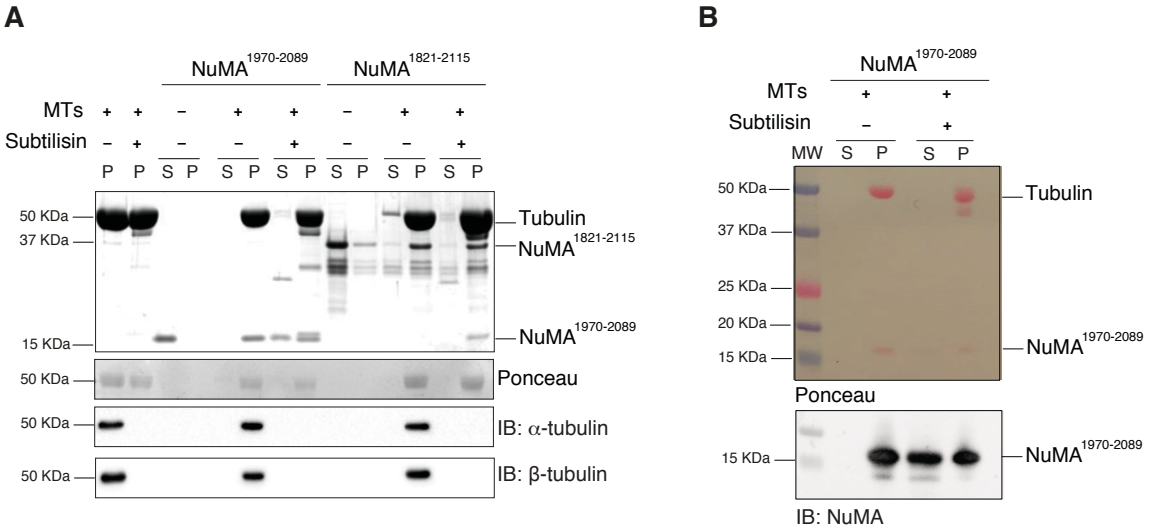

Figure 28. NuMA$^{1970-2089}$ co-sediments with untreated and Subtilisin-treated MTs. A) Co-sedimentation assay performed as reported in **Figure 26**, with 9 μM paclitaxel-stabilized MTs with or without tubulin tails and 5 μM NuMA$^{1970-2089}$ or NuMA$^{1821-2115}$ as positive control. Supernatant (S) and pellet (P) fractions were separated by SDS-PAGE and Coomassie stained. In the bottom, immunoblotting against α,β-tubulin tails revealed complete lack of the tails in the Subtilisin-treated MTs sample used for co-sedimentation assay. **B)** Western blot analysis of NuMA$^{1970-2089}$/MT co-sedimentation samples shown in panel A with anti-NuMA rabbit monoclonal antibody (Abcam) to detect the presence of NuMA into the pellet and supernatant fractions of MTs with or without tails. The experiment shows that NuMA$^{1970-2089}$ binds both the MTs lattice and the tubulin tails.

3.2.5 NuMA$^{1970-2089}$/tubulin interaction is compatible with DARPin1 binding

Based on the previous co-sedimentation assay (**Figure 28A**), I speculated that NuMA$^{1970-2089}$ could bind the acidic tails of tubulin dimers contributing to stabilize the intrinsically

disordered tubulin tails, and I decided to try to crystalize NuMA$^{1970-2089}$ in complex with tubulin dimer. In trying to crystallize the NuMA/tubulin dimer complex, I reasoned that increasing the NuMA/tubulin sample concentration above 3-5 mg/ml high for crystallization might have resulted in tubulin polymerization. To overcome the problem, I looked for biochemical tools to block MT assembly that could preserve the association of α,β-tubulin dimers with NuMA. To this end, I tested whether the binding of the plus-end capping protein DARPin1 (Pecqueur et al. 2012) (see **paragraph 1.1.1**) was compatible with NuMA$^{1970-2089}$/tubulin interaction. To this aim, I incubated tubulin, DARPin1 and NuMA$^{1970-2089}$ in a 1:1.3:1.3 molar ratio, and performed analytic SEC experiments on a Superdex-200 Increase 3.2/300 column (**Figure 29**). The SEC elution profile of the sample indicates that DARPin1 and NuMA$^{1970-2089}$ are able to bind concomitantly α,β-tubulin dimers and with the same stoichiometry, preventing tubulin polymerization.

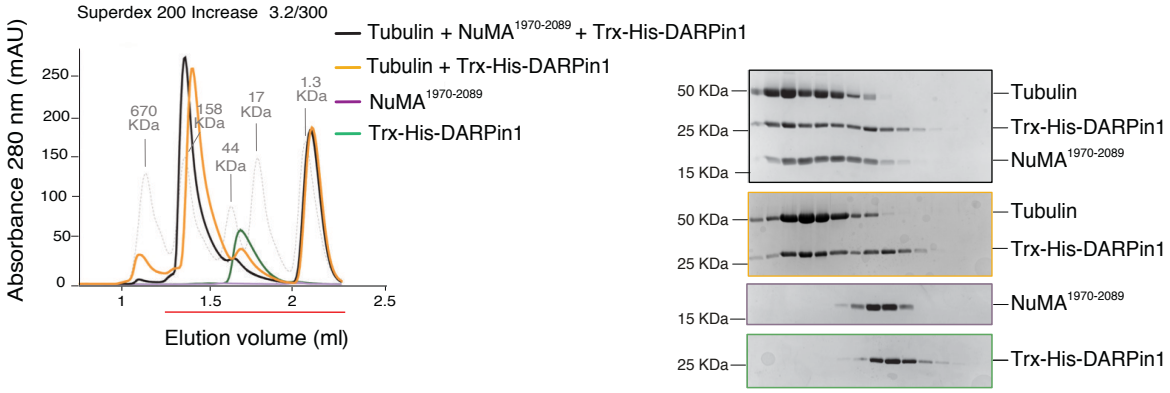

Figure 29. NuMA$^{1970-2089}$, DARPin1 and α,β-tubulin form a stoichiometric complex in solution. SEC elution profiles (left) and Coomassie-stained SDS-PAGE (right) of the complex formed between α,β-tubulin (20 µM), NuMA$^{1970-2089}$ (26 µM) and Trx-His-DARPin1 (26 µM) (purified in frame with the N-terminal hexa-histidine and Thioredoxin (Trx) tags) showing that NuMA$^{1970-2089}$ and DARPin1 are able to concomitantly bind tubulin dimers in solution (black line). Purified proteins were mixed, loaded on a Superdex-200 Increase 3.2/300 column equilibrated in GT buffer (80 mM PIPES pH 6.8, 1 mM $MgCl_2$, 1 mM EGTA) supplemented with 60 mM NaCl and 1mM DTT, and eluted in 50 µl fractions. The elution profile of globular markers is reported as a dashed grey line. Individual runs of NuMA$^{1970-2089}$ (purple line), DARPin1 (green line) and tubulin/DARPin1 mixed (yellow line) are shown for comparison.

3.2.6 Crystallization attempts of the NuMA$^{1970-2089}$/tubulin/DARPin1 complex

To prepare a sample suitable for crystallization experiments, the NuMA$^{1970-2089}$/tubulin/DARPin1 complex was purified on a Superdex-200 Increase 10/300 column

equilibrated in 80 mM Pipes pH 6.8, 1 mM $MgCl_2$, 1 mM EGTA, 60 mM NaCl and 1mM DTT. Fractions containing the complex were pooled and concentrated by centrifugation to a 25 mg/ml (**Figure 30**).

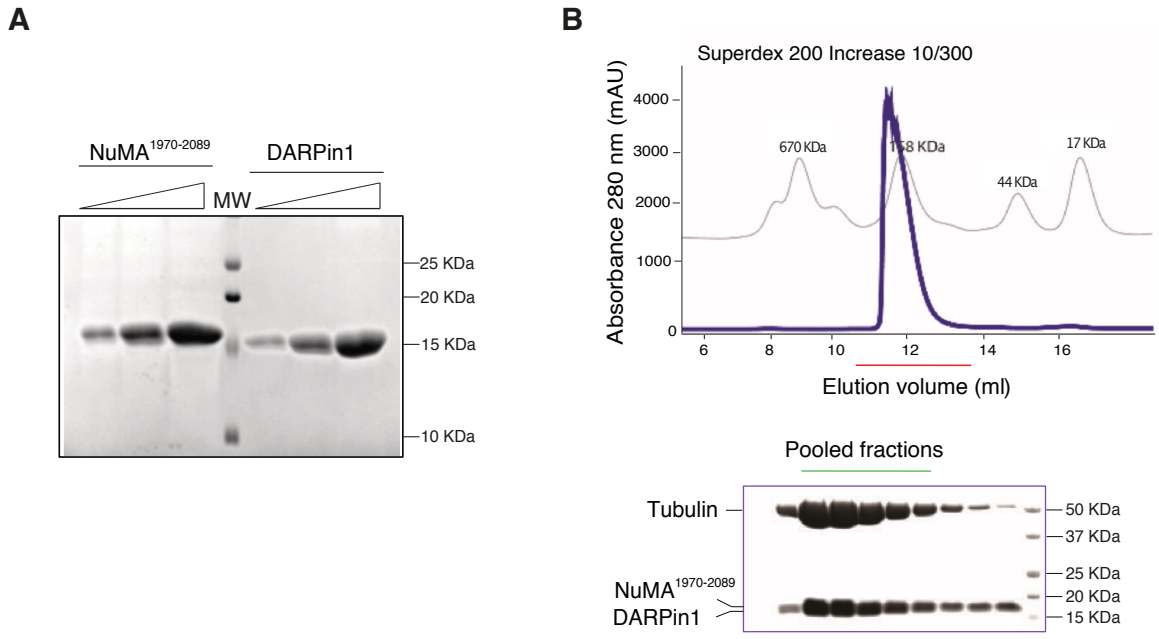

Figure 30. NuMA$^{1970-2089}$/tubulin/DARPin1 complex large-scale purification. A) SDS-PAGE and Coomassie stained of increasing amount of purified NuMA$^{1970-2089}$ and DARPin1 (lacking the Trx-His-tag) to monitor the quality samples prior to crystallization. **B)** The complex appears on SEC elution profile as a single peak. Tubulin protein was isolated from porcine brain (Cytoskeleton Inc., HTS03-A) and the lyophilized material was dissolved in General Tubulin (GT) buffer (80 mM Pipes pH 6.8, 1 mM $MgCl_2$, 1 mM EGTA). Tubulin with purified DARPin1 and NuMA$^{1970-2089}$ were incubated in a 1:1.3:1.3 molar ratio for 1 hour at 4 °C. The complex was further purified by gel filtration on a Superdex-200 Increase 10/300 column (GE Healthcare) equilibrated in GT buffer supplemented with 60 mM NaCl and 1mM DTT, and concentrated to 25 mg/ml.

I conducted initial crystallization attempts by sitting-drop vapor-diffusion methods using the commercial sparse-matrix screens ProPlex (Molecular Dimensions) and Additive (Hampton), which contain low ionic strength precipitants and don't contain glycerol to enhance tubulin disassembly. I then tried to optimized a few conditions of crystalline precipitate combining several strategies, *e.g.* hanging and sitting drop methods, different temperatures and protein concentrations, various ratios of reservoir to protein volume. However, all attempts were unsuccessful. I reasoned that NuMA$^{1970-2089}$ could not stabilize completely the high degree of flexibility of α,β-tubulin tails, thus way hampering crystallization.

For this reason, I removed the tails from the α,β-tubulin dimers by proteolytic digestion and performed SEC experiments with Subtilisin-treated tubulin and NuMA$^{1970-2089}$ (**Figure 31**). Consistently with results from MT co-sedimentation assays, NuMA$^{1970-2089}$ showed a strongly reduced affinity to tails-depleted α,β-tubulin as visible in a minimal shift of NuMA$^{1970-2089}$ elution profile of the complex compared to NuMA$^{1970-2089}$ in isolation. This result prevented further crystallization attempts of the NuMA/tubulin complex.

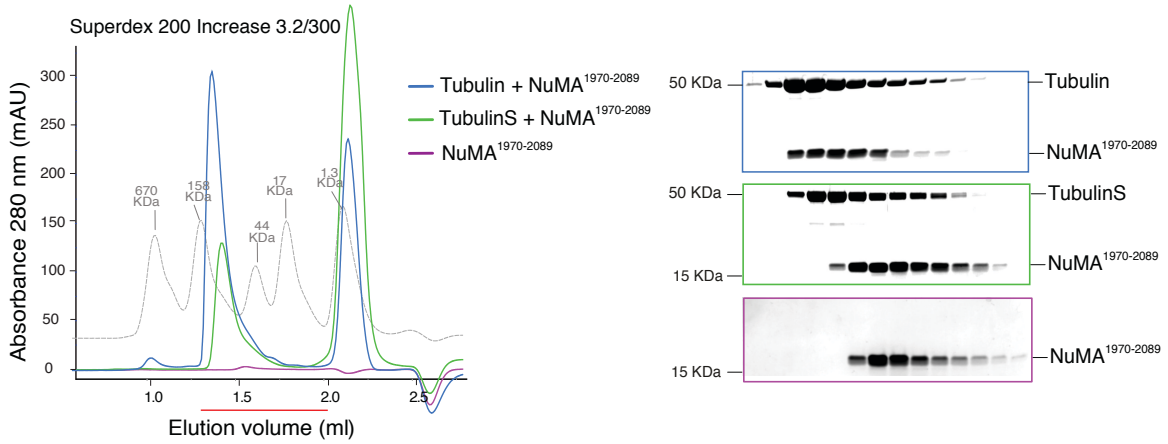

Figure 31. NuMA$^{1970-2089}$ is not able to bind soluble α,β-tubulin without tails. SEC analysis of NuMA$^{1970-2089}$ mixed with tubulin dimers with C-terminal tails (blue line) or with proteolytical cleaved tails (green line). Individual run of NuMA$^{1970-2089}$ (purple line) is shown for comparison. SEC analysis was conducted loading a complex assembled with 20 µM tubulin or 20 µM Subtilisin-treated tubulin were mixed with 26 µM NuMA$^{1970-2089}$ on a Superdex-200 Increase 3.2/300 column equilibrated in GT (80 mM Pipes pH 6.8, 1 mM $MgCl_2$, 1 mM EGTA) buffer supplemented with 60 mM NaCl and 1mM DTT, and eluted fractions were analyzed by Coomassie staining. The sample of α,β-tubulin hetero-dimers without the C-terminal tails was prepared starting from tubulin powder dissolved in GT buffer supplemented with 1 mM GTP to prevent ring-forming conformation of tubulin sample without tails (Knipling, Hwang, and Wolff 1999). Tubulin solution was incubated with Subtilisin A Carlsberg (Sigma-Aldrich) in a 1:100 weight ratio for 45 min at room temperature. Proteolytic digestion was stopped with the addition of 10 mM PMSF, and further incubated on ice for 30 min.

3.2.7 NuMA$^{2002-2115}$ is required to cortical recruitment and orient the spindle

To investigate the relevance of the newly identified MTBD of NuMA in cells, Chiara Gaddoni and Laura Pirovano in the lab analyzed NuMA cortical recruitment in HeLa cells depleted of the endogenous protein and transfected with NuMA-WT and NuMA-ΔMT constructs (**Figure 32A**). Depletion of endogenous NuMA in these experiments is required

to prevent dimerization of the rescue constructs with the endogenous protein. Wild-type NuMA localized at cortical regions above the spindle poles, while NuMA-ΔMT did not enrich at the cortex, and maintained only the spindle poles localization (**Figures 32B** and **32C**). Consistently, when NuMA-ΔMT is expressed in HeLa cells lacking NuMA, metaphase cells divide with an average angle of 14˚, while cells transfected with NuMA-WT display a mean angle of division of 7˚ (**Figures 32D** and **32E**). Therefore, NuMA-ΔMT mutant does not localize at the cortex and is not able to rescue misorientation phenotype induced by the loss of endogenous NuMA.

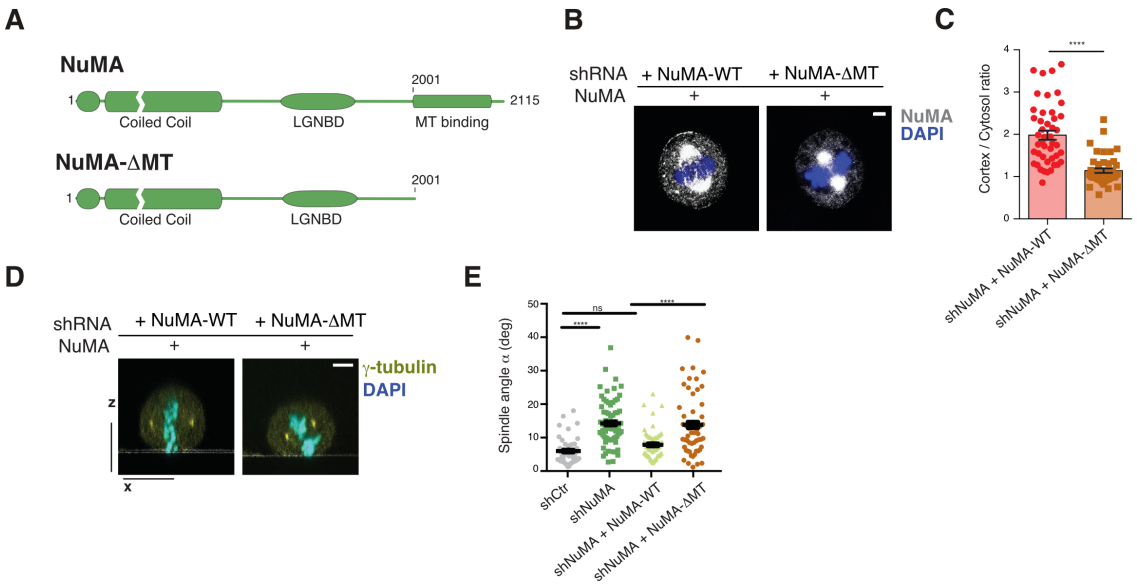

Figure 32. NuMA MTBD functions in HeLa cells. A) Schematic representation of the domain structure of NuMA wild-type and NuMA-ΔMT. **B)** Representative images of HeLa cells depleted of endogenous NuMA and transfected with mCherry-NuMA-WT and mCherry-NuMA-ΔMT. Cells were stained with NuMA (white) to visualize cortical signal and with DAPI (blue). **C)** Quantification of NuMA cortical signal, with histograms representing the cortex-to-cytoplasm fluorescent ratio. Means ± SEM are shown for three independent experiments, with n>45. **** p<0.0001 by Mann-Whitney test. **D)** Representative images of HeLa cells depleted of endogenous NuMA and transfected with mCherry-NuMA-WT and mCherry-NuMA-ΔMT. Cells were stained with γ-tubulin (yellow) to visualize the spindle poles and with DAPI (cyan). **E)** Distribution of the spindle angles in metaphase for NuMA shRNA rescue experiments in HeLa cells imaged in panel D. Mean ± SEM are shown for four independent experiments, with n>55. **** indicates p<0.0001, by the Krustal-Wallis test.

For immunofluorescence analysis, HeLa cells were plated on 13 mm coverslips coated with 5 µg/ml fibronectin and pre-synchronized with a single thymidine block/release (as reported in **Figure 22**). To visualize NuMA (**Figure 32B**), cells were fixed with methanol at -20 °C for 10 minutes. To detect γ-tubulin (**Figures 32D**), cells were fixed with 4% paraformaldehyde (PFA) for 10 minutes at room

temperature, followed by permeabilization with 0.3% Triton X-100 in PBS for 5 minutes. For all conditions, blocking was performed with 3% BSA in PBS for 1 hour at room temperature. Depending on the experiment, cells were stained with mouse anti-NuMA (1:3000, Mapelli lab) or rabbit Cy3 conjugated anti-γ-tubulin (1:200, Sigma-Aldrich, C7604). DNA was stained with DAPI. Confocal images were acquired on a Leica SP2 AOBS confocal microscope controlled by Leica confocal software. For HeLa cells analysis, a 63X oil-immersion objective lens (HC PL APO 63X/1.40 OIL CS2) was used. All images were processed using the software Fiji.

Quantification of cortical signals of mCherry-NuMA wild-type or mCherry-NuMA-ΔMT was conducted on confocal sections of metaphase cells in Fiji as follows. A 30-pixel-wide line was manually drawn from the spindle pole to the nearest cellular cortex perpendicularly to the metaphase plate, to obtain the intensity profile of the immunostained proteins along the line. Using the software Matlab, the "protein at the cortex" was calculated by integrating the profile of a 10 pixel-wide area of the peak, whereas the "protein in the cytosol" the 10 pixel-wide area, 5-pixel distant from the peak. The cortex to cytoplasm ratio was used to monitor cortical enrichment of the proteins.

4. RESULTS: NuMA and β-catenin generate mitotic complexes

In the last part of my PhD, I focused on the biochemical characterization of the mitotic interactions between NuMA and the Wnt pathway components. All data reported within the following paragraphs are result of my work and contribution, and have not been published yet.

4.1 NuMA interacts with Wnt3 pathway components in mammalian cells

Converging evidence is accumulating for the role of Wnt3 pathway effectors in spindle positioning, orientation and mitotic progression (Niehrs and Acebron 2012; Stolz et al. 2015). A question here is whether the localization of Wnt-players at the mitotic spindle during mitosis is an indication of the direct involvement of the Wnt pathway in spindle functions, or whether these effectors have different functions in mitosis independently of their canonical role in the Wnt signaling (Červenka and Čajánek 2018).

Since NuMA is a key player of spindle orientation in vertebrate cells, we wondered whether and how NuMA could interact with Wnt pathway components in mitosis. To start addressing this issue, I used HEK293T cells bearing no know mutations in key Wnt pathway components (Vora, Fassler, and Phillips 2020), and cultured these cells for immunoprecipitation experiments in different conditioned media (CM), either with Wnt3a or Dkk1. Dkk1 is a negative regulator of the Wnt signaling that competitively binds to LRP5/6 (Agostino and Pohl 2020; Niida et al. 2004). Wnt3a CM was produced using the stable cell line L-Wnt-3A (Bilić et al. 2007; Davidson et al. 2005), while Dkk1 CM using a transiently transfection of HEK293T cells (Bafico et al. 2001). First, I examined the effect of Wnt3a stimulation on putative mitotic complexes of NuMA with components of the Wnt pathway. To this aim, I transfected N-terminally GFP-tagged NuMA full-length in HEK293T cells using a Calcium Phosphate protocol (as detailed in the Material and Method **section 6.3.5**). After 32 hours of expression I treated the cells with 2.5 μM STLC (an Eg5 inhibitor; see **paragraph 1.1.2**) for 16 hours to synchronized them in prometaphase with monopolar spindle. In the last three hours of the STLC treatment, cells were supplemented with Wnt3a or Dkk1 CM. Cells were lysed with 50 mM Hepes pH 7.5, 2 mM, EGTA, 1 mM EDTA, 2 mM $MgCl_2$, 0.15 M KCl, 0.2% NP40 and 10% glycerol, in the presence of protease and phosphatase inhibitors, and after centrifugation the soluble fraction was incubated with α-GFP antibody conjugated to agarose beads (MBL). Wnt-related proteins retained on the beads after extensive washing were analysed by immunoblotting (**Figure 33**). This experiment revealed that NuMA immunoprecipitates endogenous β-catenin, Axin1 and

Dishevelled2 (Dvl2), and that the interactions does not seem to be regulated by Wnt3a stimulation. Interestingly, in spite of the fact that in Dkk1 condition the cytosolic amount of endogenous β-catenin is lower than in Wnt3a condition, due to the higher rate of phosphorylation and degradation, the amount of β-catenin immunoprecipitating with NuMA is the same in both conditions.

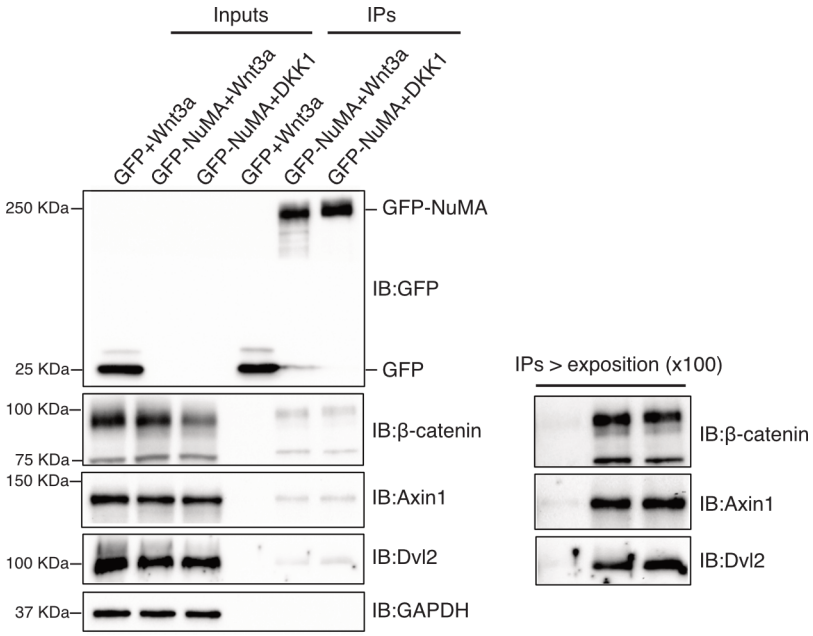

Figure 33. NuMA immunoprecipitates endogenous β-catenin, Axin1 and Dishevelled2. NuMA binds to the main components of the destruction complex in mitotic HEK293T lysates of cells transfected with 10 μg pCDH-GFP-NuMA full-length or 0.7 μg pCDH-GFP used as negative control, and treated with Wnt3a or Dkk1 conditioned media (CM). Wild-type 70% HEK293T confluent cells were transfected with appropriate vectors using Calcium Phosphate protocol. 32 hours post-transfection cells were synchronized with 2.5 μM STLC (Merk) for 16 hours. In the last three hours of the STLC treatment, cells were supplemented with Wnt3a or Dkk1 CM (1:5). Mitotic cells were lysed on ice in lysis buffer containing 50 mM Hepes pH 7.5, 2 mM, EGTA, 1 mM EDTA, 2 mM $MgCl_2$, 0.15 M KCl, 0.2% NP40, 10% glycerol, with protease (Calbiochem) and phosphatase inhibitors (Sigma), with 30 minutes 11,000 g. 1.5 mg of cleared lysates were incubated with 40 μl α-GFP antibody conjugated to agarose beads (MBL) for 2 hours at 4 °C, with gentle agitation on the wheel. After supernatant removal, beads were washed 3 times with 0.5 ml lysis buffer, and Laemmli sample buffer was added to the beads. Input and IP samples were resolved by SDS-electrophoresis and transferred onto a nitrocellulose membrane for 18 hours at 30 V, 4 °C for immunoblotting. Membranes were blocked with 5% milk solution in TBS and 0.1% Tween for 1 hour and incubated for 18 hours at 4 °C with rabbit monoclonal anti-GFP antibody, rabbit polyclonal anti-β-catenin antibody, rabbit monoclonal anti-Dishevelled2 antibody, rabbit monoclonal anti-Axin1 antibody or mouse monoclonal anti-GAPDH antibody. Western blotting are shown as representative of three

independent immunoprecipitation experiments using the indicated antibodies. On the right panel an increased exposure of proteins in the co-IPs compared to inputs is shown. GAPDH was used as loading control for the inputs and as IP negative control.

4.2 NuMA binds to endogenous β-catenin

To understand the topology of the β-catenin/NuMA interaction, we reasoned that the armadillo-domain of β-catenin and the TPR domain of LGN present a similar rigid helical architecture, and hypothesized that the two domains might bind NuMA in a similar manner (**Figure 8**). Interestingly, β-catenin consists of an N-terminal degron (residues 1-137) required for phosphorylation-dependent protein degradation, a central domain composed of 12 armadillo (ARM) repeats (residues 138-664), followed by a C-terminal helical domain (residues 665-781) (Xing et al. 2008) (**Figure 34A**). The positively charged grooved of the concave inner surface of the armadillo domain constitutes the binding surface for the majority of β-catenin partners including APC, Axin, E-cadherin, LEF/Tcf family (Huber, Nelson, and Weis 1997; Huber and Weis 2001). Starting from these observations, I decided to test the binding of the C-terminal region of NuMA encompassing residues 1821-2115 to β-catenin. First, I performed a pull-down experiment with mitotic HEK293T lysates with 0.3% Triton X-100, and GST-NuMA$^{1821-2115}$ purified from bacterial source (**Figure 34B**). The assay indicated that NuMA$^{1821-2115}$ binds specifically to endogenous β-catenin. Moreover, a GST pull-down assay with GST-β-catenin full-length on Glutathione-Sepharose (GSH) beads at 3 μM concentration and purified NuMA$^{1821-2115}$ at 10 μM or 20 μM increasing concentration in solution revealed a putative direct binding between β-catenin and the C-terminal region of NuMA, both expressed in bacteria (**Figure 34C**).

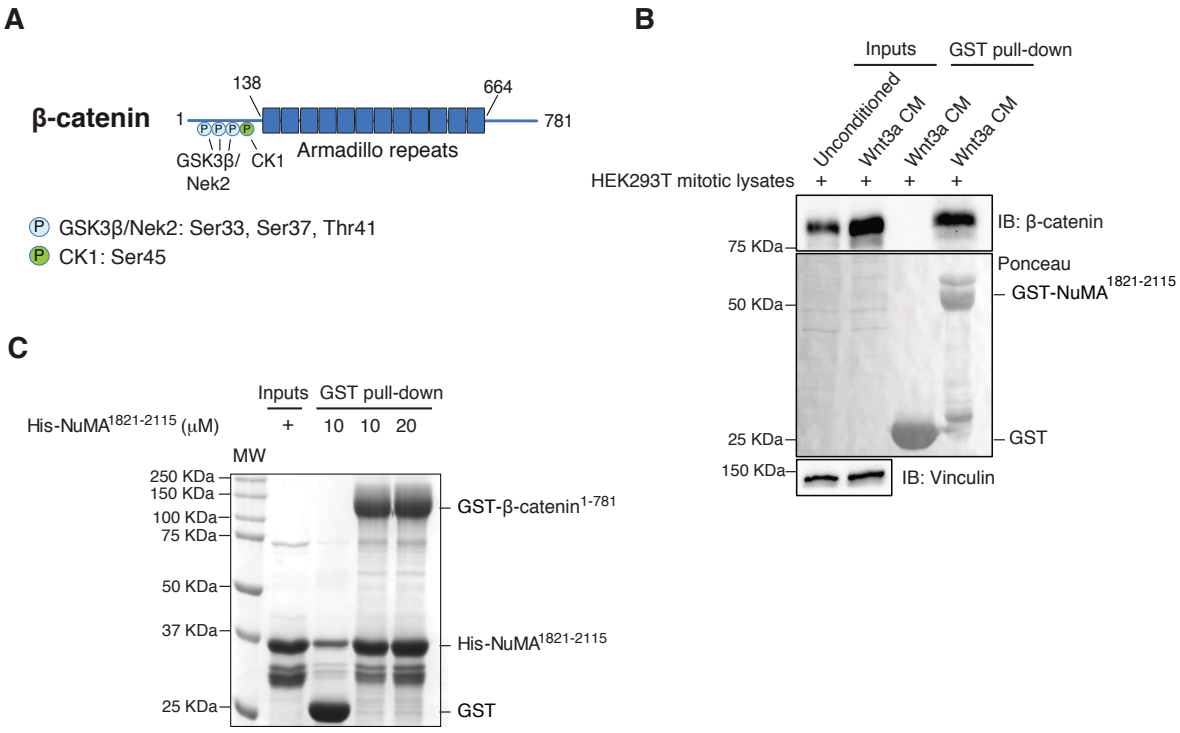

Figure 34. NuMA$^{1821-2115}$ pull-downs endogenous β-catenin. A) Schematic representation of the domain structure of β-catenin with a central core of 12 armadillo repeats (residues 138–664) flanked by two likely unfolded flexible N- and C-terminal regions. The β-catenin N-terminal region contains phosphorylation consensus sites for the Wnt-kinases GSK3β and CK1, and the mitotic kinase Nek2. **B)** GST pull-down of purified NuMA$^{1821-2115}$ and β-catenin from mitotic lysates of HEK293T cells cultured in Wnt3-conditioned medium. Specifically, wild-type HEK293T cells were treated with 2.5 μM STLC (Merk) for 16 hours to synchronized them in prometaphase. In the last three hours of the STLC treatment, cells were supplemented with Wnt3a CM (1:5) to increase the cytoplasmic amount of endogenous β-catenin compared to unconditioned HEK293T cells. Mitotic cells were lysed with 50 mM Hepes pH 7.5, 2 mM, EGTA, 1 mM EDTA, 2 mM $MgCl_2$, 0.15 M KCl, 0.3% Triton X-100, 10% glycerol, protease (Calbiochem) and phosphatase inhibitors (Sigma) to 7 mg/ml final concentration of soluble fraction obtained by total lysate centrifugation (30 minutes 11,000 g). 2 mg of cleared lysates were incubated with 5 μM GST-NuMA$^{1821-2115}$ or GST bound to GSH resin for 2 hours at 4 °C, with gentle agitation on wheel. Beads were washed 3 times with 0.5 ml lysis buffer, and species retained on beads were analyzed by SDS-PAGE and blotted with rabbit polyclonal anti-β-catenin antibody. Vinculin was used as loading control. **C)** GST pull-down with purified proteins from bacteria sources. The assay was performed with 3 μM GST-β-catenin$^{1-781}$ adsorbed on glutatathione (GSH) beads, and incubated with 10 μM or 20 μM of purified NuMA$^{1821-2115}$ for 1h on ice. Pull-down assays were conducted in 100 μl volume of pull-down buffer consisting of 50 mM Hepes pH 7.5, 0.1 M NaCl, 5% glycerol, 1 mM DTT. After washes, proteins bound to beads were separated by SDS-PAGE and visualized by Coomassie staining.

4.3 Studying NuMA/β-catenin interaction

Based on the previous results, I tested whether the interaction of NuMA and β-catenin is direct using both purified proteins in solution. I purified to NuMA-1821-2115 (**Figure 35A**) by His-tag affinity chromatography followed by a cation exchange chromatography, and full-length β-catenin (**Figure 35A**) by a single-step of GSH-affinity chromatography followed by the GST-tag cleavage and elution from beads. I then conducted analytical SEC experiments by loading equimolar amounts of two proteins (from 10 µM to 90 µM) on a Superose6 3.2/300 column equilibrated in 50 mM Hepes pH 7.5, 5% glycerol, 1 mM DTT and increasing salt concentration (from 0.1 M to 0.3 M NaCl) (**Figure 35B**). Both proteins in isolation are stable, soluble, and elute from the SEC column according to their size. Nevertheless, when they are mixed together an abundant precipitate immediately appears in the Eppendorf tube (**Figures 35C** and **35D**), and none of the proteins remain in solution as assessed by SEC analysis (**Figure 35B, yellow line**).

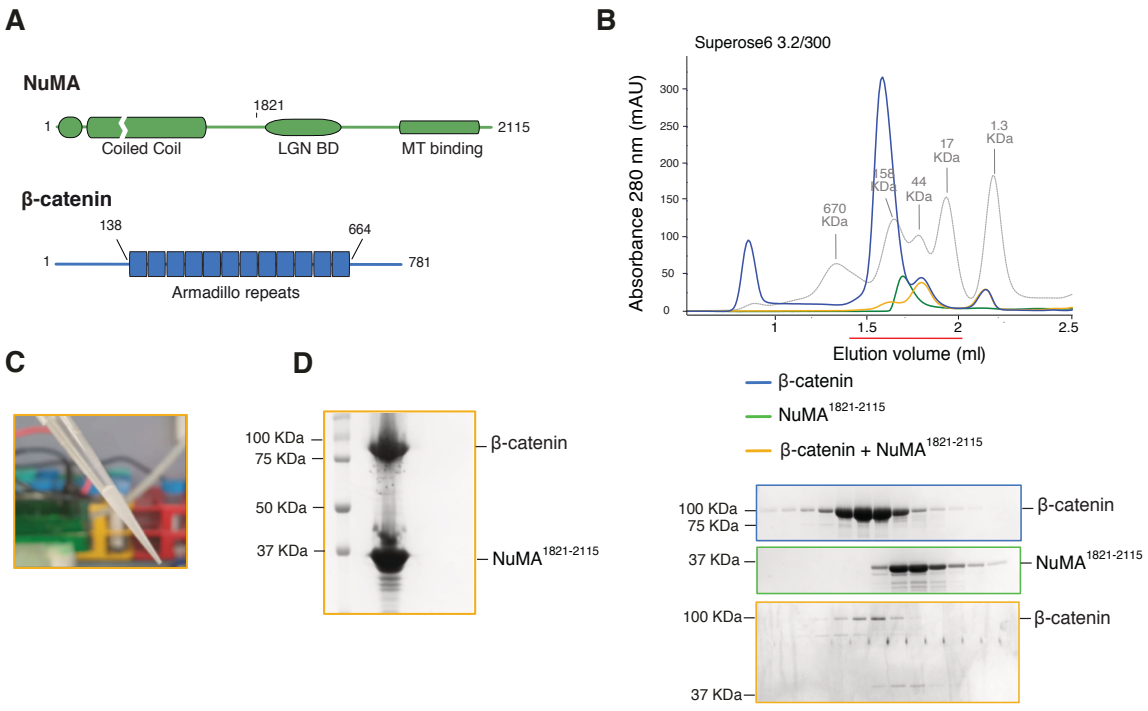

Figure 35. Analysis of purified NuMA/β-catenin reconstitution complex. A) Schematic representation of β-catenin and NuMA depicted with C-terminal boundaries both used in this study. **B)** SEC analysis and corresponding SDS-PAGE showing that β-catenin (blue line) and NuMA$^{1821-2115}$ (green line) are stable in the same buffer (50 mM Hepes pH 7.5, 0.1 M NaCl, 5% glycerol, 1 mM DTT), and precipitate when are mix together at 80 µM (orange line; SEC experiments representative concentration and buffer). Analytical SEC analyses were conducted loading from 10 µM to 90 µM β-catenin$^{1-781}$ and NuMA$^{1821-2115}$ singularly or in combination in equimolar ratio on a Superose6

3.2/300 equilibrated in 50 mM Hepes pH 7.5, 5% glycerol, 1 mM DTT and increasing salt concentration (from 0.1 M to 0.3 M NaCl). The presence of the proteins in the elution volume was monitored by absorbance at 280 nm (expressed as mAU), and subsequently checked by SDS-PAGE followed by Coomassie staining. **C)** White heavy precipitate observed upon mixing equimolar amounts of β-catenin and NuMA$^{1821-2115}$. **D)** β-catenin and NuMA$^{1821-2115}$ precipitate were separated by SDS–PAGE and visualized by Coomassie staining.

This evidence seems to suggest that also the GST-pull-down experiment presented in **Figure 34C** might result from aspecific precipitation of NuMA$^{1821-2115}$ on GST-β-catenin GSH beads. To explain this behaviour, I hypothesized that when two proteins are mixed together a conformational change occurs that exposes hydrophobic surfaces either of NuMA or β-catenin causing precipitation. I tried to change the salt concentration in the buffer to increase the stability of two proteins in complex without success. Therefore, I reasoned that post-translational modifications on β-catenin or additional intermediate interactors are required to stabilize the NuMA/β-catenin interaction.

4.4 Overexpression of β-catenin increases the binding to NuMA$^{1821-2115}$

To confirm the idea that the β-catenin phosphorylations are required to reconstitute the NuMA/β-catenin complex, I performed co-IP experiments from HEK293T mitotic lysates expressing GFP-tagged NuMA full-length or NuMA$^{1821-2115}$ and wild-type β-catenin, harvested with and without phosphatase inhibitors (**Figure 36**). In the presence of phosphatase inhibitors (**Figure 36, red box)**, the amount of β-catenin immunoprecipitating with NuMA$^{1821-2115}$ increases significantly, even compared to the amount of β-catenin found in complex with full-length NuMA (**Figure 36, blue box)**.

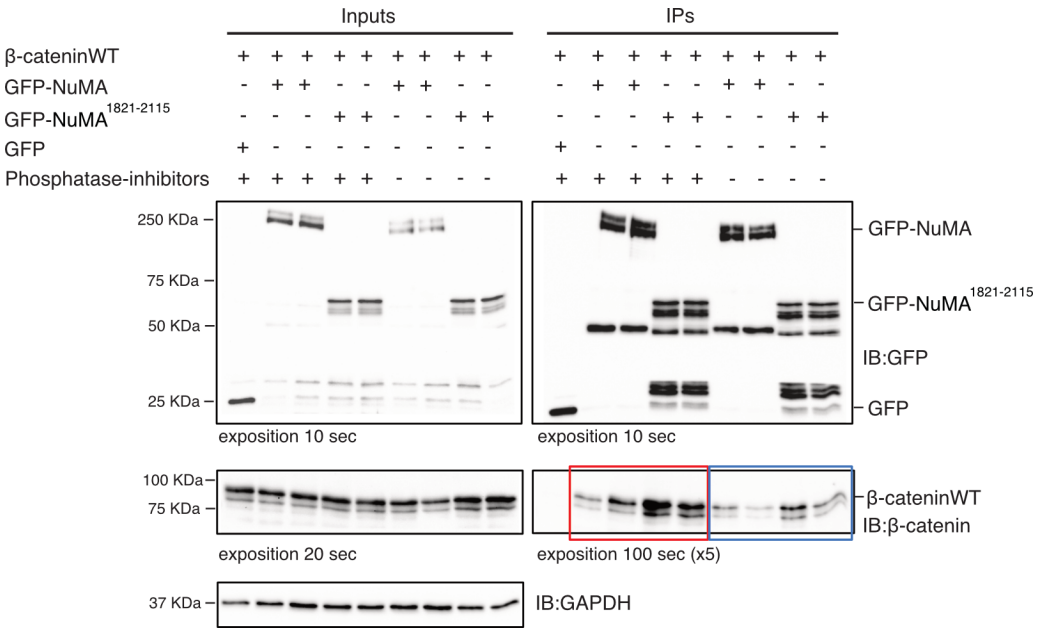

Figure 36. β-catenin wild-type enriches in the NuMA C-terminus immunoprecipitated fraction. Immunoblotting of mitotic HEK293T lysates co-transfected with 8 µg pCDH-GFP-NuMA full-length and 2 µg pCI-neo-β-catenin full-length or 5 µg pCDH-GFP-NuMA$^{1821-2115}$ and 2 µg pCI-neo-β-catenin full-length or 0.5 µg pCDH-GFP and 1 µg pCI-neo-β-catenin full-length, and immunoprecipitated with GFP-beads. The immunoprecipitation assay was performed as reported in **Figure 33.** Mitotic cells were lysed on ice in lysis buffer containing 50 mM Hepes pH 7.5, 2 mM, EGTA, 1 mM EDTA, 2 mM $MgCl_2$, 0.15 M KCl, 0.2% NP40, 10% glycerol, protease (Calbiochem) inhibitors, with or without phosphatase inhibitors (Sigma). β-catenin amounts in the IP are boxed in red (with phosphatase inhibitors) and blue (without phosphatase inhibitors). GAPDH was used as loading control for the inputs.

SEC analysis of lysates overexpressing wild-type β-Catenin and GFP-NuMA$^{1821-2115}$ revealed slight elution volume shifts of two proteins co-transfected together (**Figure 37)**, that might be consistent with the complex observe by co-IP.

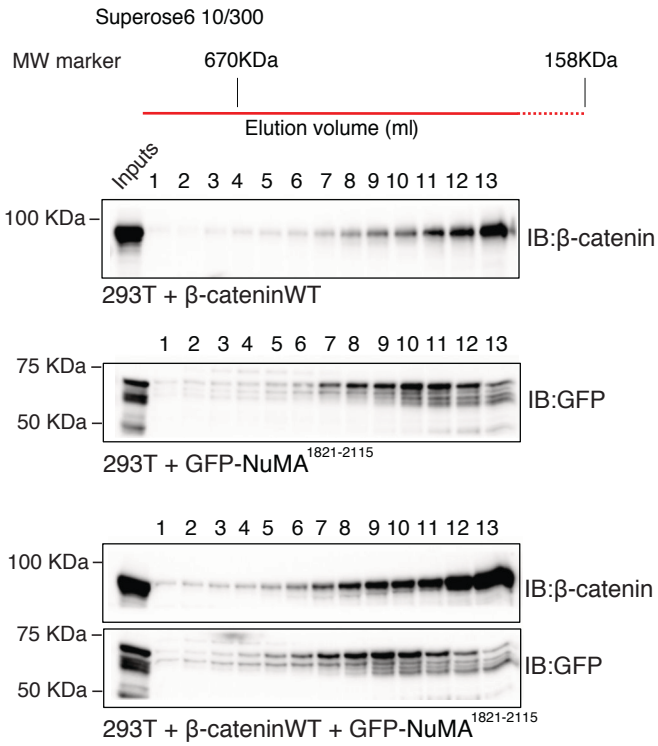

Figure 37. SEC analysis of wild-type β-catenin and NuMA$^{1821-2115}$. Immunoblotting of the Size Exclusion Chromatography elution profiles of mitotic HEK293T lysates singularly transfected or co-transfected with 5 μg pCDH-GFP-NuMA$^{1821-2115}$ or 2 μg pCI-neo-β-catenin full-length. Cell lysates prepared in lysis buffer 50 mM Hepes pH 7.5, 2 mM, EGTA, 1 mM EDTA, 2 mM $MgCl_2$, 0.15 M KCl, 0.2% NP40, 10% glycerol, 5 mM DTT, protease (Calbiochem) and phosphatase inhibitors (Sigma) were filtered (0.22 μm filter) and quantified. 0.5 ml of cell lysates at a concentration of 7 mg/ml were loaded on a Superose6 10/300 equilibrated in 50 mM Hepes pH 7.5, 0.15 M NaCl, 10% glycerol, and 5 mM DTT. Lysates were loaded on a Superose6 10/30 column equilibrated in 50 mM HEPES pH 7.5, 0.15 M KCl, 10 % glycerol, and 5 mM DTT. Eluted fractions were collected, separated by SDS- PAGE (18 μl each fraction and 20 μg of total cell lysate as input), and analyzed by immunoblotting with rabbit monoclonal anti-GFP antibody or rabbit polyclonal anti-β-catenin antibody.

5. DISCUSSION

5.1 Molecular organization of LGN/NuMA/dynein complexes directing cortical pulling forces on astral MTs

The studies described in the second and third result chapters provided evidences that in mitotic mammalian cells NuMA engages with the dynein/dynactin MT motors at the cell cortex, with the scaffold protein LGN forming oligomers, and with MTs to coordinate cortical forces generation required for spindle orientation.

Specifically, part of the studies of my PhD project focused on the characterization of the binding interfaces of NuMA with the light intermediate chains (LICs) of dynein, and demonstrated that this interaction is necessary for spindle orientation in metaphase.
Consistent with previous evidences showing that NuMA immunoprecipitates dynein in mitotic lysates (Kotak, Busso, and Gönczy 2012), we determined that the N-terminal region of NuMA encompassing residues 1-705 recognizes the LIC1 and LIC2 variants of dynein, similarly to other known dynein/dynactin activating adaptors (**Figure 14**). Within this region, we identified the presence of a monomeric globular head of about 153 residues followed by a dimeric coiled-coil, in agreement with the notion that the central portion of NuMA contains a long coiled-coil, and our evidences that NuMA self-assemble in cell (Pirovano et al. 2019). Crystallographic analysis carried out on $NuMA^{1-153}$ revealed a hook domain fold. Notably, the NuMA hook domain recognizes both the LIC1 and LIC2 dynein subunits, suggesting that in cells NuMA can work with dynein pools carrying either LIC isoforms. The NuMA hook domain differs from that of Hook proteins for the presence of an additional helix α9 that packs against the hydrophobic core of the fold conferring increased stability (**Figure 16**). In addition, the Hook proteins analysed so far show a structured helix between helices α7 and α8 contributing to the organization of a hydrophobic cleft hosting the helix α1 of LIC. The corresponding NuMA residues adopt a flexible disordered conformation. Nonetheless, NuMA shares with the Hook adaptors the same LIC-binding interface consisting of the α7-α8 loop and the helix α8, with the conserved residues $Gln124^{NuMA}$ and $Leu131^{NuMA}$ that, if mutated, impairs LIC binding *in vitro*. Whether the NuMA region between α7 and α8 of the hook domain undergoes a conformational change upon LIC binding and assumes a helical topology, or whether it remains partly disorganized accounting for the low affinity of the NuMA/LIC interaction compared to Hook3 is an

interesting open question, that only future structural studies can answer. Unfortunately, we did not succeed in reconstituting and crystallizing the NuMA/LIC-α1 complex due to the low affinity, but we believe it might be possible to obtain structural information on this interface by cryo-EM studies of the entire NuMA/dynein/dynactin assembly.

Through sequence investigation and biochemical analysis, we discovered a second LIC binding interface retained into the coiled-coil region of NuMA comprising residues 360-385, which is related to the CC1-box used by dynein/dynactin adaptors like BICD2 or Spindly to associate with LIC. Interestingly, this newly discovered stretch, that we named *CC1-box-like,* is highly conserved across the NuMA orthologs. Sequence analysis revealed that the *CC1-box-like* does not entirely conform to the CC1-box because the two central alanine residues have a one-residue frameshift compared to the canonical CC1-box motif and lack the conserved glycine residue (**Figure 18**). Nonetheless, *in vitro* binding assay with murine mitotic lysates showed that mouse NuMA, that contains a single alanine corresponding to A369 of human NuMA, binds to LIC1, indicating that $A369^{NuMA}$ is likely sufficient for the NuMA/LIC binding.

With structural and biochemical analyses, we proved that NuMA recognizes the α1 helix of the LIC subunits of dynein similarly to other dynein/dynactin activating adaptors. However the unexpected finding that NuMA harbors two LIC-binding interfaces suggests the possibility that it forms multi-subunits complex in which two dynein motors assemble with one NuMA dimer and one dynactin, as has been observed recently for BICDR1, Hook3, and BICD2 (Urnavicius et al. 2018) (**Figure 38**). Future structural information is required to clarify whether this is the case.

Recently, using a photo-inducible system, Okumura *et al.* revealed that optogenetic recruitment of dynein and dynactin cannot generate enough forces to displace the spindle and that cortical NuMA is required (Okumura et al. 2018). Molecularly, it is possible that NuMA confers high processivity to dynein that moves on astral MTs. Spindle orientation rescue experiments were conducted with NuMA mutants lacking both the hook domain and the *CC1-box-like* motif (NuMA-Δ1-705) characterized *in vitro* or either one NuMA/LIC binding interfaces (NuMA-Δ1-153 or NuMA-Δ154-705). This assay revealed that HeLa cells both LIC-interacting motifs are essential for correct spindle assembly and mitotic progression (**Figure 22**). Specifically, only the expression of NuMA-WT fully rescued the correct orientation of the spindle, while expression of NuMA-Δ1-153, NuMA-Δ154-705 or NuMA-Δ1-705 did not. However, in HeLa cells, the double point mutant in the *CC1-box-like* region (NuMA-A368V/A369V) restored spindle alignment to the substrate almost to the same extent of wild-type NuMA. Certainly, NuMA-Δ154-705 mutant is unable to interact

with LIC and to sustain spindle orientation, indicating that either the *CC1-box-like* sequence or the dimer nature of the coiled-coil in this region (**Figure 15**) are essential for dynein/dynactin complex formation and activation of MT-pulling forces. To uncouple the contribution of the *CC1-box-like* from the coiled-coil of the N-terminal portion of NuMA, one would need to conduct the same kind of spindle orientation assay presented on **Figure 22** using a point mutant in the hook domain of NuMA that strongly impairs the binding to LIC1/2 *in vitro* (for instance NuMA-L131A).
In summary, the combination of our biochemical, structural and cell biology evidences shed light on the organizational principles of NuMA/dynein/dynactin complexes, adding support to the notion that NuMA acts as a mitotic dynein-activating adaptor for what concerns spindle orientation processes.

During vertebrate cell division, spindle orientation relies on Gαi/LGN/NuMA complexes at the cell cortex, which recruit spindle motors and instruct spindle positioning (Pietro, Echard, and Morin 2016). Structural studies from our lab revealed that NuMA and LGN engage in high-order oligomers suggesting a new function of NuMA and LGN in promoting motor proteins cluster at the cortex. Specifically, we showed that the region $NuMA^{1861-1928}$ and LGN^{TPR} interact with a 3:3 stoichiometry. Crystallographic structure of the NuMA/LGN hetero-hexamers shown that these oligomers arrange in a donut-shape architecture, in which the α-helices upstream and downstream the TPR repeats of LGN and the region of NuMA spanning residues 1861-1899 are essential for oligomerization (**Figure 23**). Based on biochemical and structural evidences, we asked whether NuMA/LGN high-order complexes exist in cells and what can be their functional role in spindle orientation. To this end, I conduced co-IP experiments in mitotic HEK293T cells depleted of NuMA and expressing a monomeric NuMA C-terminal fragment (residues 1821-2115) containing the LGN-binding site (**Figure 24**). We then co-transfected these cells with either GFP-LGN-WT and FLAG-LGN-WT or GFP-LGN-ΔOLIGO and FLAG-LGN-ΔOLIGO, and tested whether in mitotic lysates the GFP-tagged version of LGN could immuno-precipitate the FLAG-tagged version of LGN together with $NuMA^{1821-2115}$. The experiment revealed that only GFP and FLAG-tagged LGN wild-type can form complexes with $NuMA^{1821-2115}$, while LGN-ΔOLIGO cannot. This evidence supports the notion that LGN and NuMA assemble high-order oligomers in mitotic cells, and that the same mutations impairing oligomerization *in vitro* disrupt oligomer formation in cells, suggesting that the same topology of the oligomer revealed by the structural work can occur *in vivo*. It is important to stress that the $NuMA^{1821-2115}$ construct that was used to assess the existence of high-order NuMA/LGN complexes in

cells does not retain all the NuMA functionalities in spindle assembly and orientation processes.

Clearly, in co-IP experiments the information regarding the localization of the LGN/NuMA complexes is lost. We believe that Proximity Ligation Assays (PLAs) combined with super-resolution microscopy technologies (such as single-molecule localization microscopy, including STORM – Stochastic Optical Reconstruction Microscopy) might help understanding the stoichiometry of endogenous LGN/NuMA complexes at the mitotic cortex. Imaging experiments in cells can also uncover how the activity of endogenous NuMA full-length is spatially organized at the cell cortex, and how this organization is retained in shorter NuMA proteins lacking the N-terminal dynein-binding domain, the coiled-coil region, the oligomerization domain with LGN, and the C-terminal MT binding fragment.

In summary, co-IP experiments with wild-type and oligomerization-deficient LGN (LGN-ΔOLIGO, lacking residues 1-12 and 350-366) confirmed that LGN/NuMA form high-order oligomers in cells depending on the ability of LGN to oligomerize with NuMA.

Importantly, we also found out that LGN-ΔOLIGO cannot rescue spindle orientation defects caused by LGN depletion (**Figure 23)**, demonstrating that LGN/NuMA oligomerization is fundamental for proper spindle orientation in mitosis.

To further explore the organizational principles of cortical force generators, I characterized the MT binding activity of NuMA, focusing on the C-terminal MT binding region of NuMA which lies downstream of the LGN binding domain (Gallini et al. 2016). Subtilisin-treated-MTs co-sediment with NuMA$^{2002\text{-}2115}$, indicating that NuMA can contact the MT-lattice regardless of the tubulin tails (**Figure 26**). Interestingly, SEC experiments showed that NuMA$^{2002–2115}$ associates stoichiometrically with α,β-tubulin dimers (**Figure 25**), indicating that NuMA also interacts with depolymerized tubulin. In the context of NuMA cortical functions, these evidences suggest that NuMA may act as astral MT plus-ends binding protein facilitating their shrinkage by catching free tubulin available near MTs nucleation sites, similarly to what have been shown for Stathmin, or by bending the MT protofilaments as kinesin-13 (see **paragraph 1.1.1**). Another possibility is that the binding of NuMA to MTs stabilizes the protofilament/tubulin-dimer interface similarly to TOG-domain proteins (see **paragraph 1.1.1**) conferring processivity to dynein movement towards the minus-ends. Comparative studies on NuMA$^{2002\text{-}2115}$ and NuMA C-terminal fragment encompassing residues 1970-2089 confirmed that 2002-2115 recapitulates the MT binding functions of NuMA. In absence of the tubulin tails, the affinity of NuMA$^{1970\text{-}2089}$ for MTs decreases,

indicating that both the MT lattice and the tubulin tails are recognized by this fragment. Unfortunately, *in vitro,* the NuMA$^{2002\text{-}2115}$ construct is prone to degradation at high concentration, and this behavior hampers crystallization studies of the NuMA$^{2002\text{-}2115}$:α/β-tubulin complex. We think that obtaining a pure and stable sample of the NuMA C-terminal region suitable for crystallization experiments with Subtilisin-treated α/β-tubulin dimers will require further effort. An interesting possibility would also be to use the NuMA C-terminal construct that recapitulates the MT-binding activity of NuMA to decorate taxol-stabilized MTs for cryo-Electron-Microscopy studies, as this kind of experiments do not require highly concentrated samples.

We found that the NuMA truncation mutant lacking the MT binding region (NuMA-ΔMT lacking residues 2002-2115) does not reach at the cortex, although it binds LGN which is the cortical recruiting factor for NuMA in metaphase (**Figure 32B**). We can explain this considering that the impaired NuMA-ΔMT cortical recruitment during metaphase could be due to the depletion of the Aurora-A phosphorylation site on Ser2047 (Gallini et al. 2016). The finding that in HeLa cells a NuMA truncation mutant lacking the MT binding region 2002-2115 (NuMA-ΔMT) cannot rescue misorientation defects caused by NuMA depletion are consistent with the notion that cortical NuMA assists the dynein-orientation functions (**Figure 32D**). However, we need to consider that NuMA-ΔMT also localizes less at the spindle poles compared to NuMA wild-type (**Figure 32B**), making it difficult to uncouple the polar and cortical function of NuMA in mitosis.

Collectively, these data support the notion that is not the cortical presence of NuMA and dynein, but rather a supra-molecular organization of NuMA with LGN, dynein and astral MTs that is required for the production of pulling forces on mitotic spindle poles necessary to orient the spindle in metaphase (**Figure 38**).

My research activities showed that: 1) NuMA contains the hook domain and a *CC1-box-like* region, and both engage with the α1-helix of LIC1 and are required to proper mitotic spindle orientation; 2) NuMA/LGN forms high-order oligomers in mitotic mammalian cells; 3) the C-terminal portion of NuMA encompassing residues 2002-2115 and containing the MT binding domain is essential for the spindle orientation functions of NuMA, though the exact molecular mechanism for this activity still remains elusive.

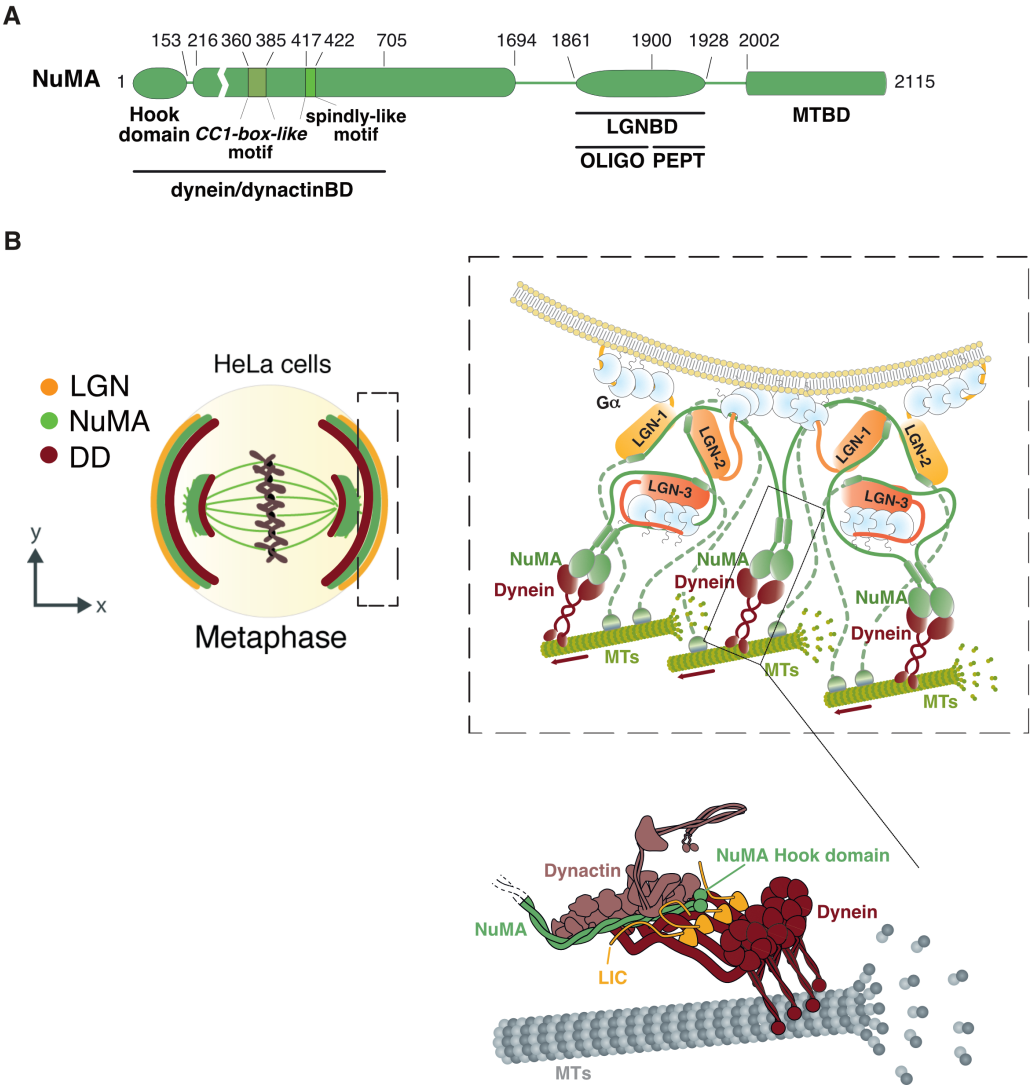

Figure 38. Schematic representation of the mitotic cortical function of LGN/NuMA/dynein complexes according to our studies. A) Domain structure of NuMA that recapitulate the boundaries of structural and functional mapping analyzed in this study. Recently, Okumura et al. (Okumura et al. 2018) identified a spindly-like motif sequence within the N-terminal region of NuMA, that was discovered as the binding interface for dynactin in dynein-adaptors (Gama et al. 2017). **B)** During metaphase, a pool of NuMA/dynein/dynactin (dynein/dynactin: DD, in brown) complexes accumulate at the spindle poles, and concomitantly NuMA (in green) is recruited at the cell cortex by LGN/Gαi association, and engages into cortical donut-shape oligomers with LGN (in orange). The self-dimerizing coiled-coil of NuMA bound to LGN in hetero-hexameric rings promotes the formation of cortical dynein clusters that pull on astral MTs to orient the mitotic spindle. In such arrangement, the C-terminal MT binding domain of NuMA associates with depolymerizing MT lattice, and the N-terminus is involved in dynein/dynactin adaptor function of NuMA. Dimeric coiled-coil NuMA interacts with the LIC subunits of dynein (in yellow) through the hook domains and *CC1-box-like* motif, suggesting the possibility that two dynein molecules are recruited to the same dynactin complex and to the MT tracks.

5.2 Mitotic NuMA/β-catenin complexes

The last part of my PhD research activities dealt with the dissection of the molecular link between spindle orientation mechanisms and Wnt signaling (Červenka and Čajánek 2018; Niehrs and Acebron 2012). The studies described in the chapter 4 of results provided evidence that, in mitotic mammalian cells, the NuMA is found in complexes with components of the canonical Wnt pathway. I demonstrated that NuMA associates with β-catenin, Dishevelled2 and Axin1, and that the C-terminal region of NuMA spanning residues 1821-2115 is required for the formation of this multi-subunit complex. Notably, I observed that Wnt3a stimulation does not seem to be relevant for mitotic NuMA/β-catenin interaction when the proteins are overexpressed in mitotic HEK293T cell lysates. Conversely, I propose the existence of a direct binding between $NuMA^{1821-2115}$ and β-catenin regulated by phosphorylations on β-catenin.

I started from evidences that, in prometaphase-synchronized HEK293T cells, GFP-NuMA full-length immunoprecipitates a number of endogenous Wnt signaling effectors including the scaffold proteins of the destruction complex Axin1 and Dishevelled2, and the effector of canonical Wnt pathway β-catenin. To evaluate the effect of mitogenic Wnt3a ligand stimulation on the NuMA/Wnt-effectors complex, we analyzed immunoprecipitation experiments in both Wnt3a and Dkk1 conditioned media (CM). As discussed in **paragraph 1.3.2**, upon Wnt-ligand binding to its Frizzled receptor and LRP5/6 co-receptor, a Wnt "signalosome" is assembled at the cytoplasmic tail of these receptors, that ultimately inhibits the Axin-dependent degradation of β-catenin. Signalosome assembly depends on the binding of Frizzled intracellular tail to the protein Dishevelled (Dvl) (Bilić et al. 2007). Interestingly, dynamic polymerization of Dvl transiently increases its avidity for Axin (Bienz 2014). Consequently, the whole Axin degradasome is recruited to the plasma membrane, and the intracellular tail of LRP5/6 is phosphorylated at specific motif (PPPS/TP). This LRP5/6 phosphorylation has been shown to function as direct competitive inhibitors of GSK3β (Stamos et al. 2014). As a result, unphosphorylated β-catenin accumulates in the cytoplasm, translocate to the nucleus, and initiates its transcriptional activity this way defining what it is known as the Wnt-ON state of the signaling pathway. In absence of Wnt3 stimulation, β-catenin is phosphorylated on Ser45 by CK1, a priming event for follow phosphorylation on Ser33/Ser37/Thr41 by GSK3β. These phosphorylation events target β-catenin for Axin-dependent degradation by the degradasome. The E3 ubiquitin ligase β-Trcp binds phospho-

β-catenin, resulting in its polyubiquitination and degradation by the proteasome (Gammons and Bienz 2018). The Dickkopf Wnt signaling pathway inhibitor 1 (Dkk1) primarily acts to block canonical Wnt signaling by binding to LRP co-receptors (Bao, Zheng, and Wu 2012). Dkk1 also facilitates the Kremen-mediated endocytosis of LRP5/6 (Chen et al. 2008). Consistently, HEK293T cells grown in Dkk1 supplemented medium display lower levels of β-catenin compared to lysates from Wnt3a conditioned media (**Figure 33**). Interestingly, our co-IP experiments revealed that β-catenin immunoprecipitates with NuMA both in Wnt3-stimulated and inhibited conditions, indicating that the presence of a homogeneously distributed Wnt3a leaves the NuMA/Wnt-effectors interaction unaffected.

In invertebrate systems including *C. elegans* and *D. melanogaster*, several lines of evidence support the existence of a binding between the C-terminal region of Dvl, consisting of a DEP and a PDZL domains, and the C-terminal region of NuMA, and that this interaction is required for spindle orientation (Johnston et al. 2013; Ségalen et al. 2010). In the last years, experimental attempts were performed from other members of the lab to reconstitute the NuMA/Dvl interaction *in vitro*. However, even if an interaction can be scored by pull-down experiments, the purified domains of the proteins do not coelute from SEC column. Consistently, I could observe a co-IP of overexpressed NuMA with Dvl. In line with these previous results, to start investigating the architecture of newly discovered NuMA/Wnt-effectors complexes, I decided to focus on the structural analogy among the NuMA binding partners. As shown in **paragraph 1.3.1**, β-catenin and LGN share a rigid helical scaffold consisting of either 12 armadillo repeats or 8 tetratricopeptide-repeats (TPRs) respectively. I hypothesized that the topology of the NuMA/β-catenin interaction con be reminiscent of the NuMA/LGN^{TPR} complex. Consistently, the LGN-binding fragment NuMA$^{1821\text{-}2115}$ purified from bacterial sources binds specifically endogenous β-catenin in pull-down experiments (**Figure 34**), demonstrating that the NuMA/β-catenin interaction does not depend on C-terminal NuMA phosphorylations. However, I did not succeed to reconstitute the NuMA$^{1821\text{-}2115}$/β-catenin complex with purified components (**Figure 35**). Intriguingly, I observed a heavy precipitation upon mixing NuMA$^{1821\text{-}2115}$ and full length β-catenin. I reasoned that this behaviour might be due to a conformational change that exposes hydrophobic surfaces either on NuMA or β-catenin, causing protein instability and precipitation. Alternatively, it is possible that the NuMA/β-catenin binding requires the presence of intermediate interactors or post-translational modifications stabilizing the complex.

As described in the literature, phosphorylation events represent a key mechanism responsible for the tight control of β-catenin levels within normal cells, and for timely activation of the Wnt/β-catenin pathway (C. Gao, Xiao, and Hu 2014). In the absence of Wnt3 stimulation, the β-catenin N-terminus is phosphorylated by GSK3β (on Ser33, Ser37, Thr41) and CK1 (on Ser45), which induce β-TrCP-mediated β-catenin degradation (Z. H. Gao et al. 2002; Haraguchi et al. 2008). Moreover, the Nek2 mitotic kinase regulates the centrosome functions of β-catenin phosphorylating it at a variety of sites including Ser33, Ser37, Thr41 (Bahmanyar et al. 2008). Therefore, to understand whether phosphorylations are required for the mitotic NuMA/β-catenin interaction, I expressed β-catenin and NuMA full-length or 1821-2115 in HEK293T cells, and harvested lysates with or in the absence of phosphatase inhibitors, and found that, when the phosphorylations are preserved, the affinity of β-catenin for $NuMA^{1821-2115}$ increases. SEC analyses with mitotic lysates co-expressing β-catenin and $NuMA^{1821-2115}$ seem to suggest that phosphorylated β-catenin and NuMA interact. To reconstitute the NuMA/β-catenin binding with purified proteins it will be important to better characterize the putative β-catenin phospho-sites. Since the NuMA/β-catenin interaction occurs in Dkk1-conditioned media in which the GSK3β/CK1-phosphorylated β-catenin is enriched (**Figures 33** and **36**), I speculate that Ser33, Ser37, Thr41, and Ser45 could be the phospho-sites involved in NuMA/β-catenin binding. Performing immunoprecipitation assays upon cell treatment with GSK3β or Nek2-inhibitors could help clarifying this aspect. To preserve all required post-translational modifications, the next step could be also to express and purify β-catenin in mammalian expression system.

We observed that when both NuMA and β-catenin are overexpressed in mitotic cells the binding affinity increase and remain constant in Wnt3a-stimulated or unstimulated conditions. Immunoprecipitation of two proteins at the endogenous levels could be interesting to evaluate whether a homogenous stimulation of the mitotic cell membrane influences the NuMA/β-catenin binding similarly to what we have observed in overexpression conditions. Moreover, NuMA immunoprecipitation assays in HEK293T cells depleted of endogenous β-catenin could help to test the hypothesis that β-catenin is a direct binding partner of NuMA within the Axin1 and Dvl2-containing macromolecular complexes.

β-catenin is a key Wnt-effector, which operates a transcriptional switch to determine cell fates during embryonic development and in adult tissues. This could explain why the deregulation of β-catenin signalling is often a root cause for cancer (Cadigan and Nusse 1997). Consistently, several cancer cell lines show β-catenin mutated phenotype (i.e.

HCT116), leading to β-catenin stabilization and hence constitutive activation of the Wnt pathway. Endogenous NuMA/β-catenin co-IP experiment from colon cancer cells represents a further strategy to understand the importance of phosphorylation in NuMA/β-catenin mitotic complexes.

In summary, the biochemical evidences gathered in the last period of my PhD indicate that in mitosis NuMA associates with Wnt-effectors regardless of Wnt3a stimulation, and that the NuMA$^{1821\text{-}2115}$ suffices to interact with phosphorylated β-catenin. Further investigations will be required to reconstitute the NuMA/β-catenin binding and larger complexes containing Dvl2/Axin1 to fully understand the molecular events underlying the connection between the Wnt and orientation pathways.

β-catenin has been shown to participate in at least two distinct centrosomal functions: γ-tubulin recruitment to centrosomes and centrosome splitting during mitotic spindle assembly (Kaplan et al. 2004; Mbom, Nelson, and Barth 2013; Vora, Fassler, and Phillips 2020). Interestingly, decreased centrosome levels of S33/S37/T41 phosphorylated β-catenin are associated with centrosomes, MTs and spindle defects in neuronal progenitors (Chilov et al. 2011). We know that, in the first phases of mitosis, NuMA contributes to spindle poles focusing and organization, and a pool of NuMA/dynein enriches at MT minus-ends near the poles (Hueschen et al. 2017). We speculate that in mitotic cells phospho-β-catenin could associate with NuMA to promote the establishment of the bipolar spindle, and later to promote spindle positioning.

6. MATERIALS AND METHODS

6.1 Cloning and plasmid

6.1.1 Biochemical assay protocols

N-terminal NuMA fragments spanning residues 1-705, 154-705, and C-terminal NuMA fragments spanning residues 1821-2115, 2002-2115, 1945-2115, 1970-2089, 1945-2059, 1951-2067 were generated by PCR amplification starting to synthetic cDNA coding for human NuMA (NCBI reference sequence NM_006185) subcloned in pCDH vector, and cloned into a pETM14 vector (Novagen) in frame with a cleavable N-terminal hexa-histidine tag. $NuMA^{1821-2115}$ was also cloned in pGEX-6PI vector in frame with a cleavable N-terminal Glutathione-S-Transferase (GST) tag. For the structural studies, $NuMA^{1-153}$ was obtained introducing a stop codon in the His-$NuMA^{1-705}$ pETM14 vector by QuikChange site-directed mutagenesis (Agilent), and sequence verified. The point mutations R114A, W116A, Y121A, Q124A, L131A, L135A and A368V/A369V were introduced in His-$NuMA^{1-705}$ using the QuikChange mutagenesis kit, and sequence verified. Dynein Light Intermediate Chain 1 (LIC1) full-length ($LIC1^{1-523}$) and C-terminus ($LIC1^{390-523}$), and dynein Light Intermediate Chain 2 (LIC2) full-length ($LIC2^{1-492}$) and C-terminus ($LIC2^{379-492}$) were generated by PCR amplification using as template human LIC1 cDNA (GE Dharmacon), and a human LIC2 cDNA retrotranscribed from HeLa cells. PCR products were cloned into a pGEX-6PI vector in frame with a N-terminal GST-tag. The point mutations F447A/F448A were introduced in GST-$LIC1^{1-523}$ by QuikChange mutagenesis. The pET28a plasmid expressing human GFP-$Hook3^{1-552}$ in frame with a N-terminal His-tag was purchased by Addgene (code 74614).

The pET32a plasmid expressing DARPin1 (Designed ankyrin repeat protein 1) in frame with a cleavable N-terminal hexa-histidine and Thioredoxin (Trx) tags, due to the presence of a Thrombin recognition site, was a gift from Steinmetz lab. For structural studies, DARPin1 sequence was cloned into a pETM14 vector (Novagen) in frame with the N-terminal cleavable His-tag.

GST-β-catenin full-length was obtained by PCR, using as template the pCI-neo vector containing β-catenin cDNA (Addgene, code 16518) and carring a CMV promoter. The PCR product was cloned into pGEX-6P1 vector (GE Healthcare). The PCR primers used to generate the recombinant proteins are listed in **Table 1**.

Primer name	Sequence (5'-3')	Vector name
N103-for	GCGCGCCCATGGGTATGACCCTGCACGCTACC	pETM14-His-NuMA-1-705
N104-rev	GCGCGCGTCGACTTATTGCAGCTGCTCTTGGAG	pETM14-His-NuMA-1-705
N113-for	GAAAACTTCCTGCAAAAGTGACCCGTGCCCTCTACCTGC	pETM14-His-NuMA-1-153
N114-rev	GCAGGTAGAGGGCACGGGTCACTTTTGCAGGAAGTTTTC	pETM14-His-NuMA-1-153
N217-for	GCGCGCCCATGGGTGCTCCCGTGCCCTCTACC	pETM14-His-NuMA-154-705
N104-rev	GCGCGCGTCGACTTATTGCAGCTGCTCTTGGAG	pETM14-His-NuMA-154-705
N20-for	GCGCGCCCATGGGTAAGAAGCTAGATGTGGAA	pETM14-His-NuMA-1821-2115
N14-rev	GCGCGCGTCGACTTAGTGCTTTGCCTTGCCCTT	pETM14-His-NuMA-1821-2115
N74-for	GCGCGCCCATGGGTGAGTCTAAGAAGGCCACC	pETM14-His-NuMA-2002-2115
N14-rev	GCGCGCGTCGACTTAGTGCTTTGCCTTGCCCTT	pETM14-His-NuMA-2002-2115
N79-for	GCGCGCCCATGGGTTCCCTGAGCCTGGGC	pETM14-His-NuMA-1945-2115
N14-rev	GCGCGCGTCGACTTAGTGCTTTGCCTTGCCCTT	pETM14-His-NuMA-1945-2115
N92-for	GCGCGCCCATGGTTATGCAGCCAATCCAGATAGC	pETM14-His-NuMA-1970-2089
N99-rev	GCGCGCGTCGACTTAATAGCGCGGAGAACGGCGGGT	pETM14-His-NuMA-1970-2089
N79-for	GCGCGCCCATGGGTTCCCTGAGCCTGGGC	pETM14-His-NuMA-1945-2059
N101-rev	GCGCGCGTCGACTTAATATAGCTTCTTGGGTGTGTTGAG	pETM14-His-NuMA-1945-2059
N100-for	GCGCGCCCATGGGTATCACAGATGAGGAGATG	pETM14-His-NuMA-1951-2067
N102-rev	GCGCGCGTCGACTTAATATCCCCGCCGCAGAAGGCT	pETM14-His-NuMA-1951-2067
DY1-for	GCGCGCGGATCCATGGCGGCCGTGGGGCGA	pGEX-6PI-GST-LIC1-1-523
DY2-rev	GCGCGCGTCGACTTAAGAAGCTTCTCCTTCCGT	pGEX-6PI-GST-LIC1-1-523
DY3-for	GCGCGCGGATCCATGGCAGCTGGAAGGCCTGTG	pGEX-6PI-GST-LIC1-390-523
DY2-rev	GCGCGCGTCGACTTAAGAAGCTTCTCCTTCCGT	pGEX-6PI-GST-LIC1-390-523
DY2-1-for	GCGCGCGAATTCATGGCGCCGGTGGGGGTGGAG	pGEX-6PI-GST-LIC2-1-492
DY2-2-rev	GCGCGCGTCGACTCAGGCTTCATTTTCTGTTGAAGAG	pGEX-6PI-GST-LIC2-1-492
DY2-3-for	GCGCGCGGATCCATGGCAGCTGGAAGGCCTGTG	pGEX-6PI-GST-LIC2-379-492
DY2-2-rev	GCGCGCGTCGACTCAGGCTTCATTTTCTGTTGAAGAG	pGEX-6PI-GST-LIC2-379-492
Bc1-for	GCGCGCGGATCCATGGCTACTCAAGCTGACCTG	pGEX-6PI-GST-β-catenin-1-781
Bc2-rev	GCGCGCGTCGACTTACAGGTCAGTATCAAACCAGGC	pGEX-6PI-GST-β-catenin-1-781
N57-for	GCGGGATCCATGAAGAAGCTAGATGTGGAAGAG	pGEX-6PI-GST-NuMA-1821-2115
N14-rev	GCGCGCGTCGACTTAGTGCTTTGCCTTGCCCTT	pGEX-6PI-GST-NuMA-1821-2115
Drp1-for	GCGCGCCCATGGGTCTGGTTCCGCGTGG	pETM14-His-DARPin1
Drp2-rev	GCGCGCGTCGACTTAGTTCAGCTTCTGCAGG	pETM14-His-DARPin1

Table 1. Primer list used for biochemistry protocols.

6.1.2 Cell biology protocols

For knocking-down human NuMA, the shRNA sequence 5'CATTATGATGCCAAGAAGCAGCAGAACCA3' was cloned into a lentiviral vector carrying a GFP reporter, and used to generate stably interfered HeLa cell lines (Gallini et al. 2016). NuMA-Δ1-153, NuMA-Δ1-705, or NuMA-Δ154-705 rescue constructs were generated by PCR, using as template mCherry-tagged NuMA full-length. NuMA-A368V/A369V double mutant construct was generated by QuickChange mutagenesis (Agilent) from the synthetic NuMA gene, and sequence verified. All rescue constructs were inserted into a pCDH lentiviral vector under the Ubc promoter (SBI System Bioscience) with a N-terminal mCherry-tag.

To obtain a NuMA construct unable to bind MTs, a stop codon at residue 2002 was introduced into pCDH-mCherry-NuMA full-length by QuickChange mutagenesis (Agilent). The pCDH lentiviral vectors obtained were used to generate stable HeLa cell lines expressing mCherry-NuMA-ΔMT.

For the immunoprecipitation (**Figure 24B**), the most effective shRNA-NuMA, carrying the sequence CATTATGATGCCAAGAAGCAGCAGAACCA (Gallini et al. 2016), was used

to generate also a NuMA knockdown HEK293T stable cell line. The NuMA fragment encompassing residues 1821-2115 was amplified and subcloned into the pCDH-Ubc-Hygro vector. This construct was used to generate a stably HEK293T cell line depleted for endogenous NuMA and expressing NuMA$^{1821-2115}$ (**Figure 24A**). LGN-WT and LGN-ΔOLIGO were cloned in a pEGFP-C1 vector, in frame with the GFP-tag. The same constructs were also cloned in a pCDH vector, with a C-terminal 3xFLAG tag.

For immunoprecipitation and SEC with cell lysate experiments (**Figure 33, 36, 37**), GFP-NuMA full-length and GFP-NuMA$^{1821-2115}$ were generated by cut and paste cloning strategy and PCR amplification, respectively, using as template the synthetic NuMA gene. Both DNA fragments were cloned into pCDH vector with N-terminal GFP tag. The PCR primers used to generate the useful constructs described are listed in **Table 2**.

Primer name	Sequence (5'-3')	Vector name
N199-for	GCGCGCGCTAGCATGGCTCTGAAGGAATCCCTG	pCDH-mCherry-NuMA-Δ1-153
N200-rev	GCGCGCGGATCCGAGTGCTTAGCCTTGCCCTT	pCDH-mCherry-NuMA-Δ1-153
N218-for	GCGCGCGCTAGCTTGCAGCTGCTCTTGGAGCT	pCDH-mCherry-NuMA-Δ1-705
N200-rev	GCGCGCGGATCCGAGTGCTTAGCCTTGCCCTT	pCDH-mCherry-NuMA-Δ1-705
N213-for	AGCCTTTTGCAGGAAGTTTTCC	pCDH-mCherry-NuMA-Δ154-705
N214-rev	GCTCTGAAGGAATCCCTGAAGG	pCDH-mCherry-NuMA-Δ154-705
N81-for	GGCCCGGGAACCCCCTAGTCCAAGAAGGCTACC	pCDH-mCherry-NuMA-ΔMT
N82-rev	GGTAGCCTTCTTGGACTAGGGGGTTCCCGGGCC	pCDH-mCherry-NuMA-ΔMT
N84-for	GCGCGCGGATCCAAGAAGCTAGATGTGGAA	pCDH-NuMA-1821-2115
N58-rev	GCGCGCGGCCGCCCCTTAGTGCTTTGCCTTGCCC	pCDH-NuMA-1821-2115
LGN-1-for	GCGCGCGGATCCATGAGAGAAGACCATTCT	pEGFP-GFP-LGN
LGN-677-rev	GCGCGCGTCGACTTAATGGTCTGCCGATTTTTT	pEGFP-GFP-LGN
LGN-13-for	GCGCGCGGATCCATGGAAGCTTCTTGCCTA	pEGFP-GFP-LGN-ΔOLIGO
LGN-677-rev	GCGCGCGTCGACTTAATGGTCTGCCGATTTTTT	pEGFP-GFP-LGN-ΔOLIGO
FLAG-for	GCGCGCGGATCCGATTATAAGGATGACGATGACAAAG	pCDH-3xFLAG-LGN-WT/ΔOLIGO
FLAG-rev	GCGCGCGGCCGCGACTGATAGTGACCTGTTCG	pCDH-3xFLAG-LGN-WT/ΔOLIGO
N57-for	GCGGGATCCATGAAGAAGCTAGATGTGGAAGAG	pCDH-GFP-NuMA-1821-2115
N14-rev	GCGCGCGTCGACTTAGTGCTTTGCCTTGCCCTT	pCDH-GFP-NuMA-1821-2115

Table 2. Primer list used for cell biology protocols.

6.2 Protein expression and purification

The hexa-histidine tagged and Glutathione-S-Transferase tagged recombinant proteins were expressed in BL21 Rosetta *E. coli* cells by 16 hours induction with 0.5 mM IPTG at 20 °C. For single-wavelength anomalous diffraction (SAD) experiments, NuMA$^{1-153}$ was expressed in a methionine auxotroph (Met-) bacterial strain grown in a Se-Met minimal medium (Molecular Dimensions, MD12-501).

For His-tagged protein recombinants purification, cells were lysed in 0.1 M Tris-HCl pH 8.0, 0.3 M NaCl, 10% glycerol, 5 mM imidazole pH 8.0, 2 mM β-mercaptoethanol and protease inhibitors (Calbiochem), and cleared for 1 hour at 100,000 *g*. Clear lysates were injected on a HiTrap chelating column (GE Healthcare) loaded with $NiCl_2$, washed with 1.0 M NaCl and 15 mM imidazole. For the N-terminal NuMA fragments (NuMA$^{1-705}$, NuMA^{1-}

^{153}, NuMA$^{154-705}$, and the point mutants on the hook domain or the *CC1-box like*), proteins were eluted with a 0.02 - 0.16 M imidazole gradient. Peak fractions were dialysed overnight at 4 °C against a buffer containing 30 mM Tris-HCl pH 8.0, 0.1 M NaCl, 5% glycerol and 1 mM DTT, while incubating with PreScission protease to remove the histidine-tag for NuMA$^{1-153}$ and NuMA$^{154-705}$ structural studies and SLS experiments. Proteins was then injected onto a Resource-Q anion exchange column and eluted by a salt gradient from 0.03 to 0.2 M NaCl over 20 column volumes. Purified proteins further polished on a Superdex-200 16/60 column equilibrated in 10 mM Tris-HCl pH 6.8, 0.1 M NaCl, 5% glycerol and 1 mM DTT. Peak fractions were analysed by SDS-PAGE, pooled and concentrated prior freezing at -80 °C. In particular, Trx-His-DARPin1 sample was further purified on a 6ml-Resource-Q column (GE Healthcare) applying a gradient from 0.04 to 0.3 M NaCl over 20 column volumes.

For the C-terminal NuMA fragmants spanning residues 1821-2115, 1821-2001, 2002-2115, 1945-2115, 1970-2089, 1945-2059, and 1951-2067, the proteins were eluted by applying a 0.02 - 0.2 M imidazole gradient, and dialyzed against 20 mM Tris-HCl pH 6.8, 40 mM NaCl, 5 % glycerol, 2mM β-mercaptoethanol prior to injection onto a Resource-S cation exchange column. The His-tag was removed by incubation with His-PreScission protease (GE Healthcare) overnight at 4 °C. The proteins were eluted from Resource-S with a gradient from 0.04 to 0.25 M NaCl over 20 column volumes, pooled and stored at -80 °C.

For GST-tagged protein recombinants purification, cells were lysed in 0.1 M Tris-HCl pH 8.0, 0.3 M NaCl, 10% glycerol, 0.5 mM EDTA, 1 mM DTT and protease inhibitors (Calbiochem), and cleared for 1 hour at 100,000 *g*. Proteins were affinity purified by incubation with Glutathione–Sepharose-4 Fast-Flow beads (GE Healthcare). For GST-pull-down assays (**Figures 14B, 17D, 17E, 19A, 19B, 19C, 20, 21C**), after washing, proteins immobilized on beads were resuspended in 1:1 v/v in a buffer consisting of 50 mM Tris-HCl pH 7.4, 0.1 M NaCl, 3 mM DTT, 0.1% Tween, 0.1% Triton X-100, and 0.07% Na deoxycholate, in a buffer consisting of 50 mM Hepes pH 7.5, 0.15 M NaCl, 2 mM EGTA, 1 mM EDTA, 2 mM $MgCl_2$, 0.3% Triton X-100, 10% glycerol, 3 mM DTT set for GST-pull-down of mitotic lysates (**Figure 34B**) or in a buffer consisting of 50 mM Hepes pH 7.5, 0.1 M NaCl, 5% glycerol, 1 mM DTT (**Figure 34C**).

For SEC experiments (**Figure 35B**), GST-β-catenin full-length was first affinity purified on glutathione beads (GSH), and then incubated with PreScission protease (GE Healthcare) overnight at 4 °C to remove the GST-tag. Cleaved β-catenin construct was eluted from the GSH beads in a desalting buffer consisting of 20 mM Tris-HCl pH 8.0, 0.15 M NaCl, 5 %

glycerol, 1 mM DTT. Eluted fractions were analyzed by SDS-PAGE analysis, pooled and concentrated to 11 mg/ml prior freezing at -80 °C.

For the MT co-sedimentation assay of **Figure 26C**, Ndc80^{Bonsai} (generous gift from Andrea Musacchio) was purified as reported by Ciferri *et al*. (Ciferri et al. 2008).

6.3 Static-Light-Scattering (SLS)

Static-Light-Scattering (SLS) analyses of His-NuMA$^{1-153}$ and His-NuMA$^{154-705}$ are reported in detail in **Figure 15**.

6.4 Protein crystallization and structural determination

NuMA$^{1-153}$ at 33 and 16.5 mg/ml was supplemented with 4 mM TCEP and screened for crystallization using commercially available crystallization kits. Crystallization experiments were initially conducted in 200 nl vapour diffusion sitting drops using a Mosquito Crystal nanodispenser (TTP Labtech) in MRC-2 well plates (Swissci, Hampton research). Crystals were obtained using the Hampton Research Crystal Screen 1 and 2 at 4 °C, at 16.5 mg/ml concentration, with a reservoir containing 30% PEG-4000, 0.2 M Magnesium Chloride, and 0.1 M Tris pH 8.5. Diffraction-quality crystals were obtained by optimization at 4 °C using the hanging-drop method in 24-well VDX plates. The best crystals grew in crystallization drops consisting of a 1:1 (v/v) mixture of protein solution and well solution of 28% PEG-4000, 0.2 M Magnesium Chloride, 0.1 M Bis-Tris Propane pH 8.5. The crystals were further improved through streak-seeding. For data collection, crystals were transferred to a cryo-buffer (reservoir buffer supplemented with 15% glycerol) and flash-frozen in liquid nitrogen. X-ray diffraction data were collected to 1.54 Å resolution at the PXIII beamline X06DA of the Swiss Light Source (SLS, Villigen). All data were initially processed with XDS (Kabsch 2010) implemented in xia2 (Winter, Lobley, and Prince 2013) to define the crystallographic space group, unit cell and data collection statistics. The structure of NuMA$^{1-153}$ was determined by single-wavelength anomalous diffraction (SAD) method on Se-Met containing crystals, which were grown similarly to the native ones. Initial phases were derived using the *AutoSol* Wizard in *Phenix* (Adams et al. 2010). The unit-cell parameters are consistent with four copies of the protein per asymmetric unit. Initial model building was conducted by *AutoBuild* Wizard in *Phenix* and completed using iterative cycles of manual model building in *Coot* (Emsley et al. 2010) and refinement in *Phenix*. The model has been refined to a R_{free} of 21.5% and a R_{work} of 17.0%. PyMOL was used to generate all the illustrations of the structure (DeLano Scientific LLC). Structure superposition of NuMA$^{1-153}$

and the hook domain of Hook3 (PDB ID 6b9h) was based on the largest rigid body calculated using the RAPIDO algorithm (Mosca and Schneider 2008).

6.5 Analytical Size Exclusion Chromatography (SEC)

Details on SEC analysis conducted to evaluate the monodispercity of purified recombinant protein samples, and the protein complexes reconstitution are reported within the corresponding figure legends.

6.6 Sequence alignments

To compare NuMA and Hook proteins sequences (**Figure 17C**), *Homo sapiens* sequences of NuMA (Uniprot entry Q14980), Hook1 (Uniprot entry Q9UJC3), Hook2 (Uniprot entry Q96ED9), and Hook3 (Uniprot entry Q86VS8) were aligned with NuMA sequences from *Mus musculus* (Uniprot entry E9Q7G0), *Gallus gallus* (Uniprot entry D8MIU8), *Xenopus laevis* (Uniprot entry P70012), *Danio rerio* (NCBI entry XP_009290241.1), *Drosophila melanogaster* (Uniprot entry Q8IR55); Hook1 sequences from *Mus musculus* (Uniprot entry Q8BIL5), *Gallus gallus* (Uniprot entry Q5ZJ27), *Xenopus tropicalis* (Uniprot entry F7CDF9), *Danio rerio* (Uniprot entry Q5TZ80); Hook2 sequences from *Mus musculus* (Uniprot entry Q7TMK6), *Gallus gallus* (Uniprot entry XP_025001539.1), *Xenopus laevis* (Uniprot entry Q6NRB0), *Danio rerio* (NCBI entry NP_957405.1); Hook3 sequences from *Mus musculus* (Uniprot entry Q8BUK6), *Gallus gallus* (Uniprot entry F1NKH3), *Xenopus laevis* (Uniprot entry Q6GQ73), *Danio rerio* (NCBI entry XP_017211697.1), and with the *Drosophila melanogaster* Hook sequence (Uniprot entry Q24185) using CLUSTALΩ (Sievers et al. 2011). The multiple sequence alignment was visualized with Jalview (Waterhouse et al. 2009).

For **Figure 18A**, NuMA sequences from *Homo sapiens* (Uniprot entry Q14980), *Mus musculus* (Uniprot entry E9Q7G0), *Gallus gallus* (Uniprot entry D8MIU8), *Xenopus laevis* (Uniprot entry P70012) and *Danio rerio* (NCBI entry XP_009290241.1) were aligned with CLUSTALΩ and coloured by percentage of identity in Jalview.

To identify the CC1-box-like motif shown in **Figure 18B**, the first 720 residues of human NuMA were aligned with 120 residues around the CC1-boxes of known dynein adaptors using the following sequences: NuMA sequence from *Homo sapiens* (Uniprot entry Q14980); Spindly sequences from *Homo sapiens* (Uniprot entry Q96EA4), *Mus musculus (*Uniprot entry Q923A2), *Gallus gallus* (Uniprot entry E1BW90), *Xenopus tropicalis* (Uniprot entry B3DLE8), *Danio rerio* (Uniprot entry A7MD70), *Drosophila melanogaster* (Uniprot entry Q9VQS4); BICD1 sequences from *Homo sapiens* (Uniprot entry Q96G01),

Mus musculus (Uniprot entry Q8BR07), *Gallus gallus* (NCBI entry XP_024997118.1), *Xenopus tropicalis* (NCBI entry OCA17635.1), *Danio rerio* (Uniprot entry F1RBX3); BICD2 sequences from *Homo sapiens* (Uniprot entry Q8TD16), *Mus musculus* (Uniprot entry Q921C5), *Gallus gallus* (Uniprot entry E1C2N3), *Xenopus tropicalis* (NCBI entry XP_017952212.1), *Danio rerio* (NCBI entry XP_005155947.1), *Drosophila melanogaster* BICD sequence (Uniprot entry P16568); BICDR1 sequences from *Homo sapiens* (Uniprot entry Q6ZP65), *Mus musculus* (Uniprot entry A0JNT9), *Gallus gallus* (Uniprot entry A0A1L1RSD5), *Xenopus tropicalis* (Uniprot entry Q0V9T6), *Danio rerio* (Uniprot entry P0CF95); BICDR2 sequences from *Homo sapiens* (Uniprot entry A1A5D9), *Mus musculus* (Uniprot entry Q8CHW5), *Xenopus tropicalis* (NCBI entry NP_001004934.1), *Danio rerio* (Uniprot entry A0JMK8), *Drosophila melanogaster* BICDR sequence (NCBI entry Q8SWR2.1); TRAK1 sequences from *Homo sapiens* (Uniprot entry Q9UPV9), *Mus musculus* (Uniprot entry Q6PD31), *Gallus gallus* (NCBI entry XP_004939527.1), *Xenopus tropicalis* (Uniprot entry F6XSR9), *Danio rerio* (NCBI entry XP_021322520.1); TRAK2 sequences from *Homo sapiens* (Uniprot entry O60296), *Mus musculus* (Uniprot entry Q6P9N8), *Gallus gallus* (Uniprot entry F1NVL2), *Xenopus tropicalis* (NCBI entry XP_002936582.1), *Danio rerio* (Uniprot entry A0A0R4IDG7); HAP1 sequences from *Homo sapiens* (Uniprot entry P54257), *Mus musculus* (Uniprot entry O35668), *Gallus gallus* (NCBI entry XP_003642869.1), *Xenopus tropicalis* (Uniprot entry F6WSB3), *Danio rerio* (NCBI entry XP_017213872.1), and *Drosophila melanogaster* TRAK and HAP sequence (NCBI entry NP_001245927.1). The alignment was further edited according to the paper by Sacristan and co-workers (Sacristan et al. 2018).

6.7 Microtubule co-sedimentation assays

MT co-sedimentation assays experimental details are discussed within the corresponding figure legends. A schematic representation of the experiment is reported in **Figure 39**.

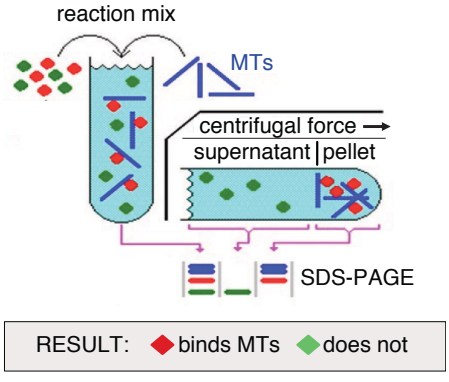

Figure 39. Schematic representation of a MT co-sedimentation experiment. The MT co-sedimentation is an *in vitro* assay routinely used to analyse the protein binding with MTs. This assay requires the incubation of the proteins with taxol-stabilized MTs, followed by the ultracentrifugation step to pellet MTs, and analysis of co-sedimented-samples.

6.8 Pull-down assays

Pull-down experiments with purified proteins and pull-down assay with mitotic cell lysates are described within the corresponding figure legends.

6.9 Cell culture

HeLa cells (ATCC, CCL-2), HEK293T (ATCC, CRL-11268) and MC38 (ATCC, CRL-2639) cells were cultured at 37°C in a 5% CO_2 atmosphere in Dulbecco's Modified Eagle Medium (DMEM) supplemented with 10% FBS, 1% L-glutamine and 50 µg/ml penicillin/streptomycin.

For HeLa and HEK293T cells expressing the shRNA targeting NuMA, the medium was supplemented also with 0.5 µg/ml puromycin, and with 5 µg/ml hygromycin for cells infected with pCDH vectors for stable expression. Protein depletion in several cell lines were monitored by western blot and immunofluorescence.

For the spindle orientation analysis (**Figure 22**), NuMA depleted HeLa cells were transiently transfected with pCDH lentiviral vector under the Ubc promoter (SBI System Bioscience) expressing mCherry-tagged NuMA full-lengh, NuMA-Δ1-153, NuMA-Δ1-705, NuMA-Δ154-705, or NuMA-A368V/A369V rescue constructs using Lipofectamine 3000 (Invitrogen) according to the manufacter's instruction. Protein depletion was monitored by western blot and immunofluorescence.

Wnt3a conditioned medium was prepared as described in Davidson et al. (Davidson et al. 2005). Briefly, mouse Wnt3a conditioned medium (Wnt3a-CM) was produced from mouse L cells stably transfected with mouse Wnt3a (American Type Culture Collection CRL-2647). Dkk1 conditioned medium was obtained with transient transfection of HEK293T cells. 10 µg of pBABE vector containing cDNA coding for mouse Dkk1 (gently gift from Myriam Alcalay's group) was transfected with 0.1% PEI in 90% HEK293T confluent cells. After 72 hours from transfection, the medium was collected, filtered and stored at -80 °C.

6.10 Immunoprecipitation

Immunoprecipitation experiments details are described within the corresponding figure legends.

6.11 SEC of cell lysates

Details on SEC experiments conducted on mitotic HEK293T lysates were discussed the corresponding figure legends.

6.12 Immunofluorescence staining, microscopy and quantification

For immunofluorescence analysis, quantification of cortical signals of mCherry-NuMA wild-type or mCherry-NuMA-ΔMT (**Figure 32B**), and spindle orientation analysis of **Figure 22** and **Figure 32D,** details are described within the corresponding figure legends.

6.13 Antibodies

Summary of the antibodies used for immunoblotting (IB) and immunofluorescence (IF) were reported on **Table 3**.

Name	**Source**	**Application**
Anti-His	Santa Cruz Biotechnology, sc-8036	1:200 (IB)
Anti-NuMA	Mapelli lab	1:200 (IB) / 1:3000 (IF)
Anti-β-catenin	Millipore, 06-734	1:2000 (IB)
Anti-Vinculin	In house IEO	1:10000 (IB)
Anti-LGN	Mapelli lab	1:500 (IB)
Anti-α-tubulin	Abcam, ab4074	1:600 (IB)
Anti-FLAG	Sigma-Aldrich, F7425	1:8000 (IB)
Anti-GFP	In house IEO	1:1000 (IB)
Anti-Dischevelled2	Cell Signaling, 3224S	1:1000 (IB)
Anti-Axin1	Cell Signaling, C76H11	1:1000 (IB)
Anti-GAPDH	Santa Cruz Biotechnology, sc-32233	1:1000 (IB)
Anti-γ-tubulin	Sigma-Aldrich, C7604	1:200 (IF)
Anti-α-tubulin YL1/2	Abcam, ab6160	1:5000 (IB)
Anti-β-tubulin JDR.3B8	Sigma-Aldrich, T8535	1:1000 (IB)
Cy3 conjugated anti-γ-tubulin	Sigma-Aldrich, C7604	1:200 (IF)
anti-mouse AlexaFluor 647	Jackson ImmunoResearch	1:300 (IF)

Table 3. Antibodies list.

REFERENCES

Acebron, Sergio P. et al. 2014. "Mitotic Wnt Signaling Promotes Protein Stabilization and Regulates Cell Size." *Molecular Cell* 54(4): 663–74. http://dx.doi.org/10.1016/j.molcel.2014.04.014.

Adams, Paul D. et al. 2010. "PHENIX: A Comprehensive Python-Based System for Macromolecular Structure Solution." *Acta Crystallographica Section D: Biological Crystallography* 66(2): 213–21.

Agostino, Mark, and Sebastian Öther Gee Pohl. 2020. "The Structural Biology of Canonical Wnt Signalling." *Biochemical Society Transactions* 48(4): 1765–80.

Akhmanova, Anna, and Michel O. Steinmetz. 2008. "Tracking the Ends: A Dynamic Protein Network Controls the Fate of Microtubule Tips." *Nature Reviews Molecular Cell Biology* 9(4): 309–22.

Al-Bassam, Jawdat et al. 2002. "MAP2 and Tau Bind Longitudinally along the Outer Ridges of Microtubule Protofilaments." *Journal of Cell Biology* 157(7): 1187–96.

Bafico, Anna et al. 2001. "Novel Mechanism of Wnt Signalling Inhibition Mediated by Dickkopf-1 Interaction with LRP6/Arrow." *Nature Cell Biology* 3(7): 683–86.

Bahmanyar, Shirin et al. 2008. "β-Catenin Is a Nek2 Substrate Involved in Centrosome Separation." *Genes and Development* 22(1): 91–105.

Baker, J., and D. Garrod. 1993. "Epithelial Cells Retain Junctions during Mitosis." *Journal of Cell Science* 104(2): 415–25.

Bao, Ju, Jie J. Zheng, and Dianqing Wu. 2012. "The Structural Basis of DKK-Mediated Inhibition of Wnt/LRP Signaling." *Science Signaling* 5(224): 1–4.

Barker, Nick. 2014. "Adult Intestinal Stem Cells: Critical Drivers of Epithelial Homeostasis and Regeneration." *Nature Reviews Molecular Cell Biology* 15(1): 19–33.

Bergstralh, Dan T., Nicole S. Dawney, and Daniel St Johnston. 2017. "Spindle Orientation: A Question of Complex Positioning." *Development (Cambridge)* 144(7): 1137–45.

Bergstralh, Dan T., Timm Haack, and Daniel St Johnston. 2013. "Epithelial Polarity and Spindle Orientation: Intersecting Pathways." *Philosophical Transactions of the Royal Society B: Biological Sciences* 368(1629).

Bergstralh, Dan T., Holly E. Lovegrove, and Daniel St. Johnston. 2015. "Lateral Adhesion Drives Reintegration of Misplaced Cells into Epithelial Monolayers." *Nature Cell Biology* 17(11): 1497–1503.

Bienz, Mariann. 2014. "Signalosome Assembly by Domains Undergoing Dynamic Head-to-Tail Polymerization." *Trends in Biochemical Sciences* 39(10): 487–95. http://dx.doi.org/10.1016/j.tibs.2014.08.006.

Bilić, Josipa et al. 2007. “Wnt Induces LRP6 Signalosomes and Promotes Dishevelled-Dependent LRP6 Phosphorylation.” *Science* 316(5831): 1619–22.

Blangy, Anne et al. 1995. “Phosphorylation by P34cdc2 Regulates Spindle Association of Human Eg5, a Kinesin-Related Motor Essential for Bipolar Spindle Formation in Vivo.” *Cell* 83(7): 1159–69.

Brouhard, Gary J. et al. 2008. “XMAP215 Is a Processive Microtubule Polymerase.” *Cell* 132(1): 79–88.

Brouhard, Gary J., and Luke M. Rice. 2018. “Microtubule Dynamics: An Interplay of Biochemistry and Mechanics.” *Nature Reviews Molecular Cell Biology* 19(7): 451–63. http://dx.doi.org/10.1038/s41580-018-0009-y.

Cadigan, Ken M., and Roel Nusse. 1997. “Wnt Signaling: A Common Theme in Animal Development.” *Genes and Development* 11(24): 3286–3305.

Carminati, Manuel et al. 2016. “Concomitant Binding of Afadin to LGN and F-Actin Directs Planar Spindle Orientation.” *Nature Structural and Molecular Biology* 23(2): 155–63.

Červenka, Igor, and Lukáš Čajánek. 2018. “Europe PMC Funders Group The Connections of Wnt Pathway Components with Cell Cycle and Centrosome : Side Effects or a Hidden Logic ?” 52(6): 614–37.

Chang, Chih Chia et al. 2017. “Regulation of Mitotic Spindle Assembly Factor NuMA by Importin-β.” *Journal of Cell Biology* 216(11): 3453–62.

Chatterjee, Chandrima et al. 2016. “Distinct Interaction Modes of the Kinesin-13 Motor Domain with the Microtubule.” *Biophysical Journal* 110(7): 1593–1604. http://dx.doi.org/10.1016/j.bpj.2016.02.029.

Chen, Lijun et al. 2008. “Structural Insight into the Mechanisms of Wnt Signaling Antagonism by Dkk.” *Journal of Biological Chemistry* 283(34): 23364–70.

Chilov, Dmitri et al. 2011. “Phosphorylated β-Catenin Localizes to Centrosomes of Neuronal Progenitors and Is Required for Cell Polarity and Neurogenesis in Developing Midbrain.” *Developmental Biology* 357(1): 259–68. http://dx.doi.org/10.1016/j.ydbio.2011.06.029.

Chishiki, Kanako, Sachiko Kamakura, Junya Hayase, and Hideki Sumimoto. 2017. “Ric-8A, an Activator Protein of Gαi, Controls Mammalian Epithelial Cell Polarity for Tight Junction Assembly and Cystogenesis.” *Genes to Cells* 22(3): 293–309.

Ciferri, Claudio et al. 2008. “Implications for Kinetochore-Microtubule Attachment from the Structure of an Engineered Ndc80 Complex.” *Cell* 133(3): 427–39.

Compton, Duane A., and Don W. Cleveland. 1993. “NuMA Is Required for the Proper Completion of Mitosis.” *Journal of Cell Biology* 120(4): 947–57.

Culurgioni, Simone et al. 2011. “Inscuteable and NuMA Proteins Bind Competitively to Leu-Gly-Asn Repeat-Enriched Protein (LGN) during Asymmetric Cell Divisions.” *Proceedings of the National Academy of Sciences of the United States of America* 108(52): 20998–3.

Davidson, Gary et al. 2005. “Casein Kinase 1γ Couples Wnt Receptor Activation to Cytoplasmic Signal Transduction.” *Nature* 438(7069): 867–72.

Desai, Arshad, and Timothy J Mitchison. 1997. “Microtubule Polymerization Dynamics.” : 83–117.

Du, Quansheng, and Ian G. Macara. 2004. “Mammalian Pins Is a Conformational Switch That Links NuMA to Heterotrimeric G Proteins.” *Cell* 119(4): 503–16.

Du, Quansheng, Laura Taylor, Duane A. Compton, and Ian G. Macara. 2002. “LGN Blocks the Ability of NuMA to Bind and Stabilize Microtubules: A Mechanism for Mitotic Spindle Assembly Regulation.” *Current Biology* 12(22): 1928–33.

Dumont, Sophie, and Timothy J. Mitchison. 2009. “Force and Length in the Mitotic Spindle.” *Current Biology* 19(17): R749–61. http://dx.doi.org/10.1016/j.cub.2009.07.028.

Dwivedi, Devashish et al. 2019. “The Dynein Adaptor Hook2 Plays Essential Roles in Mitotic Progression and Cytokinesis (Journal of Cell Biology (2019) 218:3 DOI: 10.1083/Jcb.201804183).” *Journal of Cell Biology* 218(10): 3526–27.

Emsley, P., B. Lohkamp, W. G. Scott, and K. Cowtan. 2010. “Features and Development of Coot.” *Acta Crystallographica Section D: Biological Crystallography* 66(4): 486–501.

Finegan, Tara M et al. 2019. “ Tissue Tension and Not Interphase Cell Shape Determines Cell Division Orientation in the Drosophila Follicular Epithelium .” *The EMBO Journal* 38(3): 1–18.

Fodde, Riccardo et al. 2001. “Mutations in the APC Tumour Suppressor Gene Cause Chromosomal Instability.” *Nature Cell Biology* 3(4): 433–38. https://doi.org/10.1038/35070129.

Fuchs, Elaine. 2016. “Epithelial Skin Biology: Three Decades of Developmental Biology, a Hundred Questions Answered and a Thousand New Ones to Address.” *Curr Top Dev Biol*: 357–74.

Fuchs, Elaine, and Ting Chen. 2013. “A Matter of Life and Death: Self-Renewal in Stem Cells.” *EMBO Reports* 14(1): 39–48. http://dx.doi.org/10.1038/embor.2012.197.

Gadde, Sharat, and Rebecca Heald. 2004. “Mechanisms and Molecules of the Mitotic Spindle.” *Current Biology* 14(18): 797–805.

Gallini, Sara et al. 2016. “NuMA Phosphorylation by Aurora-a Orchestrates Spindle

Orientation.” *Current Biology* 26(4): 458–69.

Gama, José B. et al. 2017. “Molecular Mechanism of Dynein Recruitment to Kinetochores by the Rod-Zw10-Zwilch Complex and Spindly.” *Journal of Cell Biology* 216(4): 943–60.

Gammons, Melissa, and Mariann Bienz. 2018. “Multiprotein Complexes Governing Wnt Signal Transduction.” *Current Opinion in Cell Biology* 51: 42–49. https://doi.org/10.1016/j.ceb.2017.10.008.

Gao, Chenxi, Gutian Xiao, and Jing Hu. 2014. “Regulation of Wntβcatenin Signaling by Modification_2014_cellbioscsience.Pdf.” : 1–20.

Gao, Zhong Hua et al. 2002. “Casein Kinase I Phosphorylates and Destabilizes the β-Catenin Degradation Complex.” *Proceedings of the National Academy of Sciences of the United States of America* 99(3): 1182–87.

Garnham, Christopher P., and Antonina Roll-Mecak. 2012. “The Chemical Complexity of Cellular Microtubules: Tubulin Post-Translational Modification Enzymes and Their Roles in Tuning Microtubule Functions.” *Cytoskeleton* 69(7): 442–63.

Gierke, Sarah, Kumar Praveen, and Wittmann Torsten. 2012. “Analysis of Microtubule Polymerization Dynamics in Live Cells.” *Methods Cell Biology* (10): 15–33.

Giet, Régis et al. 1999. “The Xenopus Laevis Aurora-Related Protein Kinase PEg2 Associates with and Phosphorylates the Kinesin-Related Protein XlEg5.” *Journal of Biological Chemistry* 274(21): 15005–13.

Gloerich, Martijn et al. 2017. “Cell Division Orientation Is Coupled to Cell-Cell Adhesion by the E-Cadherin/LGN Complex.” *Nature Communications* 8: 1–11.

Gueth-Hallonet, Catherine, Klaus Weber, and Mary Osborn. 1996. “NuMA: A Bipartite Nuclear Location Signal and Other Functional Properties of the Tail Domain.” *Experimental Cell Research* 225(1): 207–18.

Guillot, Charlène, and Thomas Lecuit. 2013. “Adhesion Disengagement Uncouples Intrinsic and Extrinsic Forces to Drive Cytokinesis in Epithelial Tissues.” *Developmental Cell* 24(3): 227–41.

Habib, Shukry J. et al. 2013. “A Localized Wnt Signal Orients Asymmetric Stem Cell Division in Vitro.” *Science* 339(6126): 1445–48.

Hadjihannas, Michel V., Martina Brückner, and Jürgen Behrens. 2010. “Conductin/Axin2 and Wnt Signalling Regulates Centrosome Cohesion.” *EMBO Reports* 11(4): 317–24.

Hao, Yi et al. 2010. “Par3 Controls Epithelial Spindle Orientation by APKC-Mediated Phosphorylation of Apical Pins.” *Current Biology* 20(20): 1809–18. http://dx.doi.org/10.1016/j.cub.2010.09.032.

Haraguchi, K. et al. 2008. “Ajuba Negatively Regulates the Wnt Signaling Pathway by Promoting GSK-3β-Mediated Phosphorylation of β-Catenin.” *Oncogene* 27(3): 274–84.

Harborth, Jens et al. 1999. “Self Assembly of NuMA: Multiarm Oligomers as Structural Units of a Nuclear Lattice.” *EMBO Journal* 18(6): 1689–1700.

Haren, Laurence, Nicole Gnadt, Michel Wright, and Andreas Merdes. 2009. “NuMA Is Required for Proper Spindle Assembly and Chromosome Alignment in Prometaphase.” *BMC Research Notes* 2: 1–6.

Haren, Laurence, and Andreas Merdes. 2002. “Direct Binding of NuMA to Tubulin Is Mediated by a Novel Sequence Motif in the Tail Domain That Bundles and Stabilizes Microtubules.” *Journal of Cell Science* 115(9): 1815–24.

Huber, Andrew H., W. James Nelson, and William I. Weis. 1997. “Three-Dimensional Structure of the Armadillo Repeat Region of β-Catenin.” *Cell* 90(5): 871–82.

Huber, Andrew H., and William I. Weis. 2001. “The Structure of the β-Catenin/E-Cadherin Complex and the Molecular Basis of Diverse Ligand Recognition by β-Catenin.” *Cell* 105(3): 391–402.

Hueschen, Christina L., Samuel J. Kenny, Ke Xu, and Sophie Dumont. 2017. “NuMA Recruits Dynein Activity to Microtubule Minus-Ends at Mitosis.” *eLife* 6: 1–26.

Ishiyama, Noboru et al. 2010. “Dynamic and Static Interactions between P120 Catenin and E-Cadherin Regulate the Stability of Cell-Cell Adhesion.” *Cell* 141(1): 117–28. http://dx.doi.org/10.1016/j.cell.2010.01.017.

Jaffe, Aron B., Noriko Kaji, Joanne Durgan, and Alan Hall. 2008. “Cdc42 Controls Spindle Orientation to Position the Apical Surface during Epithelial Morphogenesis.” *Journal of Cell Biology* 183(4): 625–33.

Jayaraman, Swaathi et al. 2017. “The Nuclear Mitotic Apparatus Protein NuMA Controls RDNA Transcription and Mediates the Nucleolar Stress Response in a P53-Independent Manner.” *Nucleic Acids Research* 45(20): 11725–42.

Johnston, Christopher A. et al. 2013. “Formin-Mediated Actin Polymerization Cooperates with Mushroom Body Defect (Mud)-Dynein during Frizzled-Dishevelled Spindle Orientation.” *Journal of Cell Science* 126(19): 4436–44.

Kabsch, Wolfgang. 2010. “Integration, Scaling, Space-Group Assignment and Post-Refinement.” *Acta Crystallographica Section D: Biological Crystallography* 66(2): 133–44.

Kam, Yoonseok, and Vito Quaranta. 2009. “Cadherin-Bound β-Catenin Feeds into the Wnt Pathway upon Adherens Junctions Dissociation: Evidence for an Intersection between

β-Catenin Pools." *PLoS ONE* 4(2).

Kapitein, Lukas C. et al. 2005. "The Bipolar Mitotic Kinesin Eg5 Moves on Both Microtubules That It Crosslinks." *Nature* 435(7038): 114–18.

Kaplan, Daniel D., Thomas E. Meigs, Patrick Kelly, and Patrick J. Casey. 2004. "Identification of a Role for β-Catenin in the Establishment of a Bipolar Mitotic Spindle." *Journal of Biological Chemistry* 279(12): 10829–32.

Kardon, Julia R., and Ronald D. Vale. 2009. "Regulators of the Cytoplasmic Dynein Motor." *Nature Reviews Molecular Cell Biology* 10(12): 854–65.

Khodjakov, Alexey et al. 2003. "Minus-End Capture of Preformed Kinetochore Fibers Contributes to Spindle Morphogenesis." *Journal of Cell Biology* 160(5): 671–83.

Kikuchi, Koji, Yohei Niikura, Katsumi Kitagawa, and Akira Kikuchi. 2010. "Dishevelled, a Wnt Signalling Component, Is Involved in Mitotic Progression in Cooperation with Plk1." *EMBO Journal* 29(20): 3470–83. http://dx.doi.org/10.1038/emboj.2010.221.

Kiyomitsu, Tomomi. 2015. "Mechanisms of Daughter Cell-Size Control during Cell Division." *Trends in Cell Biology* 25(5): 286–95. http://dx.doi.org/10.1016/j.tcb.2014.12.003.

———. 2019. "The Cortical Force-Generating Machinery: How Cortical Spindle-Pulling Forces Are Generated." *Current Opinion in Cell Biology* 60: 1–8. https://doi.org/10.1016/j.ceb.2019.03.001.

Kiyomitsu, Tomomi, and Iain M. Cheeseman. 2012. "Chromosome-and Spindle-Pole-Derived Signals Generate an Intrinsic Code for Spindle Position and Orientation." *Nature Cell Biology* 14(3): 311–17. http://dx.doi.org/10.1038/ncb2440.

———. 2013. "Cortical Dynein and Asymmetric Membrane Elongation Coordinately Position the Spindle in Anaphase." *Cell* 154(2): 391. http://dx.doi.org/10.1016/j.cell.2013.06.010.

Knipling, Leslie, Jennifer Hwang, and J. Wolff. 1999. "Preparation and Properties of Pure Tubulin S." *Cell Motility and the Cytoskeleton* 43(1): 63–71.

Knoblich, Juergen A. 2010. "Asymmetric Cell Division: Recent Developments and Their Implications for Tumour Biology." *Nature Reviews Molecular Cell Biology* 11(12): 849–60.

Kollman, Justin M., Andreas Merdes, Lionel Mourey, and David A. Agard. 2011. "Microtubule Nucleation by γ-Tubulin Complexes." *Nature Reviews Molecular Cell Biology* 12(11): 709–21.

Kotak, Sachin, Coralie Busso, and Pierre Gönczy. 2012. "Cortical Dynein Is Critical for Proper Spindle Positioning in Human Cells." *Journal of Cell Biology* 199(1): 97–110.

———. 2013. “NuMA Phosphorylation by CDK1 Couples Mitotic Progression with Cortical Dynein Function.” *EMBO Journal* 32(18): 2517–29.

———. 2014. “NuMA Interacts with Phosphoinositides and Links the Mitotic Spindle with the Plasma Membrane.” *The EMBO Journal* 33(16): 1815–30.

Kotak, Sachin, and Pierre Gönczy. 2013. “Mechanisms of Spindle Positioning: Cortical Force Generators in the Limelight.” *Current Opinion in Cell Biology* 25(6): 741–48.

———. 2014. “NuMA Phosphorylation Dictates Dynein-Dependent Spindle Positioning.” *Cell Cycle* 13(2): 177–78.

Lancaster, Oscar M., and Buzz Baum. 2014. “Shaping up to Divide: Coordinating Actin and Microtubule Cytoskeletal Remodelling during Mitosis.” *Seminars in Cell and Developmental Biology* 34: 109–15. http://dx.doi.org/10.1016/j.semcdb.2014.02.015.

Lechler, Terry, and Elaine Fuchs. 2005. “Asymmetric Cell Divisions Promote Stratification and Differentiation of Mammalian Skin.” *Nature* 437(7056): 275–80.

Lee, In Gyun et al. 2018. “A Conserved Interaction of the Dynein Light Intermediate Chain with Dynein-Dynactin Effectors Necessary for Processivity.” *Nature Communications* 9(1).

Lee, Meng-Horng, Piyush Koria, Jun Qu, and Stelios T. Andreadis. 2009. “JNK Phosphorylates B-catenin and Regulates Adherens Junctions.” *The FASEB Journal* 23(11): 3874–83.

van Leen, Eric Victor, Florencia di Pietro, and Yohanns Bellaïche. 2020. “Oriented Cell Divisions in Epithelia: From Force Generation to Force Anisotropy by Tension, Shape and Vertices.” *Current Opinion in Cell Biology* 62: 9–16.

Lu, Yan et al. 2012. “An Overview of Tubulin Inhibitors That Interact with the Colchicine Binding Site.” *Pharmaceutical Research* 29(11): 2943–71.

Mahale, Sagar P., Amit Sharma, and Sivaram V.S. Mylavarapu. 2016. “Dynein Light Intermediate Chain 2 Facilitates the Metaphase to Anaphase Transition by Inactivating the Spindle Assembly Checkpoint.” *PLoS ONE* 11(7): 1–18.

Marchesi, Stefano et al. 2014. “DEPDC1B Coordinates De-Adhesion Events and Cell-Cycle Progression at Mitosis.” *Developmental Cell* 31(4): 420–33. http://dx.doi.org/10.1016/j.devcel.2014.09.009.

Matsumura, Shigeru et al. 2012. “ABL1 Regulates Spindle Orientation in Adherent Cells and Mammalian Skin.” *Nature Communications* 3.

———. 2016. “Interphase Adhesion Geometry Is Transmitted to an Internal Regulator for Spindle Orientation via Caveolin-1.” *Nature Communications* 7(May).

Mattagajasingh, Subhendra N., Shu Ching Huang, and Edward J. Benz. 2009. “Inhibition of

Protein 4.1 R and NuMA Interaction by Mutagenization of Their Binding-Sites Abrogates Nuclear Localization of 4.1 R." *Clinical and Translational Science* 2(2): 102–11.

Mbom, Bertrade C., W. James Nelson, and Angela Barth. 2013. "β-Catenin at the Centrosome: Discrete Pools of β-Catenin Communicate during Mitosis and May Co-Ordinate Centrosome Functions and Cell Cycle Progression." *BioEssays* 35(9): 804–9.

McClelland, Levi J. et al. 2020. "Structure of the G Protein Chaperone and Guanine Nucleotide Exchange Factor Ric-8A Bound to Gαi1." *Nature Communications* 11(1). http://dx.doi.org/10.1038/s41467-020-14943-4.

Merdes, Andreas et al. 2000. "Formation of Spindle Poles by Dynein/Dynactin-Dependent Transport of NuMA." *Journal of Cell Biology* 149(4): 851–61.

Merdes, Andreas, Kasra Ramyar, Janet D. Vechio, and Don W. Cleveland. 1996. "A Complex of NuMA and Cytoplasmic Dynein Is Essential for Mitotic Spindle Assembly." *Cell* 87(3): 447–58.

Moreno, Naike Salvador et al. 2019. "The Nuclear Structural Protein NuMA Is a Negative Regulator of 53BP1 in DNA Double-Strand Break Repair." *Nucleic Acids Research* 47(6): 2703–15.

Morin, Xavier, and Yohanns Bellaïche. 2011. "Mitotic Spindle Orientation in Asymmetric and Symmetric Cell Divisions during Animal Development." *Developmental Cell* 21(1): 102–19.

Mosca, Roberto, and Thomas R. Schneider. 2008. "RAPIDO: A Web Server for the Alignment of Protein Structures in the Presence of Conformational Changes." *Nucleic acids research* 36(Web Server issue): 42–46.

Nakajima, Yu Ichiro et al. 2013. "Epithelial Junctions Maintain Tissue Architecture by Directing Planar Spindle Orientation." *Nature* 500(7462): 359–62.

Niehrs, Christof, and Sergio P. Acebron. 2012. "Mitotic and Mitogenic Wnt Signalling." *EMBO Journal* 31(12): 2705–13. http://dx.doi.org/10.1038/emboj.2012.124.

Niessen, Carien M., and Cara J. Gottardi. 2008. "Molecular Components of the Adherens Junction." *Biochimica et Biophysica Acta - Biomembranes* 1778(3): 562–71.

Niida, Atsushi et al. 2004. "DKK1, a Negative Regulator of Wnt Signaling, Is a Target of the β-Catenin/TCF Pathway." *Oncogene* 23(52): 8520–26.

Nogales E., Wolf S.G., and Downing K.H. 1998. "Structureof the A-b Tubulin Dimer by Electron Crystallography." *Nature* 6(January): 786–87.

O Morgan, D. 2007. *Cell Cycle: Principles of Control*. The Yale Journal of Biology and Medicine.

Okumura, Masako, Toyoaki Natsume, Masato T. Kanemaki, and Tomomi Kiyomitsu. 2018. "Dynein–Dynactin–NuMA Clusters Generate Cortical Spindle-Pulling Forces as a Multiarm Ensemble." *eLife* 7: 1–24.

Olenick, Mara A., and Erika L.F. Holzbaur. 2019. "Cell Science at a Glance Dynein Activators and Adaptors at a Glance." *Journal of Cell Science* 132(6): 1–7.

Oscar Hertwig, Richard Hertwig. 1884. *Untersuchungen Zur Morphologie Und Physiologie Der Zelle*. ed. Fisher.

Pan, Zhu et al. 2013. "An Autoinhibited Conformation of LGN Reveals a Distinct Interaction Mode between GoLoco Motifs and TPR Motifs." *Structure* 21(6): 1007–17. http://dx.doi.org/10.1016/j.str.2013.04.005.

Pecqueur, Ludovic et al. 2012. "A Designed Ankyrin Repeat Protein Selected to Bind to Tubulin Caps the Microtubule plus End." *Proceedings of the National Academy of Sciences of the United States of America* 109(30): 12011–16.

Peyre, Elise et al. 2011. "A Lateral Belt of Cortical LGN and NuMA Guides Mitotic Spindle Movements and Planar Division in Neuroepithelial Cells." *Journal of Cell Biology* 193(1): 141–54.

Pietro, Florencia, Arnaud Echard, and Xavier Morin. 2016. "Regulation of Mitotic Spindle Orientation: An Integrated View." *EMBO reports* 17(8): 1106–30.

Pirovano, Laura et al. 2019. "Hexameric NuMA:LGN Structures Promote Multivalent Interactions Required for Planar Epithelial Divisions." *Nature Communications* 10(1).

Prosser, Suzanna L., and Laurence Pelletier. 2017. "Mitotic Spindle Assembly in Animal Cells: A Fine Balancing Act." *Nature Reviews Molecular Cell Biology* 18(3): 187–201.

Reck-Peterson, Samara L., William B. Redwine, Ronald D. Vale, and Andrew P. Carter. 2018. "The Cytoplasmic Dynein Transport Machinery and Its Many Cargoes." *Nature Reviews Molecular Cell Biology* 19(6): 382–98. http://dx.doi.org/10.1038/s41580-018-0004-3.

Reinsch, Sigrid, and Eric Karsenti. 1994. "Orientation of Spindle Axis and Distribution of Plasma Membrane Proteins during Cell Division in Polarized MDCKII Cells." *Journal of Cell Biology* 126(6): 1509–26.

Renna, Cristina et al. 2020. "Organizational Principles of the NuMA-Dynein Interaction Interface and Implications for Mitotic Spindle Functions." *Structure*: 1–10. https://doi.org/10.1016/j.str.2020.04.017.

Rizzelli, F., M.G. Malabarba, S. Sigismund, and M. Mapelli. 2020. "The Crosstalk between Microtubules, Actin and Membranes Shapes Cell Division." *Open Biology* 10(3).

Rizzelli, Francesca, Maria Grazia Malabarba, Sara Sigismund, and Marina Mapelli. 2020.

"The Crosstalk between Microtubules, Actin and Membranes Shapes Cell Division." *Open Biology* 10(3).

Routledge, Daniel, and Steffen Scholpp. 2019. "Mechanisms of Intercellular Wnt Transport." *Development (Cambridge)* 146(10).

Rubin, Camelia Iancu, and George F. Atweh. 2004. "The Role of Stathmin in the Regulation of the Cell Cycle." *Journal of Cellular Biochemistry* 93(2): 242–50.

Sacristan, Carlos et al. 2018. "Dynamic Kinetochore Size Regulation Promotes Microtubule Capture and Chromosome Biorientation in Mitosis." *Nature Cell Biology* 20(7): 800–810.

Sana, Shrividya et al. 2018. "Plk1 Regulates Spindle Orientation by Phosphorylating NuMA in Human Cells." *Life Science Alliance* 1(6): 1–14.

Santoro, Angela et al. 2016. "Molecular Mechanisms of Asymmetric Divisions in Mammary Stem Cells." *EMBO reports* 17(12): 1700–1720.

Sato, Toshiro et al. 2011. "Paneth Cells Constitute the Niche for Lgr5 Stem Cells in Intestinal Crypts." *Nature* 469(7330): 415–18.

Scadden, David T. 2014. "Nice Neighborhood: Emerging Concepts of the Stem Cell Niche." *Cell* 157(1): 41–50. http://dx.doi.org/10.1016/j.cell.2014.02.013.

Scarpa, Elena, Cédric Finet, Guy B. Blanchard, and Bénédicte Sanson. 2018. "Actomyosin-Driven Tension at Compartmental Boundaries Orients Cell Division Independently of Cell Geometry In Vivo." *Developmental Cell* 47(6): 727-740.e6.

Schlager, Max A. et al. 2014. "Bicaudal D Family Adaptor Proteins Control the Velocity of Dynein-Based Movements." *Cell Reports* 8(5): 1248–56. http://dx.doi.org/10.1016/j.celrep.2014.07.052.

Ségalen, Marion et al. 2010. "The Fz-Dsh Planar Cell Polarity Pathway Induces Oriented Cell Division via Mud/NuMA in Drosophila and Zebrafish." *Developmental Cell* 19(5): 740–52.

Seldin, Lindsey, Andrew Muroyama, and Terry Lechler. 2016. "NuMA-Microtubule Interactions Are Critical for Spindle Orientation and the Morphogenesis of Diverse Epidermal Structures." *eLife* 5: 1–18.

Seldin, Lindsey, Nicholas D. Poulson, Henry P. Foote, and Terry Lechler. 2013. "NuMA Localization, Stability, and Function in Spindle Orientation Involve 4.1 and Cdk1 Interactions." *Molecular Biology of the Cell* 24(23): 3651–62.

Sharma, Monica, Isabel Castro-Piedras, Glenn E. Simmons, and Kevin Pruitt. 2018. "Dishevelled: A Masterful Conductor of Complex Wnt Signals." *Cellular Signalling* 47(December 2017): 52–64.

Sievers, Fabian et al. 2011. “Fast, Scalable Generation of High-Quality Protein Multiple Sequence Alignments Using Clustal Omega.” *Molecular Systems Biology* 7(539).

Silk, Alain D., Andrew J. Holland, and Don W. Cleveland. 2009. “Requirements for NuMA in Maintenance and Establishment of Mammalian Spindle Poles.” *Journal of Cell Biology* 184(5): 677–90.

Smith, Nicholas R., and Kenneth E. Prehoda. 2011. “Robust Spindle Alignment in Drosophila Neuroblasts by Ultrasensitive Activation of Pins.” *Molecular Cell* 43(4): 540–49. http://dx.doi.org/10.1016/j.molcel.2011.06.030.

Stamos, Jennifer L. et al. 2014. “Structural Basis of GSK-3 Inhibition by N-Terminal Phosphorylation and by the Wnt Receptor LRP6.” *eLife* 2014(3): 1–22.

Stolz, Ailine, Kim Neufeld, Norman Ertych, and Holger Bastians. 2015. “Wnt-mediated Protein Stabilization Ensures Proper Mitotic Microtubule Assembly and Chromosome Segregation.” *EMBO reports* 16(4): 490–99.

Tall, Gregory G., and Alfred G. Gilman. 2005. “Resistance to Inhibitors of Cholinesterase 8A Catalyzes Release of Gαi-GTP and Nuclear Mitotic Apparatus Protein (NuMA) from NuMA/LGN/Gαi-GDP Complexes.” *Proceedings of the National Academy of Sciences of the United States of America* 102(46): 16584–89.

Taneja, Nilay et al. 2016. “Focal Adhesions Control Cleavage Furrow Shape and Spindle Tilt during Mitosis.” *Scientific Reports* 6: 1–11.

Théry, Manuel et al. 2007. “Experimental and Theoretical Study of Mitotic Spindle Orientation.” *Nature* 447(7143): 493–96.

Toropova, Katerina et al. 2019. “Structure of the Dynein-2 Complex and Its Assembly with Intraflagellar Transport Trains.” *Nature Structural and Molecular Biology* 26(9): 823–29. http://dx.doi.org/10.1038/s41594-019-0286-y.

Toyoshima, Fumiko, and Eisuke Nishida. 2007. “Integrin-Mediated Adhesion Orients the Spindle Parallel to the Substratum in an EB1- and Myosin X-Dependent Manner.” *EMBO Journal* 26(6): 1487–98.

Tuncay, Hüseyin, and Klaus Ebnet. 2016. “Cell Adhesion Molecule Control of Planar Spindle Orientation.” *Cellular and Molecular Life Sciences* 73(6): 1195–1207.

Urnavicius, Linas et al. 2018. “Cryo-EM Shows How Dynactin Recruits Two Dyneins for Faster Movement.” *Nature* 554(7691): 202–6.

Vidi, Pierre Alexandre et al. 2014. “NuMA Promotes Homologous Recombination Repair by Regulating the Accumulation of the ISWI ATPase SNF2h at DNA Breaks.” *Nucleic Acids Research* 42(10): 6365–79.

Vora, Setu M., Jan S. Fassler, and Bryan T. Phillips. 2020. “Centrosomes Are Required for

Proper β-Catenin Processing and Wnt Response." *Molecular Biology of the Cell* 31(17): 1951–61.

Wang, Gang, Qing Jiang, and Chuanmao Zhang. 2014. "The Role of Mitotic Kinases in Coupling the Centrosome Cycle with the Assembly of the Mitotic Spindle." *Journal of Cell Science* 127(19): 4111–22.

Waterhouse, Andrew M. et al. 2009. "Jalview Version 2-A Multiple Sequence Alignment Editor and Analysis Workbench." *Bioinformatics* 25(9): 1189–91.

Wei, Chongjuan et al. 2012. "The LKB1 Tumor Suppressor Controls Spindle Orientation and Localization of Activated AMPK in Mitotic Epithelial Cells." *PLoS ONE* 7(7).

Widlund, Per O. et al. 2011. "XMAP215 Polymerase Activity Is Built by Combining Multiple Tubulin-Binding TOG Domains and a Basic Lattice-Binding Region." *Proceedings of the National Academy of Sciences of the United States of America* 108(7): 2741–46.

Willard, Francis S., Randall J. Kimple, and David P. Siderovski. 2004. "Return of the GDI: The GoLoco Motif in Cell Division." *Annual Review of Biochemistry* 73: 925–52.

Williams, Scott E., Slobodan Beronja, H. Amalia Pasolli, and Elaine Fuchs. 2011. "Asymmetric Cell Divisions Promote Notch-Dependent Epidermal Differentiation." *Nature* 470(7334): 353–58.

Winter, Graeme, Carina M.C. Lobley, and Stephen M. Prince. 2013. "Decision Making in Xia2." *Acta Crystallographica Section D: Biological Crystallography* 69(7): 1260–73.

Woodard, Geoffrey E. et al. 2010. "Ric-8A and Giα Recruit LGN, NuMA, and Dynein to the Cell Cortex To Help Orient the Mitotic Spindle." *Molecular and Cellular Biology* 30(14): 3519–30.

Xing, Yi et al. 2008. "Crystal Structure of a Full-Length β-Catenin." *Structure* 16(3): 478–87.

Yang, Shaomin et al. 2009. "Protein 4.1R Links E-Cadherin/β-Catenin Complex to the Cytoskeleton through Its Direct Interaction with β-Catenin and Modulates Adherens Junction Integrity." *Biochimica et Biophysica Acta - Biomembranes* 1788(7): 1458–65. http://dx.doi.org/10.1016/j.bbamem.2009.03.022.

Yang, Yunfan et al. 2014. "CYLD Regulates Spindle Orientation by Stabilizing Astral Microtubules and Promoting Dishevelled-NuMA-Dynein/ Dynactin Complex Formation." *Proceedings of the National Academy of Sciences of the United States of America* 111(6): 2158–63.

Yuzawa, Satoru et al. 2011. "Structural Basis for Interaction between the Conserved Cell Polarity Proteins Inscuteable and Leu-Gly-Asn Repeat-Enriched Protein (LGN)."

Proceedings of the National Academy of Sciences of the United States of America 108(48): 19210–15.

Zeuner, Ann, Matilde Todaro, Giorgio Stassi, and Ruggero De Maria. 2014. "Colorectal Cancer Stem Cells: From the Crypt to the Clinic." *Cell Stem Cell* 15(6): 692–705. http://dx.doi.org/10.1016/j.stem.2014.11.012.

Zhang, Kai et al. 2017. "Cryo-EM Reveals How Human Cytoplasmic Dynein Is Auto-Inhibited and Activated." *Cell* 169(7): 1303-1314.e18. http://dx.doi.org/10.1016/j.cell.2017.05.025.

Zheng, Zhen et al. 2010. "LGN Regulates Mitotic Spindle Orientation during Epithelial Morphogenesis." *Journal of Cell Biology* 189(2): 275–88.

Zheng, Zhen, Qingwen Wan, Gerry Meixiong, and Quansheng Du. 2014. "Cell Cycle-Regulated Membrane Binding of NuMA Contributes to Efficient Anaphase Chromosome Separation." *Molecular Biology of the Cell* 25(5): 606–19.

Zhu, Changjun et al. 2005. "Functional Analysis of Human Microtubule-Based Motor Proteins, the Kinesins and Dyneins, in Mitosis/Cytokinesis Using RNA Interference." *Molecular Biology of the Cell* 16(November): 3187–99.

Zhu, Jinwei et al. 2011. "LGN/MInsc and LGN/NuMA Complex Structures Suggest Distinct Functions in Asymmetric Cell Division for the Par3/MInsc/LGN and Gαi/LGN/NuMA Pathways." *Molecular Cell* 43(3): 418–31. http://dx.doi.org/10.1016/j.molcel.2011.07.011.

APPENDIX: Publications

1. Pirovano, L., Culurgioni, S., Carminati, M., Alfieri, A., Monzani, S., Cecatiello, V., Gaddoni, C., **Rizzelli, F.,** Foadi, J., Pasqualato, S., & Mapelli, M. (2019). Hexameric NuMA:LGN structures promote multivalent interactions required for planar epithelial divisions. *Nature Communications*, *10*(1). https://doi.org/10.1038/s41467-019-09999-w
2. Renna, C.*, **Rizzelli, F.*,** Carminati, M.*, Gaddoni, C., Pirovano, L., Cecatiello, V., Pasqualato, S., & Mapelli, M. (2020). Organizational Principles of the NuMA-Dynein Interaction Interface and Implications for Mitotic Spindle Functions. *Structure*, 1–10. https://doi.org/10.1016/j.str.2020.04.017
   (**co-first authors*)
3. **Rizzelli, F**., Malabarba, M. G., Sigismund, S., & Mapelli, M. (2020). The crosstalk between microtubules, actin and membranes shapes cell division. *Open Biology*, *10*(3). https://doi.org/10.1098/rsob.190314
4. Brullo, C., Rapetti, F., Alfei, S., Maric, I., **Rizzelli, F.,** Mapelli, M., Rosano, C., Viale, M., & Bruno, O. (2020). Discovery of New Antiproliferative Imidazopyrazole Acylhydrazones Able To Interact with Microtubule Systems. *ChemMedChem*, *15*(11). https://doi.org/10.1002/cmdc.202000122
5. Bruni, M.*, Cecatiello, V.*, Diaz-Basabe, A.*, Lattanzi, G.*, Mileti, E.*, Monzani, S.*, Pirovano, L.*, **Rizzelli, F.*,** Visintin, C.*, Bonizzi, G., Giani, M., Lavitrano, M., Faravelli, S., Forneris, F., Caprioli, F., Pelicci, P. G., Natoli, G., Pasqualato, S., Mapelli, M., & Facciotti, F. (2020). Persistence of anti-SARS-CoV-2 antibodies in non-hospitalized COVID-19 convalescent health care workers. *Journal of Clinical Medicine, 9*(10). https://doi.org/10.3390/jcm9103188
   (**co-first authors*)